

Anhydrous solid-state proton conduction in crystalline MOFs, COFs, HOFs, and POMs

Debolina Mukherjee, Apu Saha, Subhodeep Moni, Dirk Volkmer, Madhab C. Das

Angaben zur Veröffentlichung / Publication details:

Mukherjee, Debolina, Apu Saha, Subhodeep Moni, Dirk Volkmer, and Madhab C. Das. 2025. "Anhydrous solid-state proton conduction in crystalline MOFs, COFs, HOFs, and POMs." *Journal of the American Chemical Society* 147 (7): 5515–53.
<https://doi.org/10.1021/jacs.4c14029>.



Anhydrous Solid-State Proton Conduction in Crystalline MOFs, COFs, HOFs, and POMs

Debolina Mukherjee, Apu Saha, Subhodeep Moni, Dirk Volkmer,* and Madhab C. Das*

ABSTRACT: Strategic design of solid-state proton-conducting electrolytes for application in anhydrous proton-exchange membrane fuel cells (PEMFCs) has gained burgeoning interest due to a spectrum of advantageous features, including higher CO tolerance and ease in the water management systems. Toward this direction, crystalline materials like metal–organic frameworks (MOFs), covalent organic frameworks (COFs), hydrogen-bonded organic frameworks (HOFs), and polyoxometalates (POMs) are emerging PEM materials, offering strategic structural engineering through crystallography, thus enabling ultrahigh anhydrous proton conductivity up to 10^{-2} – 10^{-1} S/cm. This Perspective highlights significant progress achieved thus far with such crystalline platforms in the domain of anhydrous proton conduction across a wide temperature window (sub-zero to above 100 °C). Based on their structural backgrounds, these platforms are categorized into four classes (viz. MOFs, COFs, HOFs, and POMs) with a detailed evolutionary timeline since their emergence early in 2009. Insightful discussions with a key focus on the strategies undertaken to attain anhydrous proton conductivity along with implementation in fuel cell technology through membrane electrode assembly are presented. A section on “Critical Analysis and Future Prospects” provides decisive key viewpoints on those overlooked issues with future endorsement (e.g., performance assessment with CO tolerance analysis and fuel cell test stand) for further development while comparing them with other anhydrous platforms from both academic and industrial perspectives.

1. INTRODUCTION

Huge consumption of the global energy supply associated with rapid urbanization, technological advancements, industrial revolution, and population explosions has led to an abrupt hike in the rate of energy exhaustion worldwide. Most importantly, this rise in energy consumption is noted to be dynamic, as emphasized in the International Energy Outlook report from the U.S. Energy Administration in 2016 that estimated around a 50% rise in worldwide energy consumption in the next 30 years (by 2050).¹ In order to combat such a critical situation, a number of alternative energy sources have emerged globally, and among them, proton-exchange membrane fuel cells (PEMFCs) powered by hydrogen and oxygen as fuels are highly promising. Such fuel cells convert chemical energy into electrical energy and are completely detached from the fossil fuels that are linked with the emission of toxic gases such CO_x , SO_x , and NO_x causing environmental pollution and harming the health of biologically diverse species.² In PEMFCs, solid-state proton conductors (SSPCs) play an important role in the overall cell output efficiency by transporting protons from anode to cathode compartments through the proton-conducting membrane separator, which is also known as a *proton-exchange membrane* or *polymer electrolyte membrane* (PEM). Thus, ultrahigh proton conductivity (preferably on the order of 10^{-2} – 10^{-1} S/cm) is an important feature to make these SSPCs work as PEMs in fuel cell stacks under varying operating conditions.^{3,4}

Since its development in 1960, the perfluorinated sulfonated copolymer Nafion (a product of Dupont) has served as the industry-standard solid-state PEM material in PEMFCs,

exhibiting proton conductivity within the range of 10^{-2} – 10^{-1} S/cm in a narrow temperature window (70–80 °C) under high relative humidity (95–100% RH), and branded itself as a perfect PEM material for operation in low-temperature proton-exchange membrane fuel cells (LT-PEMFCs) at the commercial scale.^{5,6} However, several limitations, such as continuous maintenance of high humidity levels with the aid of external power sources, restrictions to lower operating temperatures (<80 °C), and high cost of polymeric sheets (the cost of Nafion 115 for a 12 in. × 12 in. × 0.005 in. sheet is ~\$956 from Sigma-Aldrich at the time of publication) due to the requirement of perfluorination, put a set-back on its widespread usage that interrogates the concept of sustainability.^{6,7} Another chief detractor of this technology is the risk of carbon monoxide (CO) poisoning of the Pt catalyst that severely hampers the oxidation of the H_2 (fuel) at the anode of fuel cells at lower operating temperatures. CO remains present in the H_2 fuel stream as an impurity. Globally, hydrogen fuel production (70 MMT) is accomplished by the steam reforming of natural gas/methane (76%), coal gasification technology (22%), and electrolysis (2%).⁸ The first two processes produce a synthesis gas mixture and are followed by

a water–gas shift (WGS) reaction to yield a H₂-rich stream containing several typical impurities, including CO, as listed in Table 1.^{9,10}

Table 1. Contents of Impurities in Various Hydrogen Production Methods^a

Component	Steam Reforming (%)	Coal Gasification (%)
H ₂	94.3	87.8
CO	0.1	2.6
CO ₂	2.5	3.9
N ₂	0.2	5.0
CH ₄	2.9	0.01

^aRepresentation of the global hydrogen production scenario with percentages of various impurities in each production process.⁹

In addition to the above processes, steam reforming of methanol (SRM) is a recently developed method in which the H₂ fuel is produced with fewer byproducts (only two impurities, CO₂ and CO), in the composition of H₂ (74%), CO₂ (25%), and CO (1–2%).^{11,12} In all cases, these impurities must be removed in order to obtain high-purity H₂ for its intended applications in fuel cells. Specifically, it is important to note that the elimination of trace CO impurities from the H₂ stream is pertinent to hydrogen fuel cell technologies, since even ppm levels of CO may act as a *catalyst poison* for the anodic Pt catalyst and may plague the overall performance of PEMFCs.¹⁰ For example, it has been found that, at a 100 ppm concentration of CO, the current density of PEMFCs could decrease by 73.76%, with severe deterioration in the cell performance.¹⁰ This is attributed to the ease of combination of CO impurities with the Pt catalyst through steady bond formation. In fact, CO competes with H₂ for adhering to the catalyst surface, diminishing the reaction area between H₂ and the catalyst surface, with a consequent decrease in the current density of the fuel cell. Another study revealed that even the presence of 10 ppm of CO in H₂ gas stream can cause a 50% decrease in the performance of H₂ fuel cells due to the close binding of CO to the catalyst active sites that eventually lowers the effective surface area for H₂ sorption and hampers the anodic oxidation process.⁹

LT-PEMFCs typically work in a maximum temperature range of 80–90 °C under *hydrous* conditions (95–98% RH). As evident from the preceding discussion, in general, at such low working temperatures, high amounts of CO are adsorbed on the surface of the Pt electrocatalyst that poison it. Since the adsorption process of CO on Pt catalysts is entropically negative, the adsorption is highly facile at lower temperatures and disfavored at higher temperatures. Thus, the CO tolerance of the Pt catalyst is enhanced at higher temperatures and the rate of catalyst poisoning is reduced. Moreover, a fuel cell operating with 40–50% efficiency at ~85 °C is associated with the production of huge amounts of heat (due to cathode-side oxygen reduction reaction) that need to be liberated from the system in order to maintain the lower working temperature. Thus, large heat radiators and exhaust systems are required for the operation to continue, specifically in automobile applications.¹³ In addition, for the operation of these LT-PEMFCs, an efficient water management system that can efficiently maintain the humidity (95–98% RH) throughout the entire duration of operation is a must that results in an overall increase in energy investments. *In fact, heat and water management systems are the two most critical technological aspects*

*of PEMFC systems.*¹⁴ Keeping a constant operating environment of 80–90 °C with 95–98% RH in PEM stacks (for commercial SSPCs such as Nafion in order to attain proton conductivity in the range of 10⁻¹ to 10⁻² S/cm) is energetically and technically quite exorbitant, thus impeding its widespread usage.¹⁴ These are the prime disadvantages of hydrous LT-PEMFCs. Thus, easing one of these two operating conditions (80–90 °C along with constant humidification at 95–98% RH)—for example, eliminating the water management system by using *anhydrous* proton-conducting membranes which require only the temperature to be maintained—could have a significant effect on the overall sustainability, usability, and economic viability of PEMFC systems.

In this direction, solid-state anhydrous proton conductors have gained significant attention, as a new sector of solid electrolytes that can operate mostly at temperatures >100 °C in the absence of humidity, for usage in high-temperature proton-exchange membrane fuel cells (HT-PEMFCs). Such anhydrous proton conductors enable the fuel cells to operate at slightly elevated temperatures (100–200 °C), offering several advantages such as improved catalytic activity with much reduced CO toxicity, low electro-osmotic drag coefficient, ease of heat management, reduced chance of water leakage, zero energy investment for humidification, and reduced technology costs.¹³ Especially, to address the problems of CO poisoning, the higher temperature anhydrous operation in HT-PEMFCs can be an excellent choice, since the extent of CO adsorption ($\Delta H = -ve$ and $\Delta S = +ve$) on the surface of the Pt catalyst is less at higher temperatures and the Gibbs free energy for CO adsorption continues to become less negative with increasing temperature, which eventually results in less probable adsorption of CO on the anode surface.¹¹ Moreover, the high temperature contributes toward accelerating the kinetics of proton carriers, which notably enhances proton conductivity values. In addition, under anhydrous conditions the water management system becomes irrelevant since the process does not need any additional humidification (in contrast to hydrous conductivity where both H₂ and O₂ fuels need to be humidified), thus reducing the burden of technological and overall energy investments. All of this favors a switch to anhydrous fuel cell technology which is environmentally as well as economically highly sustainable and is perfect for extensive utilization in the field of the automotive applications.

Apart from the high-temperature anhydrous conductivities mentioned above, anhydrous proton conductivity at sub-zero temperature is also highly desirable for the start-up of PEMFCs in sub-ambient environment/colder climates and high-altitude drones.¹⁵ Similar to the former case, at sub-zero conditions the commercially available Nafion suffers from a significant drop in its conductive performances (especially at temperatures below 0 °C) due to the highly hampered proton-transfer pathways (multiple ice blockages in the cathode chambers under freezing conditions) that lead to severe power loss. This urges exploration of some alternative options as PEM materials that could meet the requirements of sub-ambient anhydrous proton conductivity while maintaining the materials' stability under the stated conditions. Anhydrous proton conduction at or near room temperature is also desirable since constant maintenance of high-humidity conditions during the fuel cell operation requires an efficient water management system that is often a huge technical barrier (especially in the context of automotive applications) and serves as one of the bottlenecks, besides temperature management systems, in the operation of

PEMFCs. Operation of fuel cells under anhydrous conditions at or near room temperature would require neither humidity nor temperature control and thus could eliminate the burden of these two technological barriers to facilitate the start-up of fuel cells without much energy investment.

As mentioned earlier, Nafions are industrially used as PEM materials in LT-PEMFCs under hydrous conditions, in a constant operating environment of 80–90 °C with 95–98% RH in PEM fuel cell stacks, maintaining a steady proton conductivity in the range of 10^{-1} – 10^{-2} S/cm. However, a significant drop in conductivity beyond 100 °C limits their applicability as SSPCs in HT-PEMFCs. Overall, commercial Nafion and its family are *not* potent in the dehydrated state and under high-temperature operational conditions (>100 °C) because smooth proton transfer greatly depends on the supply of external water molecules in order to maintain the extended H-bonding pattern. At such temperatures, water molecules evaporate rapidly, thus resulting in disruption of the proton conduction pathway which in turn could cause a massive reduction in proton conductivity.

In this regard, researchers initiated the search for alternative PEMs, the performance of which could be effectively sustained under anhydrous conditions, and began to work on certain inexpensive and scalable amorphous polymers. In such polymeric systems the proton conduction does not necessarily depend on the aqueous medium; instead, water is replaced by other nonvolatile, high-boiling proton carriers such as phosphoric acid/sulfuric acid or aromatic N-rich heterocycles doped with those amorphous polymeric materials. In the mid-1980s and 1990s, some complexes of basic polymers doped with phosphoric acid, such as PBI/ H_3PO_4 , PEO/ H_3PO_4 ,^a PEI/ H_3PO_4 ,^b PEI/ H_3PO_4 ,^c PEI/ H_3PO_4 ,^d PEI/ H_3PO_4 ,^e Nylon/ H_3PO_4 , PAAM/ H_3PO_4 , PVP/ H_3PO_4 , PEO/PMMA/ H_3PO_4 , etc., were discovered as a new class of solid-state anhydrous proton conductors.¹⁶ However, they suffered from fundamental drawbacks such as poor chemical stability, low thermomechanical stability, excess doping of inorganic acids responsible for leaching, etc. Most of these acid-blended polymers typically showed a conductivity in the range of 10^{-3} – 10^{-6} S/cm below 100 °C (mostly in anhydrous conditions); however, a few of them could reach conductivity in the ultrahigh region (10^{-2}) in the temperature range of 165–175 °C (under hydrous conditions).¹⁶ In fact, most of these polymeric materials possess either amide functionalities or ether linkages in their molecular backbones that often tend to get hydrolyzed at higher temperatures in the presence of blended acids (H_3PO_4), which worsens their chemical as well as mechanical stability beyond 100 °C. From a practical viewpoint, anhydrous fuel cells need to operate above 100 °C (for the reasons highlighted earlier), and thus, such polymeric blends may not serve the purpose of anhydrous proton conductors and are inappropriate as SSPCs in HT-PEMFCs. However, amorphous polymers which lack such ether/amide functionalities (e.g., polybenzimidazole (PBI)-based polymers) have been noted to exhibit anhydrous conductivity performance beyond 100 °C.¹⁶ On the other hand, only a few crystalline phosphates and phosphonates of tetravalent metals like Zr(IV) have been tested as anhydrous proton conductors in the range of 10^{-5} – 10^{-8} S/cm, and thus, there is not much promise in this direction. Interested readers are referred to the book by Colombari.⁴ One might ask if some other popular materials like porous zeolites or silica (which have already made their ways to industry for certain applications) could be used as anhydrous

proton conductors. It should be noted that crystalline zeolites were mostly studied as proton conductors in the presence of adsorbed water (i.e., in the hydrous state) or ammonia and had conductivities in the range of 10^{-6} – 10^{-4} S/cm, while anhydrous proton conductivity could hardly be achieved with such systems.⁴ The same is true for amorphous mesoporous silica-type materials which usually show superprotonic conductivity in the hydrous state. Similarly, inorganic polymers, glasses, clays, and gels are mostly studied as proton conductors in their hydrated states.⁴

Crystalline platforms such as metal–organic frameworks (MOFs),^{6,14,17–41} covalent organic frameworks (COFs),^{5,42–45} hydrogen-bonded organic frameworks (HOFs),^{46–52} and polyoxometalates (POMs)^{53–56} serve as excellent choices for alternative SSPCs on account of their distinguished structural features such as high surface area, diversified structural topologies, scope of diverse functionalization, etc. Such highly crystalline frameworks (MOFs/COFs/HOFs/POMs) allow the pre-installation of functionalities to facilitate proton hopping in order to attain high proton conductivities in these materials *under both hydrous and anhydrous conditions*. The crystalline nature of these materials affords straightforward visualization of the plausible H-bonded conduction route by virtue of X-ray analysis, which helps in analyzing the structure–property relationship to expedite further development in this field. Their well-defined molecular arrangements allow detailed investigations on the H-bonded patterns, acidities of proton donor/acceptors, dynamic properties and prediction of proton conduction mechanisms that together help in the understanding and tuning of the proton conduction mechanism through molecular-level structure–function correlations.

MOFs are an innovative class of crystalline porous materials composed of metal ions/nodes/clusters coordinated by organic linkers, and have received a lot of attention due to their fascinating structural features like high surface area, structural tunability, infinite scope of framework functionalization, postsynthetic modification/guest incorporation, and topological versatility.^{57,58} Inspired by such intriguing structural properties, researchers have employed them in a wide spectrum of applications such as gas storage/separation,^{59–61} proton conduction in PEMs,^{6,17–41} chemical sensing,^{62–64} catalysis,^{65–69} energy applications,⁷⁰ etc. The proton conduction properties of solid-state crystalline materials (MOFs/coordination polymers (CPs)) were first reported by Kanda and co-workers in 1979; however, the poor stability of such materials hindered a detailed analysis of their conduction mechanism.⁷¹ Later the field of proton conduction with MOFs/CPs was pioneered by H. Kitagawa, S. Kitagawa, and G. Shimizu, although these materials were noted to exhibit conductivity only in the presence of high humidity (*hydrous conditions*) and in a temperature range of 60–80 °C, making them apt for operation in LT-PEMFCs.^{24–31,72–75} However, the domain of *anhydrous* proton conductivity with MOF/CP-based solid-state conductors remained completely unexplored until 2009, when Kitagawa and co-workers reported the very first example of crystalline anhydrous proton conductors based on the MIL-53 family of MOFs formed through rational encapsulation of nonvolatile, high-boiling, and amphoteric/amphiprotic heterocycles like imidazole molecules into its crystalline nanochannels, affording a unique assembly of guests to improve the proton transfer even in the absence of water.²⁸ This was followed by a series of reports on anhydrous MOF-

based proton conductors in which the nonvolatile proton carriers such as phosphates, high-boiling organic heterocycles, or counter-cations were either inherently embedded into the framework backbones or externally loaded into the micro-channels of the frameworks to achieve distinctive packing of proton carriers with high local/translational motion for improved proton transportation.^{29,72–75} Although research on sub-zero anhydrous conductivity in crystalline materials is still in its infancy, a couple of examples of MOF/CP-based materials have been reported in the literature where optimized structural engineering of the crystalline coordination networks allowed the materials to achieve substantial anhydrous conductivity over a range of low-temperature conditions (–10 to –40 °C) with complete structural retention, as will be discussed later in the respective sections.^{15,74}

COFs represent another crystalline platform that has recently attracted enormous attention due to their high surface area, porosity, scope of strategic functionalization, and high chemical and thermal robustness.^{5,42–45,77–84} However, unlike MOFs, they are built of lighter elements such as C, N, O, S, B, and H through stable covalent bonds that result in their low density and impart structural stability to these frameworks featuring unique molecular architectures. Similar to MOFs, these materials are also harnessed for diversified applications, including electrochemical sensing, electrical conductivity, photovoltaics, etc.^{77–84} COFs have shown great potential over the past few years as another solid-state crystalline proton conductor under both hydrous and anhydrous conditions, being benefitted by its excellent chemical as well as thermal stability.⁵ It is important to note that although reports on COF-based proton conductors have been increasing exponentially in the past four years, information on their applicability in anhydrous conditions is quite limited (only 15 examples), without any report on sub-zero anhydrous conductivity.

Apart from MOFs and COFs, recently HOFs have emerged as another class of crystalline materials that possess unique structural features such as pre-designability, ease of synthesis, processability, and moderate porosity along with framework tunability.^{46–52} Most importantly, these materials possess inherent intermolecular H-bonded networks that naturally hold promise in achieving high proton conductivity in hydrous environments, as reviewed recently by Das *et al.*⁴⁶ In 2009, proton conduction through HOF materials was first explored by Klapper, Müllen, and co-workers in the presence of 98% RH, although the crystal structure was not reported.⁸⁵ Thereafter a huge gap remained until 2016, when proton conductivity through HOF materials began to be explored heavily, adopting a variety of design strategies.^{46,86–89} However, in the sector of anhydrous conductivity, these crystalline materials are poorly explored, with reports limited to only six examples to date, urging further improvements in this domain. The unique assembly of hydrogen-bonded organic struts in HOF materials functionalized with several proton donor/acceptor moieties affords the incorporation of various nonvolatile proton carriers, such as imidazole, H₃PO₄, etc., within their channels that in turn aids the establishment of continuous H-bonded pathways to facilitate the smooth proton mobility associated with high proton conductivity, even in the absence of humidity (anhydrous conditions).

POMs are basically anionic metal-oxo clusters composed of Mo, W, V, etc. at their highest valence state, and they have emerged as potential crystalline proton conductors in the hydrous state owing to several exceptional features such as

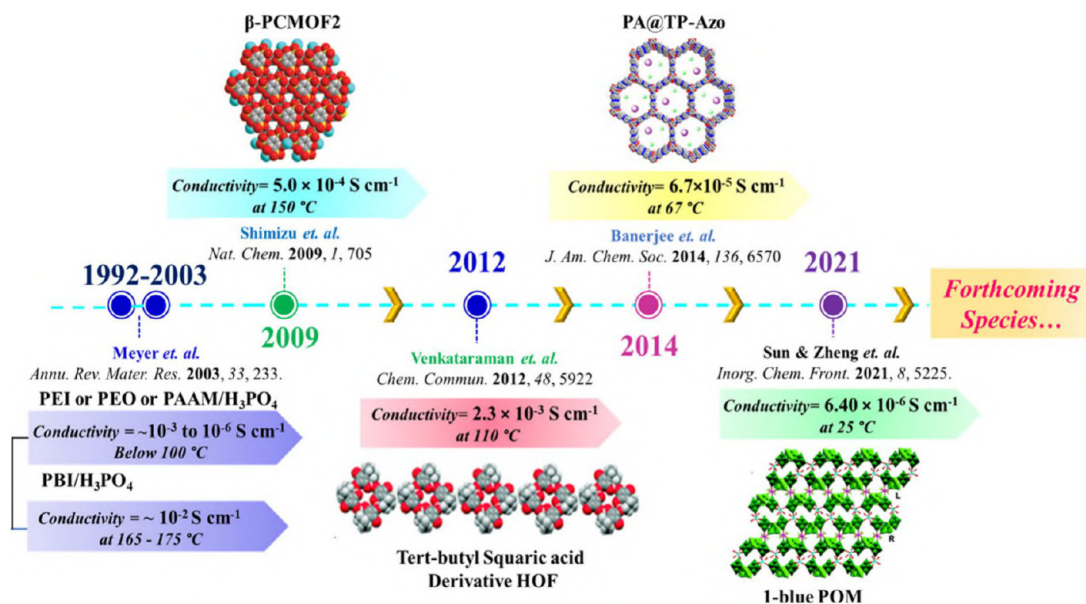
controllable structures, O-rich surface, high crystallinity, exceptional thermal stability, etc.⁵³ The pioneering work on POM-based proton conductors was initiated in 1979 by Nakamura and co-workers, who revealed the pivotal role of a large number of lattice water molecules in achieving super-protonic conductivity with such materials.⁹⁰ However, this in turn hindered the flourishing of POM-based materials in the domain of anhydrous proton conductivity due to the significant loss of active proton species in the form of crystallized lattice water molecules at elevated temperatures. Nevertheless, residual constitutional water molecules associated with the anhydrous heteropolyacids (HPAs: conjugated acids of POMs), even at high temperatures (~450 °C), could contribute significantly to the overall anhydrous proton conduction in such frameworks.⁵³ Most importantly, it is noted that the anhydrous conductivity of POMs is dependent on inherently embedded proton sources such as imidazole or isolated H⁺ that are capable of maintaining non-interrupted H-bonded matrices both under sub-ambient and above ambient conditions.

2. SCOPE OF WRITING ON ANHYDROUS PROTON CONDUCTION

The blossoming progress achieved in the design and development of crystalline SSPCs have undoubtedly grabbed immense attention from researchers in the past decades. Impressive conductivity to the order of 10^{–2} S/cm could be achieved with these crystalline framework materials, many of which could even exhibit conductivity to the order of 10^{–1} S/cm.^{6,39} Needless to say, in most cases the highest conductivity was obtained at high humidity, i.e., in the hydrous state (95–98% RH), coupled with temperatures in the range of 80–90 °C. However, achieving such high conductivity in an *anhydrous* environment, particularly in a higher temperature window (100–200 °C), would be of great interest from technical and commercial perspectives, since at such conditions the chance of CO poisoning is highly minimized and the use of additional humidifier becomes irrelevant, as discussed in the previous section, with multiple other advantages. A thorough literature survey reveals that a number of reviews have been published since 2020 (of course, a handful of reviews appeared before 2020 to establish a concrete foundation on proton-conducting MOFs,^{3,19,22,24,32,39,91–96} though no reviews appeared for HOFs, COFs, and POMs until the year 2020) highlighting the significance of such crystalline materials (MOFs/COFs/HOFs/POMs) in the domain of *hydrous* proton conduction dealing with the various aspects of their basic chemistries including designing principles, conducting media, switching behavior, proton sources, and so on.^{5,6,17,18,23,34,35,46,53} However, none of these reviews focused solely on *anhydrous* proton conduction within the domain of these crystalline platforms.

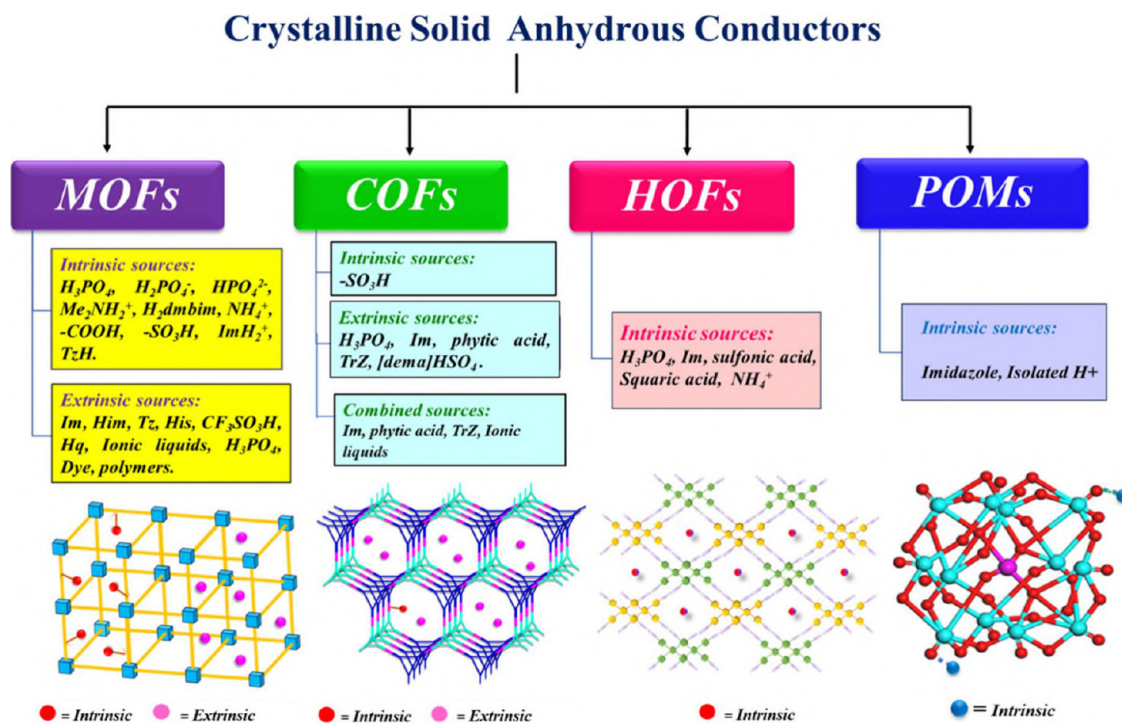
Thus, a critical perspective that specifically highlights the progress and evolution of solid-state crystalline materials (MOFs, COFs, HOFs, and POMs) in the realm of anhydrous proton conduction is still lacking in the literature and is highly demanded at the same time. In this regard, in 2021 Zhang and co-workers summarized some of their own works on anhydrous proton conductors (7 works on anhydrous conduction on MOFs), where they focused specifically on the ambient to sub-ambient temperature window for anhydrous conductivities and excluded the high-temperature zone.¹⁵ In another contribution, Zhang and Chen *et al.*

Scheme 1. Timeline Representing the Evolution of the Different Crystalline Platforms (MOFs, COFs, HOFs, and POMs) in the Domain of Anhydrous Proton Conduction^a



^aNote that amorphous blended polymers are tested as anhydrous proton conductors; however, in most cases, minimal humidity was introduced, and thus they may not be considered as strictly anhydrous conductors.

Scheme 2. Classification of Crystalline Materials as Anhydrous Protonic Conductors Based on Their Framework Backbones into Four Distinct Classes: MOFs, COFs, HOFs, and POMs



discussed 6 examples of anhydrous proton-conducting MOFs as a sub-section in their review article.¹⁷ This survey inspired us in the scope of writing this Perspective on anhydrous solid-state crystalline proton conductors.

In this Perspective, we have specifically categorized the solid crystalline anhydrous conducting materials into four classes based on their structural origin: MOFs, COFs, HOFs, and POMs, and detailed their evolutionary timelines starting from the work by Shimizu and Kitagawa et al. in 2009 (Scheme 1).

The strategies adopted for imparting high conductivity to these crystalline materials under anhydrous conditions are also discussed in detail with reference to suitable examples and corresponding Figures and Tables. Needless to say, the escalating number of reports on anhydrous conductivity attained with these materials, specifically in the past decade, essentially necessitates a Perspective article on this topic to underline and direct the rational designing strategies that could induce anhydrous proton hopping in different sectors of

crystalline materials to help in attaining ultrahigh anhydrous conductivity. Meanwhile, this Perspective aims to provide a critical analysis on the existing state of knowledge on anhydrous proton conductivity, with the challenges and prospects offered intricately (for example, instant CO tolerance testing and rapid potential assessment of these PEMs with fuel cell test stands) that will surely be appealing to the wider scientific community.

3. CRYSTALLINE SOLID-STATE MATERIALS AS ANHYDROUS PROTON CONDUCTORS

Inspired by the superior features of solid-state anhydrous proton conductors mentioned above, and synchronizing them with the beneficial features of their crystalline nature, we opted to investigate the success of solid-state crystalline proton conductors (with a huge scope of structure–conduction property relationship assessment) in the domain of anhydrous proton conductivity. Based on their molecular backbones (organic/inorganic/combination of organic and inorganic), secondary building blocks, and framework engineering; the crystalline anhydrous conductivity is divided into four prime categories as mentioned below.

1. Anhydrous Proton Conduction in Metal–Organic Frameworks (MOFs)
2. Anhydrous Proton Conduction in Covalent Organic Frameworks (COFs)
3. Anhydrous Proton Conduction in Hydrogen-Bonded Organic Frameworks (HOFs)
4. Anhydrous Proton Conduction in Polyoxometalates (POMs)

Depending upon the strategies undertaken for the facile immobilization of proton carriers onto the framework backbones, the anhydrous proton conductivities in these crystalline materials are classified as intrinsic, extrinsic, and combined (combined classification applicable only for COFs) anhydrous conductivities relating to the origin of the proton sources: whether they are inherently pre-existing or externally incorporated/loaded to improve the proton transfer (Scheme 2). Basically, the attainment of anhydrous proton conductivities in these crystalline platforms is based on two main pillars: (a) Maintaining H-bonded pathways intact to facilitate smooth proton transfer even in the absence of water molecules and (b) Stability of materials under experimental conditions (high-temperature thermal stability for HT-PEMFCs application; stability below 0 °C for conductivity measurements at sub-ambient temperature). Specifically, focusing on the first pillar, to sustain the continuity of H-bonded pathways under anhydrous conditions, the proton carriers need to be incorporated in these crystalline backbones either intrinsically (H_3PO_4 , H_2PO_4^- , HPO_4^{2-} , Me_2NH_2^+ , H_2dmbim , NH_4^+ , $-\text{COOH}$, $-\text{SO}_3\text{H}$, ImH_2^+ , TzH , sulfonic acid, squaric acid, or isolated H^+) or through an extrinsic loading approach (Im, Him, Tz, His, $\text{CF}_3\text{SO}_3\text{H}$, hydroquinone (Hq), dye, organic polymers, phytic acid, or ionic liquids such as EIMS-HTFSA, SA-EIMS), or via a combined approach (in certain cases only for COF materials). In the context of HOFs and POMs, only the intrinsic approach of proton carrier installation has been prevalent to date, leaving a huge scope for exploration on the extrinsic approach to anhydrous proton conduction. However, in MOFs and COFs, for which both approaches have been extensively explored, it is pointed out that in most cases the extrinsic strategy of proton carrier installation is associated

with low activation energies (<0.4 eV) that follows the Grotthuss-type mechanism for smooth proton hopping. Whereas the intrinsic strategy is associated with comparatively higher activation energies (>0.4 eV), indicating the vehicular mechanism of proton transfer. Despite this fact, the proton conductivity harnessed through both strategies does enter into the superprotonic zone, validating their effectivity in imparting anhydrous proton conductivities in these crystalline materials.

The mentioned regime of crystalline materials is tabulated later in Table 2 based on their structural backbones and approaches taken to install the proton species, along with their BET surface area, stability (chemical/thermal), conductivity performance, proton sources (carrier/guest molecules), temperatures at which anhydrous conductivity measurements are done, activation energy values, forms of materials used for conductivity measurement, and framework retention post measurement.

For anhydrous proton conductivity measurements, crystalline samples are typically powdered and compacted in the form of pressed pellets (with diameters ranging from 1 to 4 mm), whereas membranes that have been successfully fabricated (in some cases) must be cut into a small rectangular shape before AC impedance analysis. The AC impedance measurements are performed using a two-probe or four-probe method (preferred) with an impedance analyzer over a frequency range of 100 Hz to 10 MHz in general. To maintain the anhydrous ambience, the measurement chambers are usually flushed properly with dry N_2 gas prior to the conductivity measurements for eliminating the existence of even trace quantities of moisture. The Nyquist spectra thus obtained from the impedance measurements are fitted using specific software for estimating the resistance values. The proton conductivities (σ) are then evaluated using eq 1.

$$\sigma = \frac{L}{RS} \quad (1)$$

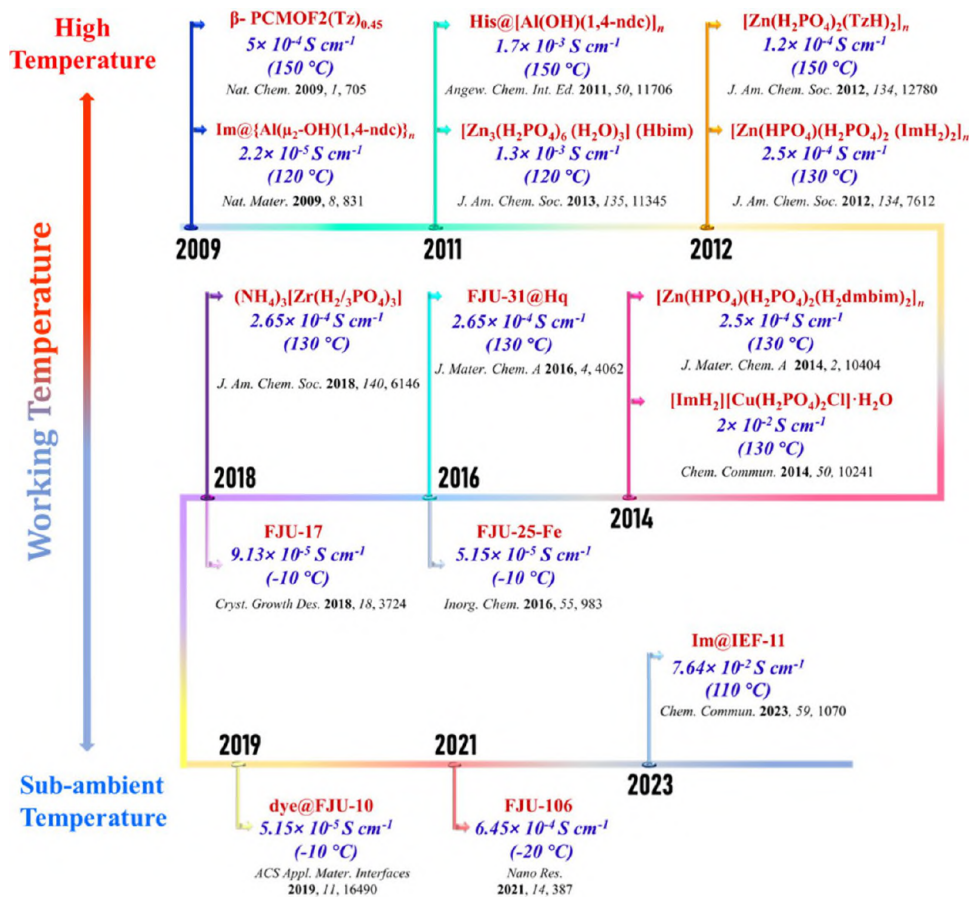
where L is the thickness of the sample pellet, S represents the cross-sectional area, and R denotes the measured impedance/resistance. Further, the activation energies (E_a) for the proton transport are deduced from the temperature-dependent conductivity measurements fitted to the Arrhenius plot by using eq 2.

$$\sigma T = A e^{-E_a/kT} \quad (2)$$

where T , A , and k are the temperature, pre-exponential factor, and Boltzmann constant, respectively.

3.1. Anhydrous Proton Conduction in Metal–Organic Frameworks (MOFs). Because of the broad spectrum of intriguing structural merits such as porosity, high surface area, structural tailorability, framework functionalization, adaptable guest loading in pore spaces, structure–function correlatability, and framework versatility, MOFs/CPs are extensively utilized as high-performance SSPCs in PEMFCs. Their conductivities are predominately noted to originate from the external water molecules through continuous H-bonding interactions among the water molecules that emerge from fuel cell operation under high-humidity conditions. However, under anhydrous conditions, the transport of active proton carriers and their mobility/molecular reorientation play the most significant roles in achieving high conductivity. Generally, nonvolatile heterocyclic organic molecules such as imidazoles, triazoles, tetrazoles, and benzimidazoles; high-boiling organic hydroxyls such as hydroquinone; nonvolatile amino acids such as

Scheme 3. Timeline Representing the Evolution of MOFs in the Field of Anhydrous Proton Conduction since 2009



histamines; and nonvolatile inorganic acids such as H₃PO₄ and H₂SO₄, with their conjugate anions, are used as proton carriers to achieve anhydrous proton conduction in MOFs/CPs. Herein, we provide a timeline (Scheme 3) that signifies the important events in the advancements of anhydrous proton conductivities in MOFs/CPs for a visualization by readers at a glance.

In the current Perspective, the approaches for designing anhydrous proton-conducting MOFs/CPs have been primarily categorized into two distinct classes based on the origin or immobilization of proton sources/carriers: either (1) through pre-installation of the proton donor/acceptor species such as imidazole/imidazolium, triazole/triazolium, benzimidazoles, ammonium ions; high-boiling organic hydroxyls such as hydroquinone; nonvolatile amino acids such as histamines; or nonvolatile inorganic acids such as H₃PO₄ and H₂SO₄, with their conjugate anions H₂PO₄⁻/HPO₄²⁻, etc. on the framework backbones through metal coordination or as counterions for charge compensation via direct synthesis (known as *intrinsic sources*) for modulating the H-bonded pathways to achieve **intrinsic anhydrous conductivity in MOFs** or (2) through extrinsic incorporation/encapsulation of several nonvolatile guest proton carriers into the nanochannels of these microporous frameworks through *ex situ* loading synthesis procedures (known as *extrinsic sources*) to secure free translational/rotation motion of the proton carriers for attainment of superprotonic **extrinsic anhydrous conductivity in MOFs** (Figure 1). It is to be noted that H₃PO₄, imidazole, triazole, and benzimidazole could serve both as intrinsic and extrinsic proton carriers, depending upon the way they are

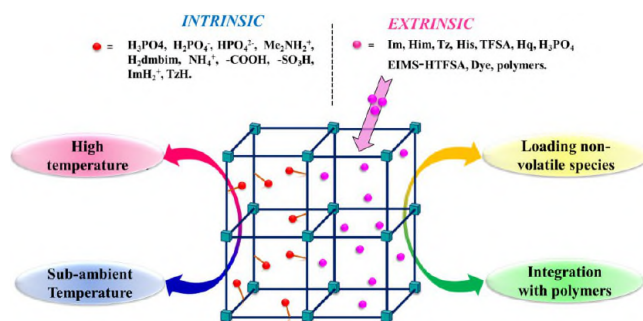


Figure 1. Illustration for the incorporation of intrinsic and extrinsic proton carriers in the backbone of MOFs/CPs to attain anhydrous proton conductivity and their classifications based on working conditions and proton carrier loading/integration.

installed into the framework (*in situ* and *ex situ*, respectively). A critical review of these categories, along with their significance in the context of the materials' application as real-time SSPCs in PEMFCs, is provided below.

3.1.1. Intrinsic Anhydrous Conductivity in MOFs. As mentioned earlier, the strategic inherent installation of proton carrier functionalities such as N-rich heterocycles (like imidazoles, triazoles, tetrazoles, benzimidazoles, histamines, etc.), phosphates (like H₃PO₄, H₂PO₄⁻, HPO₄²⁻), or dimethylammonium (Me₂NH₂⁺), NH₄⁺, formamidinium cations as charge-balancing agents into the backbones of MOFs/CPs (through *in situ* or straightforward synthesis) that ensures smooth transfer of protons even in the absence of water to achieve stable and efficient anhydrous proton conductivity

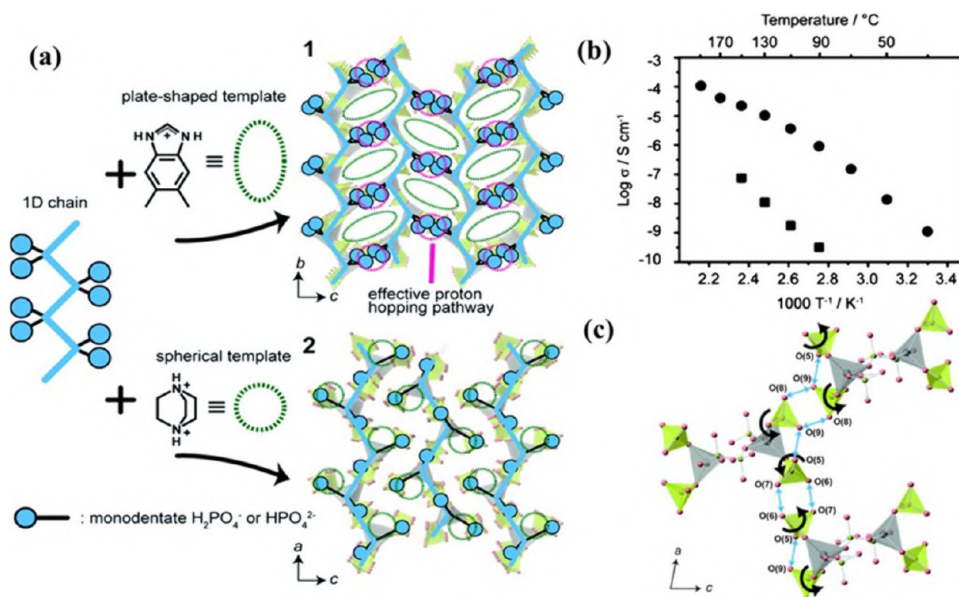


Figure 2. (a) Illustration of template effects on the crystal structure and proton conduction pathways in **1** and **2**. (b) Arrhenius plot for anhydrous proton conduction in **1** (denoted by solid circles, temperature range 30–190 °C) and **2** (denoted by solid squares, temperature range 90–150 °C). (c) Proton-hopping pathway by virtue of rotation in monodentate H₂PO₄⁻ and HPO₄²⁻ in **1**. Reproduced with permission from ref 74. Copyright 2014, Royal Society of Chemistry.

defines this class (Figure 1). Basically, for attaining intrinsic proton-conductive carrier concentration, acidity and structural features play the pivotal roles. Although each of these factors has a significant influence, structural optimization is the dominant one that regulates the distance, dynamics, mobility, and cooperativity for continuous proton hopping. In the context of such structural optimization, factors such as variation of the metal ions (for tailoring the pore aperture), template-aided alignment control (for increasing hopping sites), framework interpenetration (channel size tuning), structural phase transitions, strategic pore engineering (to facilitate the motional entropy of carriers), postsynthetic modifications, etc. also influence the establishment of continuous H-bonded matrices for smooth transfer of protons via the active carrier species mentioned above under anhydrous conditions at various working temperatures. Considering the large number of examples of MOFs/CPs that exhibit intrinsic anhydrous conductivity at higher temperature conditions and also at sub-zero temperatures, here we have sub-categorized these MOFs/CPs with intrinsic proton sources based on their operating temperature and discussed the examples under the following sub-classes: (a) **high-temperature intrinsic anhydrous conductivity** (with working window 100 °C or beyond) and (b) **sub-ambient temperature intrinsic anhydrous conductivity** (with working window under sub-zero conditions).

3.1.1.1. High-Temperature Intrinsic Anhydrous Conductivity in MOFs. Taking advantage of the superior anhydrous proton-transfer ability of 1,2,4-triazole (Tz) compared to imidazole,⁹⁷ in 2009 Shimizu and co-workers reported a crystalline porous sulfonated coordination network, β -PCMOF2 (Na₃(2,4,6-trihydroxy-1,3,5-benzenetrisulfonate)), possessing one-dimensional channels that could be loaded with N-rich heterocycles via *in situ* synthesis to exhibit anhydrous proton conduction at 150 °C.⁷² The hexagonal pore channels in β -PCMOF2 are quite large (diameter ~5.65 Å) and are beautifully decorated with oxygen atoms of sulfonate moieties that can form effective hydrogen-bonding

matrices with guest species to improve the proton transfer. Initially, the proton conduction property of the parent framework β -PCMOF2(H₂O)_{0.5} with per-sulfonated pore walls was investigated, which revealed that a conductivity of 5.0×10^{-6} S/cm could be achieved at 30 °C; however, the conductivity was noted to fall drastically with temperature increment (<70 °C) to the range of 10⁻⁸ S/cm, a phenomenon typically observed for sulfonated polymers. To resolve this issue and achieve anhydrous superprotonic conductivity, the guest water in the framework was replaced by superior nonvolatile anhydrous proton-transferring agents like Tz. The guest triazole species were loaded intrinsically into the pore structure of MOF via a straightforward *in situ* direct synthesis procedure (that is why this is categorized as an intrinsic approach) that in turn yielded β -PCMOF2(Tz)_x (where *x* represents different loadings: *x* = 0.3, 0.45, 0.6). AC impedance analysis with the guest-loaded samples revealed an improved conductivity beyond 100 °C when compared to the unloaded hydrated framework. Ultimately, at 150 °C, the intrinsically triazole-incorporated framework achieved the maximal conductivity of 5.0×10^{-4} S/cm with an optimum stoichiometric loading of *x* = 0.45. Further, in order to understand the mechanism of anhydrous proton conduction in β -PCMOF2-(Tz)_{0.45}, the activation energy was calculated to be 1.8 eV at the lower temperature range, 50–90 °C, and 0.56 eV at higher temperature range, 80–150 °C, which could be correlated well with the enhancement in proton mobility at higher temperatures. However, as the MOF material contains sodium ions as charge-balancing units, the overall conductivity could have some ionic contribution from this species as well, which needs to be analyzed further.

With an aim to install multiple anhydrous proton-conducting species onto a single crystalline platform, in 2012 Kitagawa and co-workers reported the intrinsic proton conduction in a Zn²⁺-based coordination polymer, {[Zn-(H₂PO₄)₂(TzH)₂]_n}, with coordinated orthophosphates and triazole units that displayed conductivity >10⁻⁴ S/cm at 150

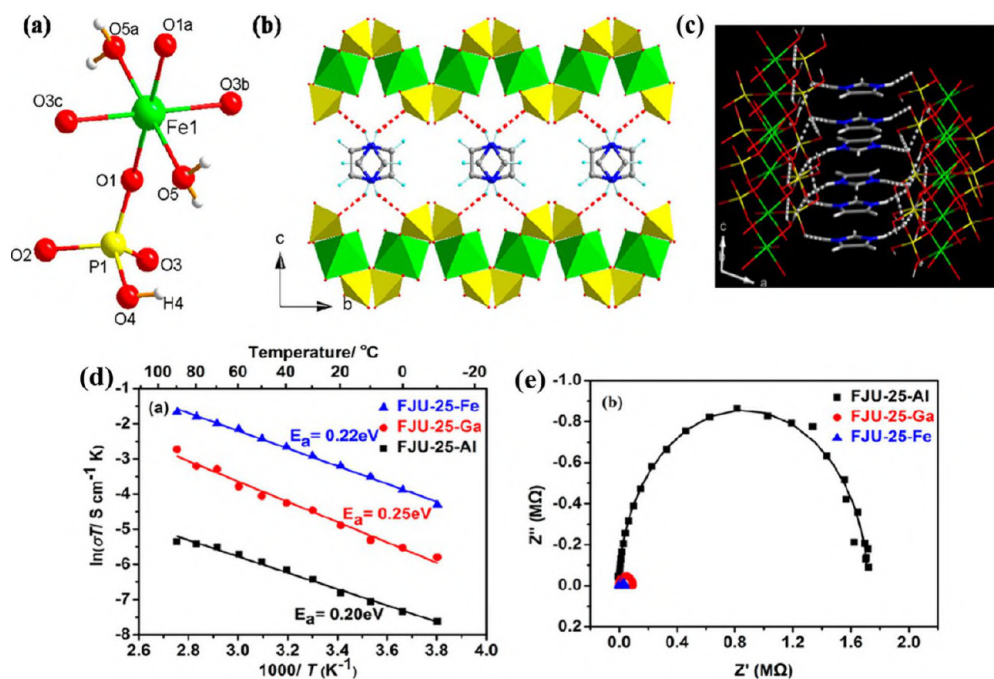


Figure 3. (a) Asymmetric unit of FJU-25-Fe. (b) View across the crystallographic *a*-axis with the H-bonding mediated through templated imidazole cations. (c) Proton conduction mechanism in FJU-25-Fe. (d) Arrhenius plot for anhydrous conductivity in the temperature range from -10 to 90 °C. (e) Nyquist plots of three frameworks at 90 °C. Reproduced with permission from ref 98. Copyright 2016, American Chemical Society.

°C under anhydrous conditions without any additional guest support.⁷³ The framework contained 2D sheets stacked across the crystallographic *c*-axis composed of Zn^{2+} metal nodes bridged via a triazole ligand (TzH) and axially monocoordinated with orthophosphate that participates in the *intra*- as well as *interlayer* H-bonding. Moreover, the triazole ligand also possesses acidic protons which additionally form interlayer H-bonding across the crystallographic *ab* plane. Although the framework contained a high density of proton carriers in the interlayer space, the optimal interval of acidic protons emerging from the appropriate positioning of coordinated phosphates accounted for the facile proton transfer. Additionally, the bridging TzH ligands afforded the ideal positioning of phosphates to make all the acidic protons H-bonded, to facilitate smooth proton transfer to achieve superprotonic conductivity of 1.2×10^{-4} S/cm at 150 °C under anhydrous conditions. An activation energy of 0.60 eV indicated vehicular hopping of protons over long ranges. Moreover, to validate the intrinsic nature of the conductivity, impedance tests on a single crystal showed an in-plane conductivity of 1.1×10^{-4} S/cm, whereas the out-of-plane conductivity value was noted to be 2.9×10^{-6} S/cm. This affirmed the anisotropic proton diffusion and proved the intrinsic origin of the proton conductivity.

Besides installation of multiple proton carriers of high melting and boiling points onto the crystalline platforms as discussed in previous examples, one should pay attention to the thermal stability of the host framework as well, which is a critical issue for their implementation as proton conductors in anhydrous HT-PEMFCs. Along this line, Kitagawa and co-workers proposed a template-directed strategy to create proton-conductive dynamic hydrogen-bonded pathways in the coordination frameworks under anhydrous conditions with varying thermal stability.⁷⁴ Two zinc-based coordination networks, namely, $[\text{Zn}(\text{H}_2\text{PO}_4)_2(\text{HPO}_4)] \cdot (\text{H}_2\text{dmbim})_2$ (**1**)

and $[\text{Zn}(\text{H}_2\text{PO}_4)_2(\text{HPO}_4)] \cdot \text{H}_2\text{dabco}$ (**2**), were synthesized that possessed one-dimensional anionic coordination chains composed of Zn^{2+} and phosphate units with the cationic templates H_2dmbim^+ (protonated 5,6-dimethylbenzimidazole) and $\text{H}_2\text{dabco}^{2+}$ (diprotonated 1,4-diazabicyclo[2.2.2]octane) as charge balancing agent for **1** and **2**, respectively (Figure 2a). The mutual π - π stacking among the close-packed plate-shaped H_2dmbim^+ units in **1** induces thermal stabilization up to 190 °C, whereas the lack of any such type of interactions among the spherically shaped $\text{H}_2\text{dabco}^{2+}$ units in **2** causes it to be unstable beyond 160 °C. Thus, the anhydrous conductivity of **1** was measured at 190 °C; it exhibited superprotonic conductivity of 2×10^{-4} S/cm with an activation energy of 0.66 eV (Figure 2b) that remained constant for over 3 h. In contrast, **2** exhibited much lower conductivity (8×10^{-8} S/cm) at 160 °C with its activation energy being as high as 1.2 eV. Such a difference could be primarily ascribed to the different cationic templates used in **1** and **2** that significantly controlled and directed the alignment of the H-bonded networks. The assembly of H_2dmbim^+ cations in **1** commands the alignment of 1D zinc phosphate chains (with rotatable and H-bonded monodentate phosphates) by bridging the adjacent frameworks to facilitate smooth and effective proton hopping across the crystallographic *a*-axis (Figure 2c). However, in the case of **2**, the shape and size of the cationic template forces the assembly on 1D chains in an interdigitated manner containing isolated monodentate phosphates that lack H-bonding interactions, thereby resulting in poor conductive performance.

3.1.1.2. Sub-ambient Temperature Intrinsic Anhydrous Conductivity in MOFs. To achieve anhydrous proton conductivity under sub-zero temperatures for fuel cell start-up under freezing conditions, specifically in the cold countries, MOFs/CPs possessing inherent proton carriers with enhanced motional entropy could be an excellent choice. To execute this, in 2016 Xiang and co-workers reported three isostructural

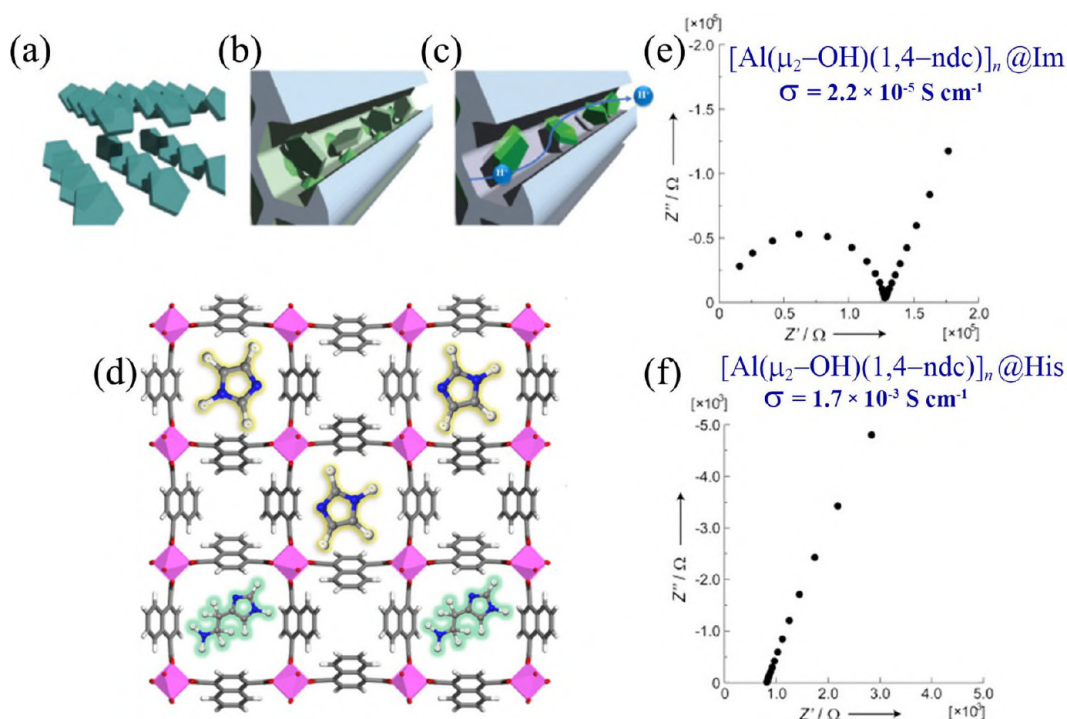


Figure 4. (a) Packing of imidazole molecules in their bulk solid state. (b) Imidazole molecules accommodated in the nanochannels of **2** (**2@Im**) through strong host-guest interactions that deter their mobility. (c) Imidazole molecules accommodated in the nanochannels of **1** (**1@Im**) without strong interactions, allowing for faster mobility. Reproduced with permission from ref 28. Copyright 2009, Nature Publishing Group. (d) Structural encapsulation of $[\text{Al}(\mu_2\text{-OH})(1,4\text{-ndc})]_n$ (**1**) with imidazole and histamine. (e) Nyquist plots for **1@Im**. (f) Nyquist plots for **1@His**. Reproduced with permission from ref 29. Copyright 2011, WileyVCH.

metal-phosphate-based CPs, **FJU-25-X** ($[\text{ImH}_2][\text{X}(\text{HPO}_4)_2(\text{H}_2\text{O})_2]$, $\text{X} = \text{Al}/\text{Ga}/\text{Fe}$), templated with imidazole cations (ImH_2^+), through rational tuning of the metal nodes based on their size.⁹⁸ The frameworks contained corrugated anionic layers of metal phosphates built from alternating layers of XO_6 octahedra ($\text{X} = \text{metal ions}$) and PO_4 tetrahedra with charge-balancing imidazole cations occupying the interlayer spaces (Figure 3a, b). These protonated imidazolium cations are in turn involved in the formation of multiple hydrogen bonds with the orthophosphate moieties that give rise to an intrinsic smooth array of H-bonded matrices appropriate for facile proton transfer (Figure 3c). Thus, proton conductivity was measured under anhydrous conditions in a wide temperature range from -10 to $+90$ °C through AC impedance analysis. Interestingly, it was noted that at -10 °C, the intrinsic proton conductivity of **FJU-25-Fe** was the highest (5.15×10^{-5}), followed by **FJU-25-Ga** (1.16×10^{-5}) and **FJU-25-Al** (1.88×10^{-5}), and at 90 °C under anhydrous conditions, **FJU-25-Fe/Ga/Al** exhibited superprotonic conductivities of 5.21×10^{-4} , 1.80×10^{-4} , and 1.30×10^{-4} S/cm, respectively. The higher conductivity of **FJU-25-Fe** as compared to its analogous counterparts could be nicely correlated with the size of the metal nodes that regulate the density of packing of imidazolium cations (ImH_2^+) per unit cell and thus eventually control the free dynamic motion of these carriers for their facile transfer in attaining high anhydrous conductivities. The activation energies were calculated to be 0.22, 0.25, and 0.20 eV for **FJU-25-Fe/Ga/Al**, nicely attributable to the Grotthuss mechanism of proton conduction, signifying smooth proton hopping (Figure 3d,e).

While protonated imidazole and monohydrogen phosphate were assimilated into the MOF structures (discussed above) to

impart anhydrous proton conductivity, dimethylammonium cations could serve the same purpose as demonstrated in two anionic In(III)-based MOFs, namely **FJU-16** ($[(\text{CH}_3)_2\text{NH}_2][\text{In}(\text{L})] \cdot 2.5\text{DMF} \cdot 2\text{H}_2\text{O}$) and **FJU-17** ($[(\text{CH}_3)_2\text{NH}_2][\text{In}(\text{L})] \cdot 4.5\text{DMF} \cdot 16\text{H}_2\text{O}$), with different degrees of interpenetration and containing the dimethylammonium cations in the pore spaces as protonic species.⁹⁹ Although both **FJU-16** and **FJU-17** possess similar net structures, the former contains 4-fold interpenetrations with reduced pore sizes ($8.35 \text{ \AA} \times 11.09 \text{ \AA}$, across a -axis) and smaller solvent-accessible void volume (36.45%), whereas the latter contains 2-fold interpenetrations with comparatively larger pore channels ($20.02 \text{ \AA} \times 25.92 \text{ \AA}$ across the c -axis) and a solvent-accessible void volume (73.8%) responsible for the accumulation of higher numbers of counter-cationic $(\text{Me}_2\text{NH}_2)^+$ protonic guests in the square-shaped channels. AC impedance measurements were performed over a broad temperature window (-40 to 100 °C) under anhydrous conditions. Both frameworks exhibited reasonably high intrinsic conductivity at temperatures as low as -40 °C under anhydrous conditions, with values of 2.90×10^{-6} and 9.13×10^{-5} S/cm for **FJU-16** and **FJU-17**, respectively. The highest conductivity achieved by **FJU-16** was 1.25×10^{-3} S/cm at 80 °C, whereas **FJU-17** exhibited an ultrahigh superprotonic conductivity of 1.08×10^{-2} S/cm at 100 °C, both under anhydrous conditions. Activation energies of 0.38 and 0.29 eV were calculated for **FJU-16** and **FJU-17**, respectively, which are indicative of the Grotthuss mechanism of continuous proton hopping. The enhanced intrinsic conductivity and lower activation energy achieved with **FJU-17** (2-fold interpenetrated) compared to **FJU-16** (4-fold interpenetrated) could be ascribed to the larger available spaces with abundant confinement of proton carriers

(Me_2NH_2^+) in the former case, which imparts the potential for faster migration of protons in achieving ultrahigh superprotonic conductivity under anhydrous conditions. Thus, the work highlights that controlling the interpenetration degree could be highly effective to tune the anhydrous proton conductivities of the frameworks.

3.1.2. Extrinsic Anhydrous Conductivity in MOFs. As discussed above, the pre-installation of proton donor/acceptor moieties appended to framework backbones is undoubtedly an excellent strategy to achieve anhydrous conductivity. However, this sort of framework designing is quite unpredictable and is associated with complications in the synthetic procedures of ligands. In this regard, frameworks with nonvolatile guest molecules extrinsically loaded (such as inorganic acids: H_3PO_4 and H_2SO_4 ; aromatic heterocycles: imidazoles, triazoles, and tetrazoles; organic hydroxyls; etc.) into the porous channels of MOFs/CPs have essentially exhibited high conductive performance, as evident from Table 2. In fact, the incorporation of these proton carrier molecules into the nanochannels imparted their unique assemblage through preferential interactions with host frameworks that enhances their rotational or translation local motions and improves the proton-transfer kinetics. Moreover, these channels afford the desirable working space for free movement of the carriers with high mobility and appropriate packing to achieve improved conductivity at high temperatures. Besides, in certain cases, proton-conductive polymers such as sulfonated polyether ether ketone (SPEEK), poly(vinylphosphonic acid) (PVPA), polybenzimidazole (PBI), etc. are integrated with the MOF materials, which helps in the establishment of continuous hydrogen-bonded pathways and triggers smooth proton transportation for improved conductivity under anhydrous conditions.⁹⁴ Hence, the extrinsic anhydrous conductivity is sub-categorized into two classes: (a) extrinsic loading of nonvolatile species in MOFs and (b) extrinsic integration with proton-conducting polymers in MOFs.

3.1.2.1. Extrinsic Loading of Nonvolatile Species in MOFs. This particular class encompasses the external incorporation/loading of nonvolatile species such as inorganic acids (like H_3PO_4), N-rich aromatic heterocycles (like triazoles, tetrazoles, benzimidazoles and histamines), or organic molecules (like cyclohexanol, butanol, hydroquinone, etc.) that can participate and aid proton diffusion even in the absence of water to achieve anhydrous conductivity. Employing this strategy, in 2009 Kitagawa and co-workers first proposed the approach of guest encapsulation in porous aluminum coordination polymers (PCPs), where the nonvolatile proton carrier imidazole molecules were externally incorporated into the framework nanochannels through tuned host–guest interactions to achieve anhydrous conductivity at 100 °C or beyond. In this regard, two analogous porous frameworks, $[\text{Al}(\mu_2\text{-OH})(1,4\text{-ndc})]_n$ (**1**) and $[\text{Al}(\mu_2\text{-OH})(1,4\text{-bdc})]_n$ (**2**), with similar pore size (~ 8 Å) but different pore shapes and surface potentials, were synthesized.²⁸ When the guest imidazole molecules were installed extrinsically into these frameworks, they suffered unique types of packing/assembly potentiated through the nanochannel surface of these PCPs (Figure 4a–d). Under anhydrous conditions, **1@Im** exhibited a proton conductivity of 2.2×10^{-5} S/cm (Figure 4e) achieved at 120 °C, whereas the second framework **2@Im**, despite containing a higher loading of imidazole units, exhibited a much lower proton conductivity value (1.0×10^{-7} S/cm) with a comparatively larger activation energy (0.9 eV) relative to

1@Im (0.6 eV). The higher conductivity of **1@Im** (2 orders of magnitude higher conductivity) as compared to **2@Im** could be correlated to the difference in dynamic motion of imidazole units in the pore channels based on varying host–guest interactions. The nanochannels of **1** (Figure 4d) exhibited steric hindrance on account of the bulky naphthalene rings (lining the pore spaces) that deterred interactions among the hydrophilic $\mu_2\text{-OH}$ /carboxylate moieties of **1** with the polar guest imidazole molecules and allowed the proton carrier imidazole molecules to move freely in the pore channels, resulting in the higher anhydrous proton conductivity of **1@Im** molecules. In contrast, the absence of such bulky hydrophobic moieties in **2** prompted the surface-exposed hydrophilic polar sites ($\mu_2\text{-OH}$ /carboxylate) to interact strongly with the polar imidazole guest molecules, resulting in framework shrinkage, decelerating the mobility of imidazole molecules (hindering their free translational/rotational movement), and leading to poor proton conductive performance in **2@Im**. Thus, the work highlighted the significance of fine-tuning of the pore spaces in the PCPs to house appropriate pore environments to provide optimum mobility to the encapsulated guest molecules in order to achieve superior proton conductivities. After that publication appeared in 2009, a series of other reports based on extrinsic loading of nonvolatile carriers for achieving high-temperature anhydrous conductivity were subsequently published.

As a continuation of the work discussed above on guest encapsulation in PCPs, the same group in 2011 again fabricated another composite with compound **1** as a porous support, while the optimized nanochannels being extrinsically encapsulated by the nonvolatile histamine molecules as proton carriers to generate **1@His**.²⁹ The anhydrous proton conductivity of **1@His** was noted to increase linearly from 3.0×10^{-5} S/cm at room temperature to 1.7×10^{-3} S/cm at 150 °C (Figure 4f). Strikingly, at 150 °C the proton conductivity of **1@His** was almost 100 times that of **1@Im** at 120 °C. While investigating the large differences in the conductivity performances of **1@His** than **1@Im**, it was noted that the proton carrier concentrations, structural packing and conformations of proton carriers in the pore channels, and intermolecular H-bonding among the amine groups and imidazole rings in histamines were responsible for the increased anhydrous proton conductivity of **1@His** compared to **1@Im**. Moreover, the proton transportation in **1@His** occurred with an activation energy of 0.25 eV (remarkably lower than the 0.6 eV for **1@Im**), signifying a Grotthuss mechanism of proton hopping that allowed for the intramolecular proton transfer due to molecular reorientation in histamine, unlike that of imidazole molecules. Thus, the work highlights the replacement of imidazole units with histamine proton carriers as a beneficial tool to attain high anhydrous proton conductivity in MOFs with lower activation energy, inciting further research in this domain through extrinsic encapsulation of other nonvolatile amino acids in the MOF channels. However, pre-functionalization of the framework backbones with histamine moieties (intrinsic pre-installation of histamines) could be an interesting strategy since in that case concerns about leaching stemming from external loading would be totally eliminated.

Besides nonvolatile N-rich heterocycles, high-boiling organic hydroxyls such as hydroquinone (Hq), cyclohexanol (Ch), and butanol (Bu) possesses excellent potential for proton donation as well as acceptance and could also serve as efficient proton

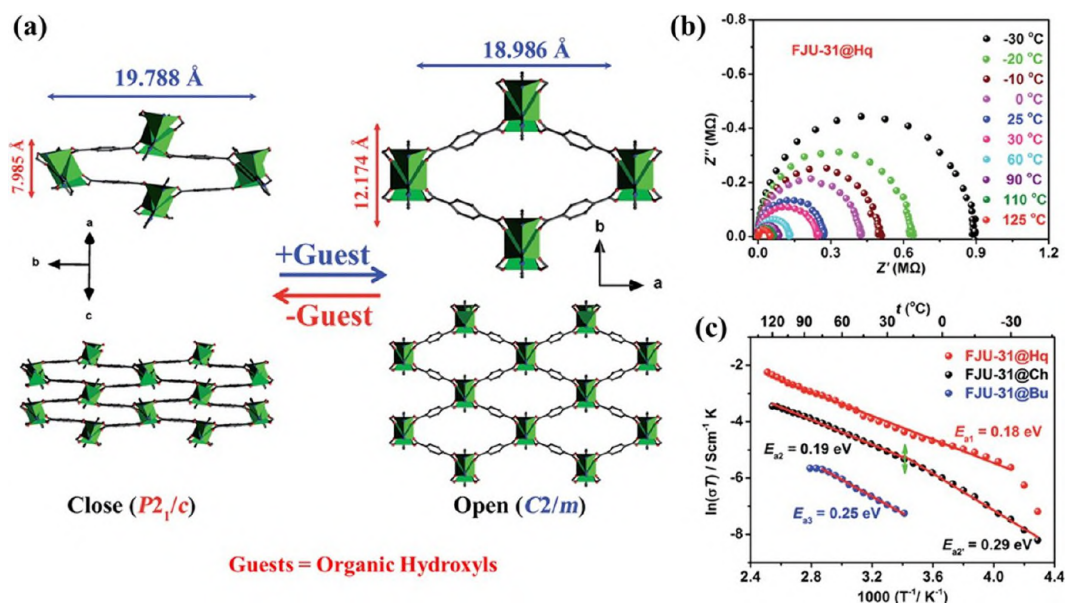
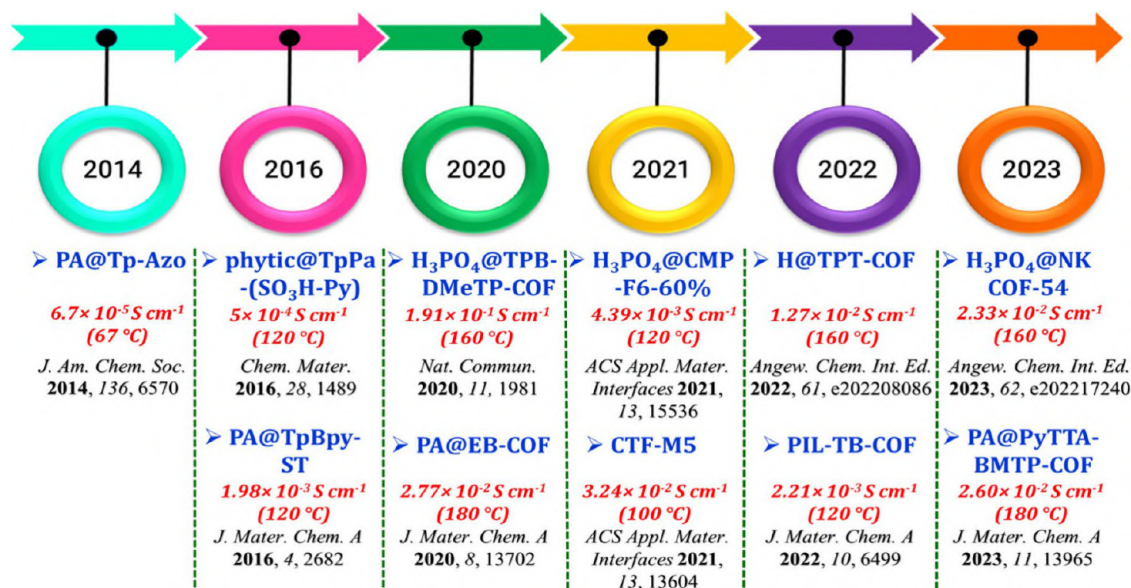


Figure 5. Representation of rhombic channels in FJU-31 during degassing (closed pore) and after organic hydroxyl loading (open pore). (b) Nyquist plot for temperature-dependent anhydrous conductivity in FJU-31@Hq. (c) Activation energy plots for FJU-31@Hq, FJU-31@Ch, and FJU-31@Bu. Reproduced with permission from ref 100. Copyright 2016, Royal Society of Chemistry.

carriers under anhydrous conditions. Along this direction, Zhang and co-workers loaded a variety of organic hydroxyl guest protonic species extrinsically in a flexible MOF, $[\text{Zn}_3(\text{tz})_2(\text{bdc})_2]_n$ (FJU-31), that showed anhydrous proton conduction over a wide temperature range from sub-zero to 125 °C.¹⁰⁰ The framework skeleton was composed of trinuclear $\{\text{Zn}_3(\text{COO})_4\}$ units doubly bridged by triazole ligands to give one-dimensional rods of $\{\text{Zn}_3(\text{COO})_4(\text{tz})_2\}$ that are connected to four phenyl rings of bdc linkers to achieve a 3D flexible framework with rhombic channels across the crystallographic *c*-axis that showed large breathing up to 65% upon loading of guest molecules during the transition from the closed pore to open pore phase (Figure 5a). These extrinsic organic hydroxyl units provide continuous H-bonded pathways for proton transfer under anhydrous conditions and attained conductivities of 3.24×10^{-6} and 1.17×10^{-6} S/cm for FJU-31@Hq and FJU-31@Ch, respectively, under sub-zero (-40 °C) conditions. Importantly, the conductivity value of FJU-31@Hq remains higher than those of FJU-31@Ch and FJU-31@Bu over the whole temperature range, in accordance with the pK_a values of the hosted hydroxyls (pK_a for Hq, Ch, and Bu = 9.85, 17, and 18, respectively). Thus, hydroquinone, with the lowest pK_a value, exhibits a comparatively higher tendency for proton hopping that eventually resulted in higher proton conductivities. The conductivity of FJU-31@Hq increased sequentially with the temperature, and ultimately at 125 °C, the conductivity value stepped into the superprotonic region, at 2.65×10^{-4} S/cm under anhydrous conditions (Figure 5b). Besides high conductivity, FJU-31@Hq exhibited a low activation energy of 0.18 eV, signifying the Grotthuss mechanism of proton transfer (Figure 5c) mediated through high-boiling organic hydroquinone moieties units with pK_a values even lower than those of the nonvolatile N-rich heterocycles. Hence, that work confirms flexible MOFs are excellent hosts for extrinsically encapsulating various organic proton carriers to achieve high anhydrous proton conductivity with remarkable low activation energy barriers.

3.1.2.2. Extrinsic Integration with Proton-Conducting Polymers in MOFs. Apart from achieving ultrahigh conductivity, robustness, thermal stability and mechanical endurance of PEM materials play significant roles in determining their practicality to operate under anhydrous conditions in fuel cells. Hence, the development of composite membranes through extrinsic integration of MOF materials (that act as nanofillers with adaptable loading) with proton-conducting polymers such as PBI, SPEEK, PVPA, etc. has upgraded these materials' conductive performance (owing to the combined effects of individually incorporated proton carriers in the crystalline materials and the polymeric matrices) along with enhancing the overall stability of the PEM materials to achieve two aims at once. In this regard, Compan and co-workers reported three composite membranes formed through the integration of PBI with Zn^{2+} -based ZIF-8, Co^{2+} -based ZIF-67, and their combination, i.e., a binary mixture of ZIF-8 and ZIF-67 (ZIF-mix), externally doped with H_3PO_4 to improve proton transfer through increased carrier concentration.¹⁰¹ As expected, after polymeric integration, the thermal stability of the materials was enhanced and the materials could be used as PEMs up to 250 °C. After the integration of ZIFs with the polymeric matrix of PBI, the proton transportation of all the composite membranes were enhanced as compared to that of the pristine ZIFs and PBI. Interestingly, at 200 °C, the conductivity achieved with PBI@ZIF-67 (4.1×10^{-2} S/cm) was higher than that of PBI@ZIF-8 (3.1×10^{-2} S/cm), which could be ascribed to the higher affinity of phosphates toward the Co^{2+} metal ions as compared to the Zn^{2+} metal ions. Finally, the binary composite PBI@ZIF-mix achieved a conductivity of 9.1×10^{-2} S/cm at 200 °C, which signifies the synergistic promotion of conductivity through mutual cooperation between the PBI and the ZIF-mix. In order to investigate the mechanism, the activation energies were calculated to be 0.34, 0.31, and 0.20 eV for PBI@ZIF-8, PBI@ZIF-67, and PBI@ZIF-mix, respectively, which implies a Grotthuss mechanism of proton transportation in all three cases. In fact, the multiple H-bonded matrices existing among

Scheme 4. Timeline Representing the Evaluation of COFs in the Field of Anhydrous Proton Conduction since 2014



the PBI polymeric chains, the imidazole rings of the ZIFs, and H₃PO₄ assisted the continuous proton hopping from one site to another, which eventually resulted in ultrahigh superprotonic conductivity at 200 °C under anhydrous conditions. Thus, the work investigates the further research scope on MOF-based polymeric membranes capable of operation in a broad temperature window while maintaining the anhydrous conditions.

Besides benzimidazole-based organic polymers, proton-conducting sulfonated polymers such as sulfonated poly(ether sulfone) (SPES) could induce anhydrous proton conductivities in MOF materials. Along this line, in 2018 Zhiani and co-workers reported a SPES-MOF composite membrane doped with phosphoric acid as an ultrahigh anhydrous superprotonic conductor in the high-temperature window.¹⁰² An amino-functionalized Cr-MIL-101 (Cr-MIL-101-NH₂) was anchored onto the flexible aryl ether backbone of the SPES polymer via the Hinsberg reaction to form cross-linked bonds that not only resulted in a high thermal stability of the membrane (390 °C) but also increased its mechanical stability (in terms of high tensile strength and elongation at break), making it appropriate as a PEM material in real-time fuel cells. In the SPES backbone, the attached MOFs created some proton-hopping channels uniformly filled with -NH₂ and -SO₂NH groups that form strong hydrogen bonds with the externally doped phosphoric acid (PA) units, resulting in a continuous proton conduction pathway. The proton conductivity of the PA-doped membrane thus fabricated was 4.1 × 10⁻² S/cm when measured at 160 °C under anhydrous conditions. Moreover, the proton-transfer activation energy was calculated to be 0.21 eV, which signified a Grotthuss mechanism of proton jumping among the continuously hydrogen-bonded phosphate units and -SO₂NH moieties of the polymeric backbones and manifested that the successful treatment of MOFs with commercial polymers could guarantee their application in future HT-PEMFCs.

3.2. Anhydrous Proton Conduction in Covalent Organic Frameworks (COFs). COFs represent an emerging class of functional nanostructures that possess a unique combination of several intriguing features such as highly

ordered crystalline structures, high surface area, pore space tunability, low mass density, etc.^{42–45,77–84} Basically, they are the metal-free counterparts of MOFs, formed via covalent linking of lighter elements (such as B, C, N, and O) in a periodic manner to form chemically as well as thermally stable 2D/3D structures. In addition, their high tolerance over a wide acidic as well as basic pH range, water retention capability, high processability, and excellent compatibility with the polymeric matrices (on account of its organic background for membrane fabrication in membrane electrode assembly (MEA) construction) definitely count among the several superior features that provided sufficient reason for researchers to explore COF materials in the field of proton conductivity. Moreover, the existence of multiple covalent bonds in COF backbones makes them mechanically stable as well for film/membrane fabrication. However, it was not until 2014 when the proton conductive properties of these COF materials were explored by Banerjee and co-workers.¹⁰³ Since then, a series of reports have arrived on the utilization of these COF materials as excellent superprotonic conductors, approaching even the ultrahigh conductivity 10⁻²–10⁻¹ S/cm range in certain cases.⁵ Nevertheless, although a bunch of reports have been published on proton conduction through COFs under hydrated conditions, reports on anhydrous proton conduction are comparatively limited. A timeline of the origin and development of COF materials in the field of anhydrous conductivity is provided in Scheme 4 for rapid visualization. Importantly, although two review papers have been published summarizing various examples of COFs for proton conduction under hydrous condition,^{5,43} a critical review highlighting anhydrous proton conductivity with in COF materials is high in demand to provide future direction to researchers for exploring this aspect of anhydrous proton conductivity in COF-based materials for their real-time applicability in anhydrous fuel cells.

Akin to the cases of MOFs, for achieving anhydrous proton conduction through COFs, the strategies can be sub-divided into three classes on the basis of proton immobilization, namely, **intrinsic proton conductivity in COFs**, where the carrier species such as -SO₃H are either inherently installed

into the framework backbones or the proton carriers (such as nonvolatile heterocycles or acids) are *in situ* doped during the synthesis procedures, which has been largely unexplored to date; **extrinsic proton conductivity in COFs**, where nonvolatile proton carriers like PA, phytic acids, imidazoles, triazoles, and proton-conducting ionic liquids (PIL) are externally loaded into the nanoporous crystalline channels of the framework to achieve superprotonic anhydrous conductivity; and **combined proton conductivity in COFs**, where the mutual cooperation of both intrinsic and extrinsic approach is synchronously used to achieve anhydrous conductivity. In the context of anhydrous proton conductivity with COFs, to date the majority of published reports have utilized the extrinsic conductivity approach, where rational encapsulation/loading of nonvolatile proton bearers into the nanochannels of COF materials resulted in ultrahigh conductivities. A few reports have manifested intrinsic anhydrous proton conduction through pre-installed framework functionalization ($-\text{SO}_3\text{H}$ only) in COFs, whereas others revealed that adopting a combined approach, i.e., cooperative harmony of intrinsic proton sources with extrinsically loaded proton carriers and their mutual interplay, aided the achievement of high anhydrous conductivity (Figure 6).

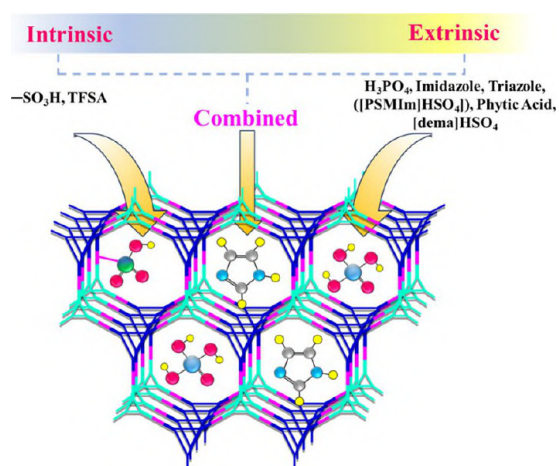


Figure 6. Representation of COFs with nonvolatile proton carriers incorporated inside the framework intrinsically, extrinsically, or via a combined approach for anhydrous proton conduction.

3.2.1. Intrinsic Proton Conductivity in COFs. This particular class involves the intrinsic pre-installation of various proton-donor/carrier functionalities (such as sulfonate moieties or nonvolatile superacids) into the covalent backbones of COFs through direct synthesis procedures that can ensure stable H-bonded proton-conducting pathways in anhydrous conditions. Usually, these groups remain appended (uncoordinated) inside the pore apertures, which not only increases the acidity of the pore channels but also aids in enhancing the carrier concentration as well as the kinetic mobility of protons, in turn triggering efficient proton conductivities.

Along this line, an intrinsic $-\text{SO}_3\text{H}$ -functionalized COF material named **TpPa-SO₃H**, with periodically arranged $-\text{SO}_3\text{H}$ groups flanking the hexagonal channels, was developed by Banerjee and co-workers in 2016.¹⁰⁴ The presence of a continuous array of proton-conducting/hopping sites in the COF backbone helped in maintaining an extensive H-bonded pathway even in the absence of any external humidity, and thus

made **TpPa-SO₃H** perfectly suited for studying the anhydrous proton conductivity. The material displayed a proton conductivity of 1.7×10^{-5} S/cm under anhydrous condition at 120 °C, thereby making it an inventive example of anhydrous intrinsic proton-conducting COFs.

Apart from the intrinsic framework functionalization strategy mentioned above, *in situ* doping of nonvolatile proton carriers in the pore channels of COFs is another exciting strategy whereby intrinsic proton conductivity could be harnessed. Hence, a series of covalent triazine framework membranes (**CTF-M_x**) having an intrinsically doped high-boiling superacid, trifluoromethanesulfonic acid (TFSA), with different quantities of *N*-methyl-4-piperidone contents was developed by Ma and co-workers in 2021.¹⁰⁵ The materials possessed unique structural features on account of strong electrostatic interactions as well as acid–base interactions among the CTF and TFSA that imparted high mobility to proton carriers to improve anhydrous proton conductivity in free-standing membranes. These COF membranes were identified as **CTF-M2** to **CTF-M6**, based on the sequential increase in the content of piperidones in the parent framework that imparted flexibility to the membranes. Among the CTFs, **CTF-M5** offered the highest proton conductivities within a broad temperature range under anhydrous conditions (1.21×10^{-3} S/cm at -40 °C and 3.24×10^{-2} S/cm at 160.15 °C). Such high superprotonic conductivities even at sub-zero temperatures could be attributed to the high piperidone content leading to a greater absorption of TFSA molecules via acid–base interactions. The spontaneous migration of protons in the TFSA-doped **CTF-M_x** was further supported through DFT calculations that revealed a reduction in the proton dissociation energy of TFSA by 1.14 eV (from 4.68 eV in pristine TFSA to 3.54 eV in TFSA-doped CTF). This suggests a weak interaction between the $-\text{SO}_3\text{CF}_3^-$ anion and triazine ring in the CTF skeleton (CTF $\cdots\text{H}\cdot\text{SO}_3\text{CF}_3$ interaction), resulting in free migration of protons and contributing toward excellent anhydrous superprotonic conduction. Furthermore, the activation energy (E_a) of **CTF-M5** was the lowest ($E_a = 0.11$ eV) among all the TFSA-doped **CTF-M_x**. The reduced activation energy in **CTF-M5** emerged from the strong acid–base interaction between the TFSA and the N atoms of piperidine rings that provided enormous basic sites for smooth proton transfer via the Grotthuss mechanism of proton conduction. Thus, the work represents the first example where *in situ*-doped proton carriers (TFSA and *N*-methyl-4-piperidone) played a significant role in achieving ultrahigh anhydrous proton conductivity in triazine-based COFs (CTFs) employing the intrinsic proton conductivity approach over a wide temperature range, which broadens the scope for further explorations on such intrinsic proton-conducting COF-based membranes.

3.2.2. Extrinsic Proton Conductivity in COFs. The presence of pre-installed nonvolatile proton carrier functionalities into the COF backbones is undoubtedly an excellent strategy to achieve anhydrous conductivity, as mentioned earlier; however, such structures are highly difficult to synthesize and require arduous synthetic treatments. External incorporation of various nonvolatile species such as H_3PO_4 (PA), phytic acids, N-rich heterocycles (triazole, imidazole), or their combination into the pore channels of the COFs could help in establishing continuous H-bond matrices that aid facile proton hopping with low activation energy barriers in anhydrous conditions.

Anhydrous proton conduction across the mesoporous channels of crystalline **TPB-DMTP-COF** through external incorporation of nonvolatile N-rich heterocycles like triazole and imidazole into the pore spaces of COF was reported by Jiang and co-workers in 2021.¹⁰⁶ The parent COF (**TPB-DMTP-COF**) exhibited a high BET surface area of 2072 m² g⁻¹ with a pore volume of 1.34 cm³/g that exhibited poor conductive performance ($\sim 10^{-12}$ S/cm). However, when the organic proton carrier triazole species were externally loaded (180 wt%) into the pore channels COF, the material (**trz@TPB-DMTP-COF**) exhibited superprotonic conductivity of 1.1×10^{-3} S/cm at 130 °C under anhydrous conditions with a low activation energy barrier of 0.21 eV, implying a Grotthuss type of continuous proton hopping through triazole moieties in 1D mesoporous channels. Eventually, this triazole-loaded COF performed better than the state-of-the-art triazole-loaded **β PCMOF-2** under the same conditions. The material was further investigated through extrinsic loading of proton carrier imidazole moieties (with a maximum loading of 164%) into the pore spaces of the framework through vapor diffusion methods to generate **im@TPB-DMTP-COF**. It is interesting to note that **im@TPB-DMTP-COF** exhibits a 4 times superior conductivity of 4.37×10^{-3} S/cm at 130 °C as compared to **trz@TPB-DMTP-COF** with similar activation energies. The superior proton conductivity performance of the imidazole-loaded framework as compared to the triazole counterpart could be attributed to the lower concentration of protons in the triazole, with lone pairs on its two N atoms, that decreases the charge carrier concentration as well as mobility, resulting in its slightly lower conductivity as compared to the imidazole molecules, with only one lone pair-containing N atom. The work highlights the importance of extrinsic heterocycle guest (nonvolatile proton carriers) encapsulation as an effective tool to attain superprotonic conductivity with low activation energies under anhydrous conditions in mesoporous COFs materials.

Apart from the nonvolatile heterocycle guest loading discussed above, external doping of PA is considered as an efficient strategy to achieve anhydrous conductivities due to its nonvolatile nature (boiling point 158 °C) with high proton mobility that results in extended H-bonded networks stemming from three ionizable –OH bonds, which guarantee uninterrupted proton hopping even at anhydrous conditions. In this direction, Du and co-workers developed a series of COFs, **TPB-COF** (with a benzene core), **TPT-COF** (with a triazine core), and **TPB-TPT-COF** and **TPT-TPB-COF** (combinations of benzene and triazine cores), through variation of the numbers and chemical positions of triazine units and explored their anhydrous proton conductivities after extrinsic incorporation of H₃PO₄ inside the channel walls to yield **H@COFs**.¹⁰⁷ Although the parent COFs exhibited nearly insulating behavior due to the absence of proton carriers, the proton conductivities of 18% H₃PO₄-loaded COFs were noted to increase with a gradual rise in temperature from 100 to 160 °C. Comparing the conductivities of two frameworks (**TPB**- and **TPT-COFs**), the 10 times higher proton conductivity of 18% **H@TPT-COF** than that of 18% **H@TPB-COF** could be attributed to the higher surface area, highly exposed pore spaces, and larger pore volume of the former as compared to the latter. **H@TPT-COF** exhibited a conductivity of 8.84×10^{-5} S/cm at 160 °C with 18 wt% H₃PO₄ that increased to 9.34×10^{-3} S/cm at 150 °C with increasing H₃PO₄ loading up to 65 wt%, eventually stepping into the ultrahigh superprotonic

region with a conductivity of 1.27×10^{-2} S/cm at 160 °C. Thus, the superprotonic conductivity was found to be directly proportional to the increasing temperature and H₃PO₄ concentration. This 3-fold increment in conductivity could have resulted not only because of the additional proton sources from impregnated H₃PO₄ but also due to the perfect alignment of exposed triazine-N sites inside the 1D nanochannels, which facilitated the formation of a dense H-bonding network along the z-direction. Moreover, the framework 65% **H@TPT-COF** exhibited a low activation energy (0.17 eV), which is indicative for the Grotthuss mechanism of proton transportation, which correlates with the continuous and smooth proton hopping. DFT calculations revealed that H₃PO₄ is stabilized by both the imine and N atoms of the triazine core in **TPT-COF** and suggested strong binding interactions between H₃PO₄ and triazine-N atoms (energy of -37.4 kJ mol⁻¹) through N...H–O interactions. Besides high proton conductivity, durability of performance is also an important prerequisite. **H@TPT-COF** showed durability for 100 h at 160 °C and thus offered a high-temperature proton transport system by harnessing the anhydrous extrinsic proton conductivity approach. Although the strategy of phosphoric acid doping in COFs is quite interesting for the enhanced conductivity with minimal activation energies, the technique of external doping of inorganic acids is always associated with concerns about leaching of loaded acids that might hamper the proton conduction pathway, and these need to be critically analyzed before confirming the materials' practical utility.

3.2.3. Combined Proton Conductivity in COFs. At times, the isolated employment of an intrinsic or extrinsic strategy might not be the best option to impart the desired ultrahigh proton conductivity to the COFs under anhydrous conditions. As mentioned earlier, the customary practice for the development of proton-conducting materials depends on the charge carrier concentration and the availability of continuous proton-hopping sites. Hence, to accelerate the conductivity under anhydrous conditions, synchronous cooperation of intrinsic as well as extrinsic properties in a single COF system through a combined approach might be an excellent alternative, as demonstrated by Banerjee and co-workers in 2016.¹⁰⁴ The group had developed a sulfonate-functionalized framework, **TpPa-SO₃H**, that exhibited a conductivity of 1.7×10^{-5} S/cm under anhydrous conditions at 120 °C (as discussed previously in section 3.2.1). However, the conductivity performance of that material did not step into the “superprotonic” zone. To improve the scenario, two other frameworks—one with pyridine functionalization (**TpPa-Py**) and the other with both pyridinic (basic site) and sulfonic acid functionalities (acidic site) (**TpPa-SO₃H-Py**)—were synthesized.¹⁰⁵ However, neither of them exhibited significant conductivities under the aforementioned anhydrous conditions. Hence, the hybrid COF **TpPa-SO₃H-Py** was extrinsically impregnated with highly nonvolatile phytic acid molecules (even less volatile than H₃PO₄) to generate **phytic@TpPa-(SO₃H-Py)**, combining the aspects of both intrinsic and extrinsic proton sources, and achieved superprotonic conductivity of 5×10^{-4} S/cm at 120 °C. The intrinsic proton sources (–SO₃H) allowed the protonation of pyridines that resulted in the formation of pyridinium (–C₅H₃NH⁺) and sulfonate (–SO₃⁻) pairs inside the **TpPa-(SO₃H-Py)** backbone. Further, the extrinsic loading of phytic acid molecules inside the hexagonal channels of COFs enhanced the carrier concentration in the framework to improve the proton hopping with enhanced mobility, achieving

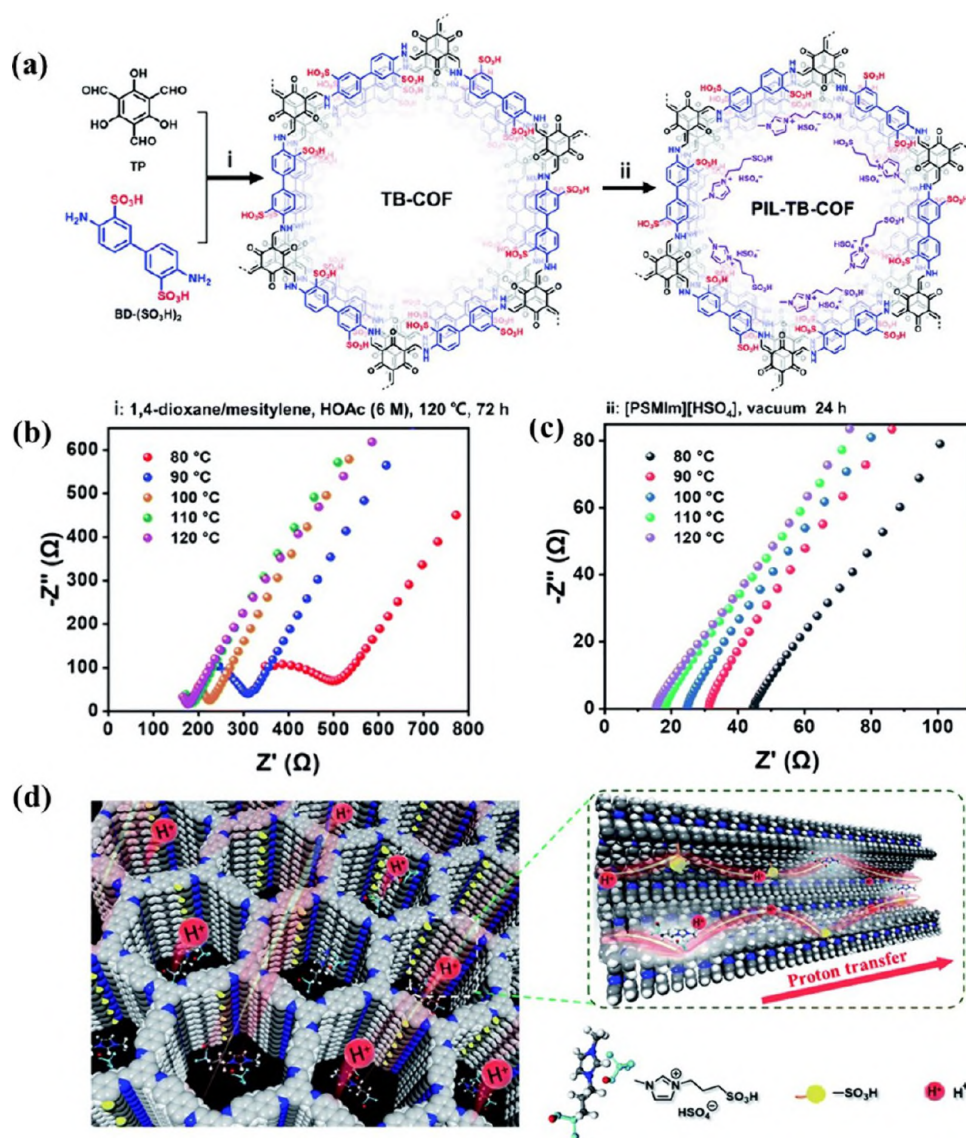


Figure 7. (a) Synthesis scheme for TB-COF and PIL-TB-COF. (b) Nyquist plots for TB-COF at different temperatures. (c) Nyquist plots for PIL-TB-COF at different temperatures. (d) Illustration of proton transfer in PIL-TB-COF. Reproduced with permission from ref 108. Copyright 2022, Royal Society of Chemistry.

superprotonic conductivity with a low activation energy of 0.16 eV that revealed smooth proton conduction via the Grotthuss mechanism. The work highlights the significance of synchronous interplay among intrinsic and extrinsic proton sources to achieve combined proton conductivity that served as an effective strategy to attain superprotonic anhydrous conductivity in the COFs.

Besides nonvolatile organic/inorganic acids and/or N-rich heterocycles, ionic liquids such as [dema]HSO₄, [dema]-H₂PO₄, and [PSMIm][HSO₄] are also interesting candidates as nonvolatile proton carriers for anhydrous proton conduction. Along this line, Yan and co-workers developed a fully sulfonated porous COF material, namely TB-COF [TpBD-(SO₃H)₂], with a high density of free -SO₃H groups and extrinsically incorporated a protic ionic liquid (PIL), 1-methyl-3-(3-sulfopropyl)imidazolium hydrogensulfate ([PSMIm][HSO₄]), inside the TB-COF to develop PIL-TB-COF (Figure 7a).¹⁰⁸ The framework PIL-TB-COF exhibited an anhydrous proton conductivity of 2.21×10^{-3} S/cm at 120 °C, which is 15 times higher than that of the parent framework

TB-COF (1.52×10^{-4} S/cm) at 120 °C (Figure 7b,c). This significant enhancement in the conductivity value could be attributed to the combined increment in the proton sources from intrinsically aligned free -SO₃H groups along with the extrinsically loaded -SO₃H groups from PILs ([PSMIm][HSO₄]) that concurrently assist the establishment of continuous H-bonding pathways for facile proton transfer (Figure 7d).

Further, the material exhibited an activation energy of 0.30 eV, attributed to the faster proton migration between the incorporated proton-defect sites i.e., -SO₃⁻/HSO₄⁻. Moreover, PIL-TB-COF exhibited almost constant proton conductivity performance over 72 h without any leakage of PIL, proving the excellent durability of this material. This work again highlighted that the cooperative participation of intrinsic as well as extrinsic proton sources in COFs can give rise to significant improvements in the conductive performances under anhydrous conditions through the combined proton conductivity approach and validated the encapsulation of

porous ionic liquids as essential tools to impart anhydrous proton conductivity in COFs.

3.3. Anhydrous Proton Conduction in Hydrogen-Bonded Organic Frameworks (HOFs). Apart from the crystalline platforms like MOFs and COFs, HOFs represent a novel class of functional crystalline networks that are assembled from organic molecular tectons through medium/strong noncovalent intermolecular hydrogen-bonding interactions.^{46–52} As H-bonding constitutes an essential component in building HOFs and the fundamental criterion for achieving high proton conductivity in solid-state PEMs is the existence of continuous H-bonded networks, hence it is obvious that these materials offer great promise for providing ultrahigh conductivity by virtue of intrinsic H-bonded matrices. The scope for diverse functionalization of organic building blocks in HOFs allow the accommodation of proton carrier guests (H_2O , Im, NH_3 , etc.) in their channels/interlayer spaces by virtue of well-defined H-bonding interactions with the functionalized organic struts that eventually result in the generation of continuous H-bonded matrices.⁴⁶ Moreover, other advantages such as simple synthesis via crystallization, solution processability, easy healing and regenerability due to the self-adaptable reversible nature of H-bonds (dynamic and flexible), and low-density features broaden its scope for as lightweight SSPCs. Although about a dozen HOFs have been explored for proton conductivity in hydrated conditions (operation under high relative humidity), to date not much work has focused on the domain of anhydrous conductivity, and remained underexplored due to the materials' poor thermal/chemical stabilities. In fact, only seven reports on anhydrous conductivity through HOFs are known to date. As mentioned earlier, to achieve anhydrous conductivity, the incorporation/encapsulation of nonvolatile proton carrier guest species that can maintain the continuous H-bonded networks even in the absence of water is necessary. So far, species such as squaric acid, $\text{H}_3\text{PO}_4/\text{H}_2\text{PO}_4^-$, imidazole, glutamic acid, and succinic acids have been explored as the anhydrous proton carriers in HOFs. Most importantly, it should be mentioned that in HOFs, to date proton conduction has solely relied on intrinsic proton sources with inherent dynamic H-bonded networks (Figure 8). In this section, we focus on some of the rare HOF materials that exhibited substantially high conductivity in anhydrous conditions.

In 2012, a discrete work on anhydrous proton conduction with four squaric acid derivatives by Venkataraman and co-

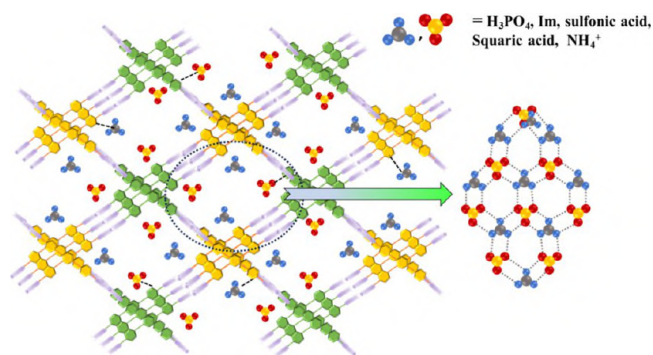


Figure 8. Representation of intrinsic incorporation of nonvolatile proton carriers in the backbone of HOFs to attain anhydrous conductivity. Extrinsic loading of protonic species in HOFs is yet to be realized.

workers marked the beginning of investigations into anhydrous conductivity with HOF-based materials.¹⁰⁹ In the context of anhydrous conduction, proton carriers play the pivotal role since the ease of dynamic movement of these carrier molecules through diffusive pathways significantly influences the conductivity. Hence, the proton carriers preferentially ought to exist in two or more tautomeric forms and must contain acidic protons that could be easily donated. Squaric acid (3,4-dihydroxycyclobut-3-ene-1,2-dione, **4**) exists in multiple tautomeric conformations and possesses proton donor as well as acceptor sites that facilitate the formation of extended H-bonded networks and long-range proton translocation. Four different derivatives of this squaric acid, namely methyl (**4a**), *n*-butyl (**4b**), *tert*-butyl (**4c**), and phenyl (**4d**), were synthesized, and their anhydrous conductivities were explored. The nonsubstituted parent squaric acid was noted to exhibit negligible conductivity, attributed to its constrained reorientation that represents the rate-limiting step in anhydrous conduction. For the methyl and phenyl derivatives (**4a** and **4d**) the conductivities were also very poor ($\sim 10^{-8}$ S/cm even at 160 °C). However, for **4b** and **4c**, the conductivities were noted to be 2.2×10^{-5} and 2.3×10^{-3} S/cm at 120 °C with activation energies of 0.643 and 0.415 eV, respectively. The superior conductivity of the *tert*-butyl derivative (**4c**) as compared to the *n*-butyl derivative (**4b**) could be correlated with the existence of ordered intrinsic H-bonding tetrameric chains in **4c** under high-temperature conditions, unlike **4b**, in which only dimeric H-bonded units are present, as established from a wide-angle X-ray scattering (WAXS) experiment.

As seen from previous studies on MOFs and COFs, imidazoles and phosphoric acids are extensively used as proton conductors *mostly* by extrinsic incorporation onto pores. Dekura, Mori, and co-workers took a different approach to crystallize these two proton-conducting species together into a single HOF platform, namely, the phosphoric acid imidazolium dihydrogen phosphate (**1**) framework.¹¹⁰ The O–H...O hydrogen bonds among the H_2PO_4 and H_3PO_4 molecules give rise to $[\text{H}_5\text{P}_2\text{O}_8]^-$ units that are again hydrogen bonded to each other to form an overall 3D hydrogen-bonded structure with 1D pore channels across the crystallographic *a*-axis (Figure 9a–c). These channels are inhabited by ImH^+ cations

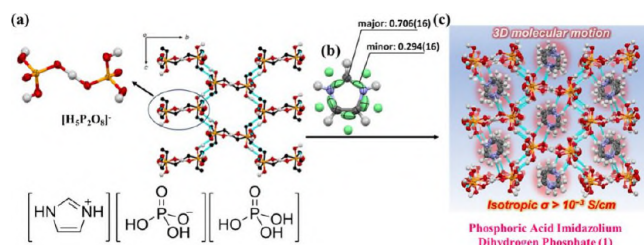


Figure 9. (a) Representation of the 3D hydrogen-bonded phosphate network in **1**. (b) Intrinsically incorporated orientationally disordered ImH^+ cations. (c) Crystal structure of **1** across the crystallographic *a*-axis at 286.6 K. Reproduced with permission from ref 110. Copyright 2022, Wiley VCH.

that form strong N–H...O hydrogen bonds with phosphate networks. The 1D ladder-like H-bonded chains along with uniform H-bond lengths in the phosphate networks are noted to be primarily responsible for the isotropic superprotonic anhydrous conductivities of 1.15×10^{-3} and 1.31×10^{-3} S/cm across the crystallographic *a*- and *c*-axis, respectively, at 351 K

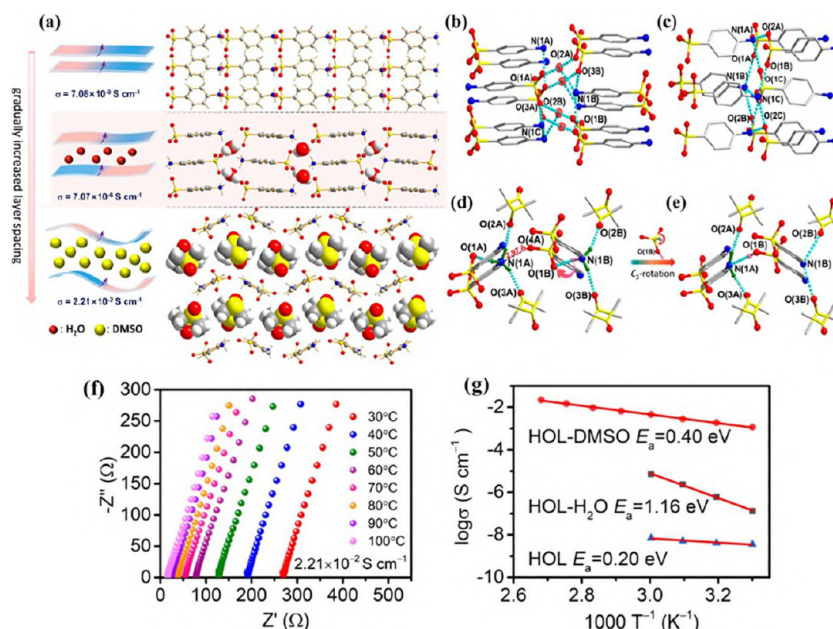


Figure 10. (a) Superprotonic conduction attained through aggregation of 4-ABS molecules in **HOL**, **HOL-H₂O**, and **HOL-DMSO** with gradual increments of interlayer spacing. H-bonded networks in (b) **HOL**, (c) **HOL-H₂O**, and (d) **HOL-DMSO**. (e) Proton hopping by rotation of sulfonic acid groups in **HOL-DMSO**. (f) Temperature-dependent Nyquist plots for **HOL-DMSO** under anhydrous conditions. (g) Activation energy for anhydrous proton conduction in **HOL-DMSO**, **HOL-H₂O**, and **HOL**. Reproduced with permission from ref 111. Copyright 2023, American Chemical Society.

under anhydrous conditions. The encapsulated imidazolium cations underwent 3D dynamic molecular motions (as established from SCXRD, DSC, and solid-state NMR) that indirectly accelerated the protons' movement through the phosphate networks to hasten the conduction mechanism. It is important to note that imidazolium cations possess small sizes with permanent electric dipole moments on the N–H species, and their electrostatic potential promotes the depolarization of H-bonded networks in **1**. In fact, when the protons migrate, significant rotation of the ImH⁺ cations aids the establishment of transient N–H···O interactions with the phosphate networks that decrease the potential barrier, for enhanced proton conduction. In addition, other factors such as the differences in p*K_a* values between H₃PO₄ (p*K_a* = 1.97) and ImH⁺ (p*K_a* = 6.99) and the molecular rotation of ImH⁺ also assist in achieving anhydrous conductivity in such HOF-based materials.

Apart from using molecules with inherent tautomeric forms containing acidic protons (the first example of squaric acid-based HOF) and assimilating two or more proton-conducting species into a single HOF platform (the second example under HOF category), HOFs constructed from zwitterionic molecules could be potential anhydrous conductors, taking into account their strong H-bonds among the tectons. In this direction, Liang, Zhang, and co-workers constructed three new proton-conducting HOFs, **HOL**, **HOL-H₂O**, and **HOL-DMSO**, based on a 4-aminobenzenesulfonic acid (4-ABS) moiety as the molecular tecton, that exhibited guest-dependent anhydrous superprotonic conductivity (Figure 10a).¹¹¹ Single-crystal structure analysis of **HOL** displayed a parallel arrangement of all 4-ABS molecules in a head-to-tail manner that generates a layered-type structure via both intra- and interlayer strong H-bonding interactions (N–H···O) between the protonated amino (–NH₃⁺) group of one 4-ABS and the deprotonated sulfonic acid (–SO₃[–]) group of the other.

However, in the cases of **HOL-H₂O** and **HOL-DMSO**, the guest solvent molecules (H₂O and DMSO) are respectively incorporated inside the layered network, that in turn assists the interlayer H-bonding interactions (Figure 10b–e). The Nyquist plot of **HOL** shows only a large semicircle in the higher frequency region, suggesting poor proton conductive performance (7.08×10^{-9} S/cm at 60 °C). Although fast proton transfer can occur in **HOL** through –NH₃⁺ and SO₃[–] species in the same layer, the restricted rotational motion of SO₃[–] and its subsequent locking through a H-bonding confinement effect between consecutive layers hinder proton movement and results in poor conductivity. For **HOL-H₂O**, temperature-dependent proton conduction analysis revealed a gradual increase in proton conduction with increasing temperature from 1.42×10^{-7} S/cm at 30 °C to 7.07×10^{-6} S/cm at 60 °C due to faster proton dissociation and transfer from –NH₃⁺ to water molecules to form H₃O⁺, which acted as a vehicle to transport the protons to the subsequent –SO₃[–] via the continuous H-bonded network with a much higher activation energy of 1.16 eV. However, in the case of **HOL-DMSO**, superprotonic conductivity as high as 1.15×10^{-3} S/cm was achieved at 30 °C, which was further enhanced to reach the ultrahigh superprotonic region at 100 °C (2.21×10^{-2} S/cm) with a much lower activation energy of 0.40 eV (Figure 10f,g). The higher anhydrous conductivity associated with the lower activation energy was ascribed to the separation of adjacent 4-ABS layers by DMSO molecules that decreased the hydrogen-bonding confinement of SO₃[–] and facilitated smooth proton transfer from –NH₃⁺ via C₃-rotation to the adjacent –SO₃[–].

3.4. Anhydrous Proton Conduction in Polyoxometalates (POMs). POMs are well-known polynuclear metal-oxo clusters that are widely recognized for their structural diversity, structural tunability, and excellent thermal stability.^{53–56} Recently, POM-based materials have emerged as exceptional

SSPCs in the hydrous state due to the large number of associated crystallized lattice water molecules.⁵³ Owing to their highly crystalline nature, similar to MOFs, COFs, and HOFs, structure–function relationships could be established for POMs, which are advantageous for further exploration of such materials. Motivated by the combined effect of excellent thermal stability and superprotonic conductivity in the hydrous state, this class of materials have also been studied recently for their applicability toward anhydrous proton conductivity. In case of POMs, so far, anhydrous proton conductivity arises mostly because of coordinated water molecules attached to the cationic charge-balancing agents or intrinsically incorporated imidazole/imidazolium molecules or from the structural acidic protons present even at high temperatures (Figure 11).

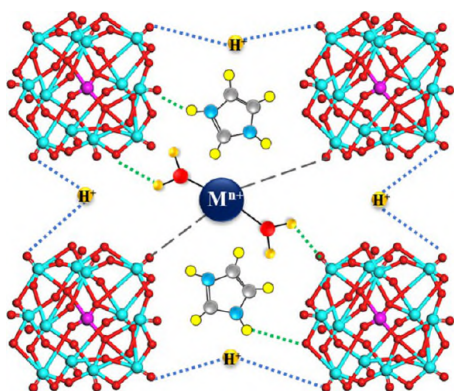


Figure 11. Representation of proton carriers intrinsically installed into native POMs for anhydrous proton conduction. Color code: yellow, hydrogen; red, oxygen; blue, nitrogen; gray, carbon; pink, heteroatom; cyan, metal ions.

However, only a handful of reports could be found on POM-based anhydrous SSPCs; thus, significant attention is needed for further development of POMs in the domain of anhydrous proton conduction.

Considering the significant role of free structural protons in anhydrous conductivity, a cobalt-containing hetero-polyoxoniobate, **1-purple** ($\text{H}_9\text{KNa}_2(\text{H}_2\text{O})_{10}[\text{Co}(\text{H}_2\text{O})_2(\text{SiNb}_{18}\text{O}_{54})] \cdot 15\text{H}_2\text{O}$) was reported by Sun, Zheng, and co-workers in 2019 that exhibited a superprotonic conductivity of 1.01×10^{-3} S/cm under hydrous conditions.¹¹² Upon heating at 60 °C, **1-purple** was gradually converted into another polymorph, dehydrated **1-blue**, with liberation of the coordinated and lattice water molecules (Figure 12a,b). The proton conductivity of **1-blue** was investigated at room temperature under anhydrous conditions, and the initial conductivity value was 6.34×10^{-6} S/cm (Figure 12c). This anhydrous proton conductivity of **1-blue** could result from the long-range H-bonding networks between free structural protons and bridging as well as terminal oxygens of the polyoxoniobate unit, which helped to form smooth proton conduction pathways under anhydrous conditions. However, the anhydrous conductivity of **1-blue** could not be measured at higher temperatures because of irregular impedance data in the Nyquist plots, suggesting complete destruction of the H-bonding pathway inside the crystal. Overall, although the anhydrous conductivity is not in the superprotonic region, the work highlighted the significant role of free structural protons in achieving anhydrous proton conduction in POM-based materials.

Besides MOFs and COFs, sub-zero anhydrous proton conduction could also be achieved for POMs as well. A 3D Keggin-type POM composed of $\{\text{Mo}_{4.55}\text{V}_{7.45}\text{PO}_{40}\}^{10.45-}$ anions and $(\text{H}_2\text{O})_{0.3}@\text{K}_6(\text{H}_2\text{O})_{12}$ clusters with the chemical formula $[(\text{H}_2\text{O})_{0.3}@\text{K}_6(\text{H}_2\text{O})_{12}]\text{H}_{4.45}[\text{PV}_{7.45}\text{Mo}_{4.55}\text{O}_{40}] \cdot 11\text{H}_2\text{O}$ exhibited anhydrous proton conductivity even at temperatures as low as -50 to -1 °C under a dry nitrogen environment

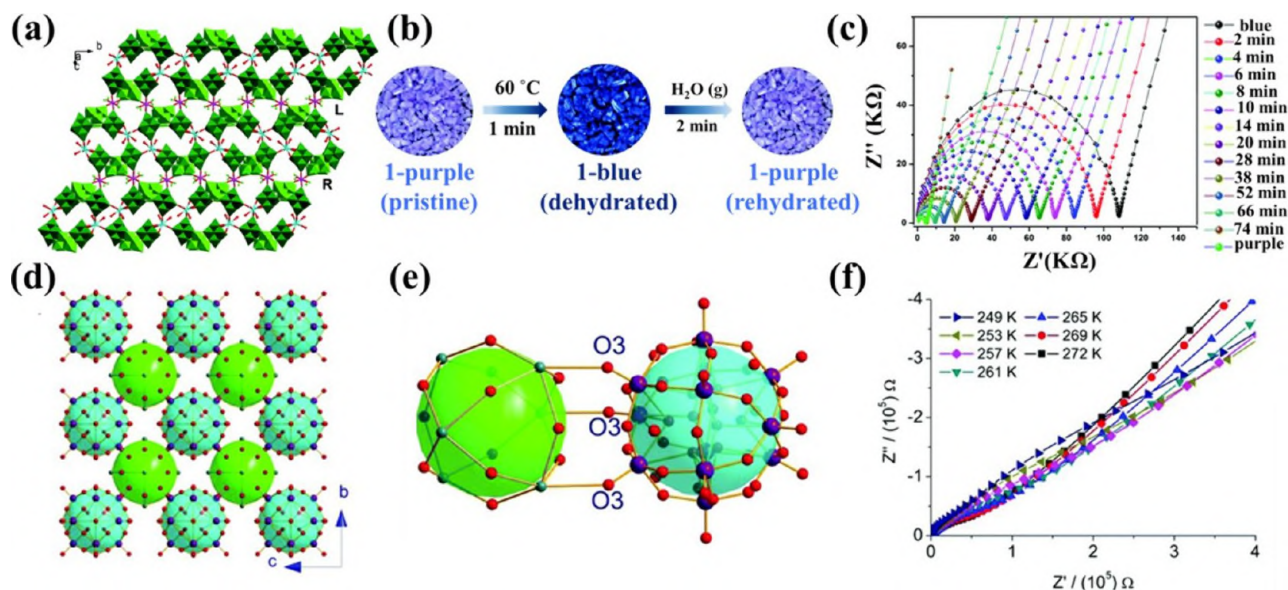


Figure 12. (a) 2D layer in **1-purple** along the a -axis. (b) Digital photographs of the chromic response (purple to dark blue) observed for **1-purple** with controlled thermal treatment (60 °C, 1 min) and revival of the original color (dark blue to purple) on rehydration. (c) Nyquist plots for **1-blue** at room temperature. Reproduced with permission from ref 112. Copyright 2021, Royal Society of Chemistry. (d) Packing diagram of Keggin-type $\{\text{Mo}_{4.55}\text{V}_{7.45}\text{PO}_{40}\}^{10.45-}$ anions (cyan balls) and $(\text{H}_2\text{O})_{0.3}@\text{K}_6(\text{H}_2\text{O})_{12}$ clusters (green balls) for **1**. (e) Connection mode among the polyoxoanion and the $(\text{H}_2\text{O})_{0.3}@\text{K}_6(\text{H}_2\text{O})_{12}$ cluster. (f) Nyquist plots in the temperature range 249–272 K for **1**. Reproduced with permission from ref 113. Copyright 2019, Royal Society of Chemistry.

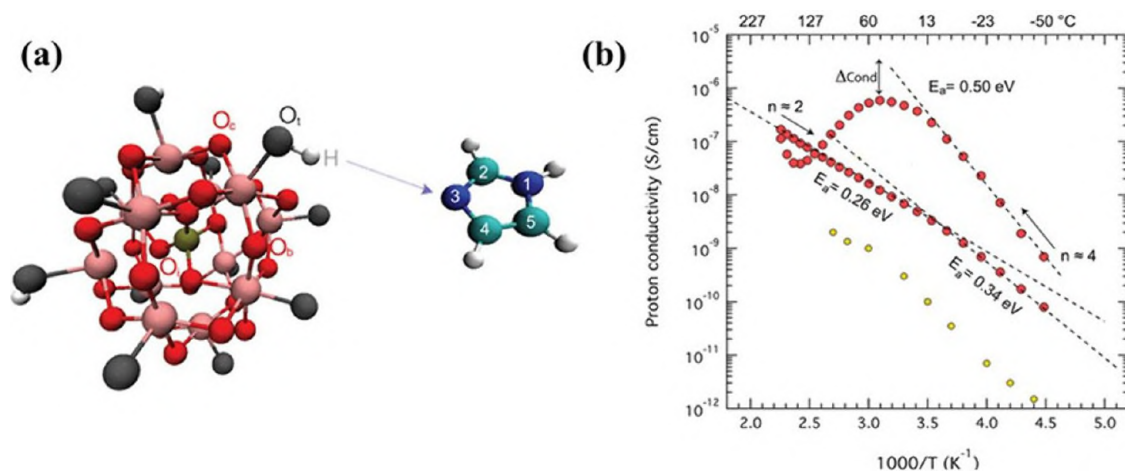


Figure 13. (a) Keggin unit of the 12-tungstophosphoric acid, H_3WPA , and imidazole in its neutral form. (b) Arrhenius plot of the proton conductivity measured for the salt hydrate $\text{Imid}_3\text{WP}\cdot n\text{H}_2\text{O}$ (red filled circles) upon heating and subsequent cooling. Reproduced/adapted from ref 56. Available under CC-BY 4.0, published 2021, American Chemical Society.

(Figure 12d,e), as demonstrated by Ren and co-workers.¹¹³ Although the material exhibited insulating behavior at temperatures below $-26\text{ }^\circ\text{C}$, when the temperature increased to $-24\text{ }^\circ\text{C}$, the anhydrous conductivity was measured to be $6.90 \times 10^{-7}\text{ S/cm}$. Subsequently, the conductivity was progressively enhanced as the temperature increased and reached $3.36 \times 10^{-6}\text{ S/cm}$ at $-1\text{ }^\circ\text{C}$ under anhydrous conditions (Figure 12f). This significant increase in anhydrous conductivity with the rise in temperature could be attributed to facile dissociation of the coordinated water molecules in the $[(\text{H}_2\text{O})_{0.3}@\text{K}_6(\text{H}_2\text{O})_{12}]^{6+}$ cluster, which allowed for the faster movement of protonic species (such as dissociated acidic protons from coordinated water and free structural protons) at higher temperatures. The Arrhenius plot revealed an activation energy of 0.44 eV, indicating the vehicle mechanism of proton transport with H_3O^+ as proton carriers that dominated proton conduction even at sub-zero temperature within the range from -24 to $-1\text{ }^\circ\text{C}$. Though the material inaugurated the exploration of anhydrous proton conductivity at sub-zero temperature in POMs, there is still huge room for improvement to reach the ultrahigh superprotonic region and meet the criteria for industrial implementation.

As discussed earlier, the large dependence of proton conductivity on the hydration level of heteropolyacids (HPAs) as a function of temperature and/or humidity not only imposes significant influence on the conductivity value but also affects the mechanism of proton transportation, which is essentially dependent on the number and orientation of protonic sources/carriers present alongside the POM anion. However, an interesting approach to overcome this limitation in anhydrous conditions could be attained by harnessing the advantage of inherent Brønsted acidity of HPAs, where complete transfer of the structural acidic protons to the anionic bases can occur feasibly to generate the salt hydrate. Toward this direction, Martinelli and co-workers designed a new POM-based SSPC, $\text{Imid}_3\text{WP}\cdot n\text{H}_2\text{O}$, where the proton transfer occurred from 12-tungstophosphoric acid to the imidazole moieties that acted as intrinsically installed proton acceptors (Figure 13a).⁵⁶ The Arrhenius plot exhibited a gradual increase in proton conductivity from $\sim 10^{-9}$ to $\sim 10^{-6}\text{ S/cm}$ with a rise in temperature from -50 to $20\text{ }^\circ\text{C}$ (Figure 13b), which could be attributed to the vehicular mechanism

($E_a = 0.50\text{ eV}$) of proton conduction via four H_2O molecules present in the salt hydrate ($\text{Imid}_3\text{WP}\cdot 4\text{H}_2\text{O}$), as observed from the TGA results. However, upon a further increase in temperature, it was noted that the proton conductivity decreased to $\sim 10^{-7}\text{ S/cm}$ at $145\text{ }^\circ\text{C}$. This could be ascribed to the generation of a pseudoanhydrous state with only ~ 2 lattice water molecules per Keggin unit ($\text{Imid}_3\text{WP}\cdot 2\text{H}_2\text{O}$). Along with proton conductivity, the activation energy also decreased from 0.50 eV at $20\text{ }^\circ\text{C}$ in $\text{Imid}_3\text{WP}\cdot 4\text{H}_2\text{O}$ to 0.26 eV at $145\text{ }^\circ\text{C}$ in $\text{Imid}_3\text{WP}\cdot 2\text{H}_2\text{O}$. This observation was correlated to the faster proton-hopping events via strong H-bonding interactions between the imidazolium cation and free imidazole with the assistance from residual structural water molecules and Keggin WP anions. This in turn contributed towards lowering the activation energy barrier for proton transport within imidazoles and water molecule, as supported by solid-state NMR spectra, MD simulations, and DFT study. Thus, the work not only depicted the role of water present in anhydrous POMs to significantly enhance the overall rate of proton movement, but also opened up new directions for further exploration of POM and N-heterocycle-based salts toward smooth anhydrous proton conduction with a lowered energy barrier.

4. CRYSTALLINE ANHYDROUS PROTON CONDUCTORS IN REAL-TIME IMPLEMENTATION VIA MEMBRANE ELECTRODE ASSEMBLY

As mentioned earlier, anhydrous proton conduction beyond $100\text{ }^\circ\text{C}$ is highly important for upholding the environmental and economic sustainability of fuel cell technologies, enabling the fuel cells to function with increased efficiency. In PEMFCs, the MEA is considered the chief component (the heart of the fuel cell), consisting of solid electrodes (anode and cathode) along with solid-state electrolyte materials (known as proton exchange membranes, PEMs). The proton-conducting solid-state electrolyte (PEM) is sandwiched between the two electrodes (by heat pressing methods) to help in transportation of protons from the anode to cathodes. In the anodic compartment, the fuel (H_2) is provided which get oxidized to protons and diffuse through the membrane material (PEM) to meet the oxidant (oxygen or air) at the cathodic compartment. There, the protons react with O_2 and receive the electrons that

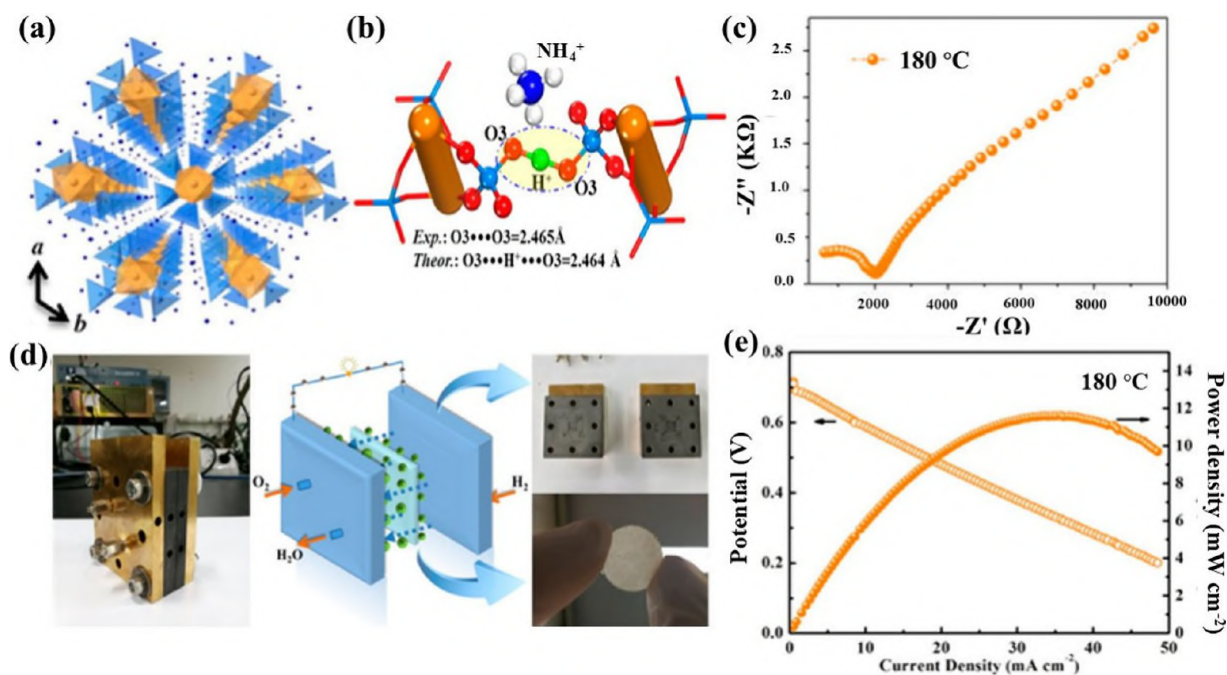


Figure 14. (a) Crystallographic packing of ZrP viewed across the c -axis, where yellow octahedra represent ZrO_6 and blue tetrahedra signify PO_4 units. (b) View of anhydrous proton-hopping pathway mediated through $\text{H}_2/3\text{PO}_4$ units and NH_4^+ ions. (c) Nyquist plot for anhydrous proton conduction with ZrP at 180°C . (d) Schematic representation of a H_2/O_2 fuel cell with pelletized ZrP as solid-state electrolyte in PEMFCs. (e) Fuel cell performance plots where solid and hollow spheres represent current–voltage and current–power measurements, respectively. Reproduced with permission from ref 114. Copyright 2018, American Chemical Society.

were separated from the fuel during oxidation to produce water as the reaction product. Finally, the fuel cell's performance is evaluated on the basis of the open-circuit voltage (OCV), obtained from the I – V plot in terms of maximum current density and power density. Thus, the cell potential is maintained and current is drawn from the cell, producing electricity which can be used for further applications (automotive applications). PEMFCs are highly fascinating on account of their sustainability (only water is produced as product) and socio-economic securities. Hence, for successful validation and to check the real-time potential of PEMs, evaluation of their performance as solid-state electrolytes in practical MEAs under anhydrous conditions is necessary. In the current section, examples of proton-conducting crystalline materials whose practical potential has been examined in MEAs are discussed.

Although a handful of MOFs/CPs are noted to exhibit anhydrous proton conductivities, some of them even in the range of 10^{-1} – 10^{-2} S/cm, utilization of MOFs in PEMFCs as practical solid electrolyte separators needs to be validated widely. Among the 39 examples of MOFs and MOF-based membranes tabulated in Table 2, so far, only 8 of them have been deployed in MEA construction for practical validation under actual (H_2/O_2) fuel cell conditions. For example, in 2009 Shimizu and co-workers reported an *in situ* triazole-incorporated framework, β -PCMOF2(Tz) $_{0.45}$, that exhibited superprotonic conductivity of 5.0×10^{-4} S/cm when operated at 150°C under anhydrous conditions (discussed previously in section 3.1.1.1).⁷² The powdered sample was sandwiched in between two electrodes for fabrication of the MEA in a H_2/air fuel cell. Surprisingly, the framework exhibited a very high maximum OCV of 1.18 V at 100°C that was constantly maintained for 72 h. However, the OCV values were decreased with further increments of temperature to 120 and 140°C

(noted to be 0.93 and 0.77 V, respectively), attributed to phenomenon of fuel crossover.

Along the same line, as mentioned in section 3.1.1.1, in 2012 Kitagawa and co-workers reported two zinc-based CPs, $\{[\text{Zn}(\text{H}_2\text{PO}_4)_2(\text{TzH})_2]_n\}$ ⁷³ and $[\text{Zn}(\text{HPO}_4)(\text{H}_2\text{PO}_4)_2] \cdot (\text{ImH}_2)_2$,⁷⁵ that exhibited superprotonic anhydrous conductivity values of 1.2×10^{-4} and 2.5×10^{-4} S/cm at 150 and 130°C , respectively. The real-time potentiality of both of these materials were validated through MEA formation and electromotive force (EMF) measurements in a H_2/air cell to determine the direct current (DC) conductivity. Detailed analysis showed that maximum OCV values of 0.65 and 0.75 V were obtained for $\{[\text{Zn}(\text{H}_2\text{PO}_4)_2(\text{TzH})_2]_n\}$ and $[\text{Zn}(\text{HPO}_4)(\text{H}_2\text{PO}_4)_2] \cdot (\text{ImH}_2)_2$ at 25 and 150°C , respectively, under anhydrous conditions. Moreover, the fuel cell performances were maintained for 1 h, validating their practicality.

Likewise, in 2014 Kitagawa and co-workers manifested the practical potentiality of a benzimidazole-templated anhydrous superprotonic zinc-based CP, $\{[\text{Zn}(\text{H}_2\text{PO}_4)_2(\text{HPO}_4)] \cdot (\text{H}_2\text{dmbim})_2\}$ (mentioned section 3.1.1.1),⁷⁴ through MEA construction with pelletized samples, and the EMF was measured in a H_2/air fuel cell, displaying a maximum OCV value of 0.95 V, achieved at temperature as high as 190°C . Although the OCV values was less than the theoretical maximum of 1.14 V at 190°C under 1 atm, the value being on the higher side signified that fuel crossover was not dominant.

In 2018, Wang and co-workers reported a Zr-based CP, $\{(\text{NH}_4)_3[\text{Zr}(\text{H}_2/3\text{PO}_4)_3]\}$ (ZrP), possessing NH_4^+ counter-cations that helped establish 1D infinite H-bonded pathways and served the role of being intrinsic proton carriers at the same time (Figure 14a,b).¹¹⁴ The framework ZrP achieved an anhydrous intrinsic superprotonic conductivity of 1.45×10^{-3} S/cm even at 180°C (Figure 14c), comparable to some of the best-performing anhydrous crystalline proton conductors.

Inspired by the material's high stability coupled with the existence of inherent proton sources, the pelletized sample was deployed in real-time H_2/O_2 fuel cells to evaluate **ZrP** as a solid-state electrolyte (Figure 14d). The EMF measurements exhibited a maximum OCV value of 0.72 V at 180 °C and afforded a high power density of 12 mW cm^{-2} even at such a high temperature. Moreover, a steady current density was constantly maintained for 15 h, validating the real-time potentiality of the material in actual HT-PEMFCs (Figure 14e).

In the very same year 2018, Zang and co-workers reported a binary MOF-based polymer composite formed through a unique combination of $-\text{SO}_3\text{H}$ -functionalized (UiO-66- (SO_3H) , A) and basic $-\text{NH}_2$ -functionalized (UiO-66- $(-\text{NH}_2)$, B) isomorphous MOFs with an inexpensive and nontoxic polymer matrix, chitosan (CS), adorned by amino and hydroxyl functionalization, and investigated its high-temperature anhydrous conductivities. This extrinsic integration of the polymer with a binary mixture of acidic and basic UiO-66 MOFs (with optimized loading of 15 and 6 wt% for MOFs A and B, respectively) aided the establishment of continuous H-bonded chains that were responsible for the attainment of anhydrous conductivity of 3.78×10^{-3} S/cm at 120 °C. Further, to validate the practicality of this dual co-filled MOF membrane composite (CS/A-6+B-15), it was employed as a solid-state conductor in a real H_2/O_2 fuel cell which exhibited an OCV of 1.0 V along with a power density of 10.6 mW cm^{-2} under the stated conditions.¹¹⁵

On a similar note, Zhiani and co-workers in 2018 fabricated a PA-doped MOF-polymer composite membrane, **SPES-Cr-MIL-101-NH₂**, that exhibited an ultrahigh superprotonic conductivity of 4.1×10^{-2} S/cm at 160 °C under anhydrous conditions. To authenticate the practical potentiality of this membrane in real-time anhydrous fuel cells, its polarization curve and power density were also measured at 160 °C. The SPES-MOF membrane exhibited an OCV value of 0.92 V along with a peak power density of 238 mW cm^{-2} and a maximum current density of 899 mA cm^{-2} , which hinted at negligible gas permeability or fuel crossover.¹⁰²

Recently, in 2020 Lan and co-workers synthesized a zero-dimensional H-bonded nickel cluster, **NNU-66a**, that exhibited superprotonic conductivity under anhydrous conditions, discussed in section 3.1.1.1. Inspired by the material's excellent chemical and thermal stability, **NNU-66a** was fabricated into a flexible membrane with PVDF (**NNU-66a@PVDF**) as the polymeric binder that imparted high elastic modulus, tensile strength, and mechanical robustness to the membrane. The employment of the developed membrane in a H_2/O_2 fuel cell showed a maximum OCV of 0.7 V with a maximum power density of 1.43 mW cm^{-2} , validating the potentiality of the material for usage in real-time intermediate-temperature anhydrous PEMFCs. In addition, the performance of the fuel cell had good stability, authenticating its real-time potentiality.¹¹⁶

In the context of practical implementations, although a couple of COFs have been deployed as solid-state electrolytes in real-time PEMFCs under hydrous conditions, the domain of anhydrous conductivity in practical fuel cells with COFs as PEM materials have remained completely unexplored to date, except for a report by Banerjee and co-workers who synthesized two COF materials, **PA@TpBpy-ST** and **PA@TpBpy-MC**, solvothermally and mechanochemically through extrinsic loading of phosphoric acids (PAs). These materials

attained ultrahigh conductivities of 1.98×10^{-3} and 2.5×10^{-3} S/cm, respectively, at 120 °C in the absence of humidity. Such high conductivities could be attributed to the abstraction of protons of the PA by the bipyridine units, that eventually resulted in the formation of an extensive H-bonded network among the H_2PO_4^- units and protonated bipyridinium moieties. Further, these COFs were explored as solid-state conductors in real H_2/O_2 fuel cells through MEA construction with powdered samples, exhibiting maximum OCVs of 0.66 ± 0.02 and 0.9 V for **PA@TpBpy-ST** and **PA@TpBpy-MC**, respectively, at 50 °C under anhydrous conditions. Increasing the flow rate of the reactant gases before cell polarization caused a further increment in the OCV from 0.90 to 0.92 V for **PA@TpBpy-MC**, eventually resulting in a maximum current density of 29 mA cm^{-2} with a high power density (7 mW cm^{-2}), ascertaining the fuel cell completion and proton conductive nature of the COF.¹¹⁷

Similarly for HOF materials, real-time potentiality checks through practical fuel cell applications under anhydrous conditions are completely underexplored. It is surprising to note that, even though HOFs are easily processable, they have never been integrated with polymers for membrane fabrication to evaluate their practicality in MEA.

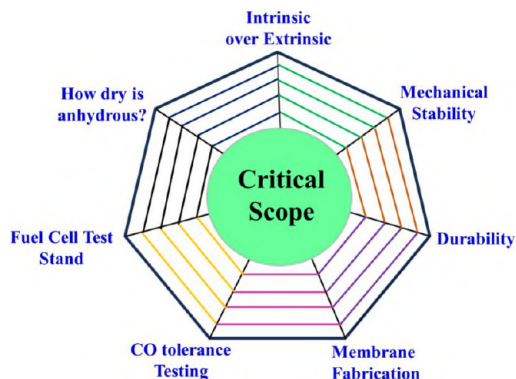
Coming to the POM materials, although native POMs have never been assembled for MEA construction, on being integrated with polymers they have successfully exhibited fuel cell performance. For example, Li and co-workers recently prepared a POM-polymer hybrid, **PN2-PA**, by combining a ternary hybridized polymer network containing poly(terphenyl piperidine) (PTP), polyvinylpyrrolidone (PVP), and a Keggin-type POM, $\text{H}_3\text{PW}_{12}\text{O}_{40}$ (PW), which exhibited an ultrahigh anhydrous superprotonic conductivity of 5.51×10^{-2} S/cm at 160 °C upon PA adsorption.¹¹⁸ This ultrahigh anhydrous superprotonic conductivity of the resulting polymer membrane could be attributed to the fast proton-hopping events from PA to PW through the strongly electrostatically bound PTP as well as the PVP polymer backbone under high temperature anhydrous conditions. This membrane also exhibited excellent thermal stability (until 160 °C) and offered a high break strength of 7.0 ± 0.8 MPa, along with a storage modulus of 72 MPa. This enhanced mechanical strength and thermal stability could be accredited to the PTP backbone of the polymer membrane, which favor practical utilization of the polymer hybrid in PEMs. Considering its comprehensive performance in terms of both mechanical stability and proton conductivity, the real-time efficiency of the membrane was tested. Hence, a high-temperature PEM fuel cell was fabricated using the **PN2-PA** membrane. Under non-humidified H_2/air conditions, the **PN2-PA** membrane offered an OCV above 0.85 V and a maximum power density of 273.6 mW cm^{-2} at 160 °C, which signified the importance of polymer hybridization for real-time implementation of the proton-conducting POMs under anhydrous conditions.

5. CRITICAL ANALYSIS AND FUTURE PROSPECTS

Although several milestones remain in the advancement of crystalline MOFs, COFs, HOFs, and POMs materials in the domain of anhydrous proton conductivity, there is still enough room for improvements in the different crystalline platforms to achieve high conductivity even in the absence of externally supplied humidity, i.e., anhydrous conductivity. Hence, certain critical insights into these materials are discussed in the following sections that necessitate further upgrades to expedite

future research in this field along with practical realizations of such anhydrous conducting materials onto PEMFC technology (Scheme 5).

Scheme 5. Illustration of Critical Scopes for Further Improvement in the Domain of Anhydrous Crystalline Proton Conductors



5.1. Importance of Intrinsic over Extrinsic Conductivity. Though dozens of MOF materials have been explored as anhydrous proton conductors (specifically for HT-PEMFCs) in the past decade, it is noted that greater efforts were invested in the construction of MOFs with externally incorporated guest molecules (protonic species) by employing the second approach of MOF-based “extrinsic anhydrous conductivity”, as evident from Table 2. Although the extrinsic guest loading/integration approach is well adopted in the literature, often these materials are susceptible to leaching of proton carrier molecules under high-temperature conditions (specifically for inorganic acids such as H_3PO_4 , H_2SO_4 , etc.) due to the weak host–guest interactions, which significantly reduces their potentiality and urges a switch back to intrinsic sources of proton conductivity, i.e., the first approach, “intrinsic anhydrous conductivity”, with reduced chances of leaching. However, at the same time it is also noted that, in most of the MOF-based intrinsic conductors, the activation energy is quite on the higher side, indicating the vehicular mechanism, whereas those with extrinsic proton sources usually display activation energies less than 0.4 eV that in turn hint at smooth hopping of protons following a Grotthuss mechanism. In order to maintain a balance in such a *double-edged sword situation*, strategic designing of MOF materials with abundant intrinsic proton sources affixed to the framework backbone at optimized positions for facilitating smooth proton hopping with lower energy barriers is absolutely necessary in the development of leach-free, efficient anhydrous PEMs. In this context, the exploration of proton conductivities on MOFs with intrinsically pre-installed phosphonate moieties (possessing free $-\text{POH}$ groups) adorning the framework backbone is indeed a nice strategy to harness the proton shuttling intrinsically. Strikingly, although a number of MOFs with phosphonate moieties containing free $-\text{POH}$ groups have been explored to determine their proton conduction (some even explored at temperatures higher than $100\text{ }^\circ\text{C}$) under hydrous conditions, as recently reviewed by Shimizu, Zheng, and co-workers,¹¹⁹ unfortunately none of them exhibit proton conductivity under anhydrous conditions (in the complete absence of relative humidity). Even those frameworks for which conductivity is

measured at temperatures higher than $100\text{ }^\circ\text{C}$ typically require high relative humidity ($\sim 95\%$ to 98% RH) to exhibit proton conduction performance. Thus, it is utterly unfortunate to note that, despite possessing enormous potentiality, none of these frameworks with free $-\text{POH}$ group (as proton sources) could transfer protons under anhydrous conditions, and this leaves huge scope for further exploration of intrinsic anhydrous proton conductors in MOF-based SSPCs. Along this line, two other phosphonate-based MOFs, namely, $(\text{Me}_2\text{NH}_2)[\text{Eu}(\text{L})]^{76}$ and $\text{LiBr}@(\text{H}_3\text{O})[(\text{UO}_2)_4(2\text{pmb})_3(\text{H}_2\text{O})_3]\cdot 0.5\text{H}_2\text{O}$ ($\text{LiBr}@1$),¹²⁰ were introduced by Zang and Zheng, respectively. Although both of these frameworks exhibited proton conduction performance (1.25×10^{-3} S/cm at $150\text{ }^\circ\text{C}$ for $(\text{Me}_2\text{NH}_2)[\text{Eu}(\text{L})]$ and 1.55×10^{-1} S/cm at $110\text{ }^\circ\text{C}$ for $\text{LiBr}@1$) under pure anhydrous conditions (without any humidity), the phosphonate units were completely deprotonated in both cases, and no free $-\text{POH}$ moieties were available in either of the cases. In the first case, the Me_2NH_2^+ ion acted as the main proton donor species that interacted with uncoordinated O atoms from adjacent phosphonate groups to form $\text{N}-\text{H}\cdots\text{O}$ hydrogen-bonding interactions, whereas in the second case LiBr -encapsulated water was the chief proton carrier under higher temperature anhydrous conditions.

Compared to MOFs, where significant development has been achieved despite certain indispensable drawbacks, the domain of COF materials is comparatively less explored in terms of anhydrous conductivity (limited to only 22 examples to date). Akin to the earlier case, the extrinsic approach of proton conduction through externally loaded guest molecules is quite predominant here as well. As a matter of fact, only two COF materials are reported to date that can exhibit intrinsic conductivity under anhydrous conditions (**TpPa-SO₃H** and **CTF-MS**). Extrinsic doping with inorganic acids, particularly H_3PO_4 (PA), is quite common in the case of COFs, that in turn could be associated with leaching concerns and might severely hamper the materials’ performance in the fuel cells. Although postsynthetic modification/functionalization could be an important tool under extrinsic anhydrous conductivity approaches, in order to develop the desired COFs free from leaching of protonic species, the challenges associated with the non-uniform distribution of functionalized proton carriers cause it to lack the reliability factor and demands further improvements in the development of *ex situ* linkage of proton carrier moieties to the organic backbones of COFs. It is surprising to note that, to date, only $-\text{SO}_3\text{H}$ -functionalized organic precursors have been deployed to develop intrinsic COF-based proton conductors. To widen the scope of intrinsic anhydrous conductivity in COFs, rationalized installation of potential proton donor functionalities such as $-\text{COOH}$, $-\text{PO}_3\text{H}_2$, or proton carriers as intrinsic proton sources onto the organic backbones (motifs) could be an excellent choice that remains completely unexplored to date, though really challenging. Specifically, COFs with $-\text{COOH}$ groups appended to the framework backbones are highly promising as intrinsic proton-conducting materials for usage in PEMFCs. In fact, the $-\text{COOH}$ -functionalized COF (**COOH-COF-2**) has been shown to be a superprotonic conductor (2.6×10^{-3} S/cm) when measured at high temperature (353 K) under high-humidity conditions (98% RH).¹²¹ However, unfortunately, so far, such $-\text{COOH}$ -containing COF materials have not been explored along the direction of anhydrous proton conduction, which thus demands further investigation. It is suspected that these $-\text{COOH}$ -flanked COF materials would

Table 2. Anhydrous Proton Conductivity Achieved with the Four Types of Prime Crystalline Materials Studied So Far

SL No.	Compound	Protonic Species (Carrier/Guest Molecule) ^a	Stability (Thermal/Chemical)	BET Surface Area (m ² /g)	Form of Material	Conductivity (S/cm)	Temp (°C)	Stability Post PC Measurements	E _a (eV)	ref
Anhydrous Proton Conduction in MOFs										
<i>Intrinsic Approach</i>										
1	[Zn(H ₂ PO ₄) ₂ (TzH) ₂] _n	TzH	200 °C	-	Pellet	1.2 × 10 ⁻⁴	150	-	0.6	73
2	[Zn(H ₂ PO ₄) ₂ (HPO ₄) ₂](H ₃ dmhim) ₂	H ₃ dmhim	190 °C	-	Pellet	2 × 10 ⁻⁴	190	Retained	0.66	74
3	[Zn(HPO ₄)(H ₂ PO ₄) ₂](ImH ₂) ₂	ImH ₂ ⁺	200 °C	-	Pellet	2.5 × 10 ⁻⁴	130	-	0.47	75
4	NNU-66a	H ₂ O, SCN ⁻	180 °C	-	Pellet	1.94 × 10 ⁻³	180	Retained	0.66	116
5	{[(Me ₂ NH ₂) ₃ (SO ₄) ₂] ₂ [Zn ₃ (ox ₂) ₃] _n }	(Me ₂ NH ₂) ⁺	180 °C	-	Pellet	1.0 × 10 ⁻⁴	150	Retained	0.129	132
6	In-IA-2D-2	(Me ₂ NH ₂) ⁺	220 °C	-	Pellet	2.72 × 10 ⁻⁵	77	-	-	133
7	[ImH ₂][Cu(H ₂ PO ₄) ₂ Cl]·H ₂ O	ImH ₂ ⁺	180 °C	-	Pellet	2 × 10 ⁻²	130	-	1.1	134
8	[Co(HPO ₃) ₂][H ₂ DABCO]	H ₂ DABCO ⁺ phosphite	200 °C	-	Pellet	1.85 × 10 ⁻⁶	140	-	0.93	137
9	[Zn(H ₂ PO ₄) ₂ (C ₃ N ₃ H ₃) ₂] _n	H ₃ PO ₄ , H ₃ PO ₄ ⁻	180 °C	-	Pellet	4.6 × 10 ⁻³	150	-	0.53	140
10	ZrP (NH ₄) ₃ [Zr(H ₂ PO ₄) ₃]	NH ₄ ⁺ and phosphate	200 °C	-	Pellet	1.45 × 10 ⁻³	180	-	0.3	114
11	[Eu ₂ (CO ₃)(ox) ₂ (H ₃ O) ₂]·4H ₂ O	Coordinated water, -C ₂ O ₄ ²⁻	350 °C	-	Pellet	2.08 × 10 ⁻³	150	Retained	0.28	141
12	(Me ₂ NH ₂)[Eu(L)]	(Me ₂ NH ₂) ⁺	350 °C	-	Single crystal	1.25 × 10 ⁻³	150	Retained	0.21	76
13	FJU-25-Fe	HPO ₄ ²⁻	160 °C	-	Pellet	5.15 × 10 ⁻⁵	-10	-	0.22	98
14	FJU-17	(Me ₂ NH ₂) ⁺	350 °C	-	Pellet	1.30 × 10 ⁻⁴	90	-	-	99
15	FJU-106	(Me ₂ NH ₂) ⁺ uncoordinated COOH	360 °C	-	Pellet	9.13 × 10 ⁻⁵	-40	Retained	0.29	144
16	a-CdITz-500	H ₃ PO ₄ ⁻ , Tz	160 °C	-	Pellet	1.0 × 10 ⁻⁴	<142	Retained	1.2	146
17	[Zn ₃ (H ₂ PO ₄) ₆](Hbim)	H ₃ PO ₄ ⁻ , Hbim	140 °C	-	Pellet	1.3 × 10 ⁻³	120	Retained	1.5-0.5	149
<i>Extrinsic Approach</i>										
18	Im@[Al(μ ₂ -OH)(1,4-ndc)] _n	Im	160 °C	-	Pellet	1.80 × 10 ⁻²	70	Retained	0.6	28
19	His@[Al(OH)(1,4-ndc)] _n	His	170 °C	-	Powder	1.7 × 10 ⁻³	150	-	0.25	29
20	(β-PCMOF2)(Tz) _{0.45}	Tz (Triazole)	300 °C	-	Pellet	5 × 10 ⁻⁴	150	Retained	1.8-0.56	72
21	[Zn ₃ (tz) ₂ (bdc)] _n @Hq FJU-31@Hq	Hq	300 °C	-	Pellet	2.65 × 10 ⁻⁵	125	-	0.18	100
22	28% Im-MOF-217	Im	300 °C	-	Pellet	1.1 × 10 ⁻³	100	Retained	0.58	131
23	Im@IEF-11	Im	190 °C	-	Pellet	7.64 × 10 ⁻²	110	Retained	0.5	135
24	Im@UiO-67	Im	300 °C	18	Pellet	1.52 × 10 ⁻³	130	-	0.36	136
25	CAU-11_Him	Him	120 °C	354	Pellet	3.0 × 10 ⁻⁴	110	-	0.19	138
26	MOF-867-PS-100TFOH	CF ₃ SO ₃ H	-	20	Pellet	3.92 × 10 ⁻³	130	Retained	<0.4	139
27	dye@FJU-10	Dye = nitrated HPTS; -SO ₃ H and -OH groups on the dye	-	-	Pellet	3.32 × 10 ⁻⁶	-40	-	0.45	142
28	CPO-27(Mg)-NCS _{FA}	FA	240 °C	-	Pellet	7.8 × 10 ⁻⁴	140	-	0.23	143
29	Nafion/ZSNF	Hmim, -SO ₃ H	~430 °C (ZSNF)	349.68 (ZSNF)	Membrane	4.78 × 10 ⁻³	120	-	0.15	145
30	EIMS-HTFSA@MIL-101 (BIL-100)	Binary ionic liquids; EIMS-HTFSA	320 °C	-	Pellet	1.99 × 10 ⁻⁴	140	-	0.76	147
31	Im@ZrSQU-200	Im	300 °C	-	Pellet	3.6 × 10 ⁻²	110	Retained	0.53	148
32	SPPO/Fe-MIL-101-NH ₂ ∩NAPI	NAPI	200 °C	-	Membrane	4 × 10 ⁻²	160	-	-	150
33	GO@UiO-66-NH ₂ /Nafion	-NH ₂ , -SO ₃ H	~300 °C	-	Membrane	3.403 × 10 ⁻³	120	-	-	151

Table 2. continued

SL No.	Compound	Protonic Species (Carrier/Guest Molecule) ^a	Stability (Thermal/Chemical) <i>Extrinsic Approach</i>	BET Surface Area (m ² /g)	Form of Material	Conductivity (S/cm)	Temp (°C)	Stability Post PC Measurements	E _a (eV)	ref
34	PBI@ZIF-mix	PBI, Im	550 °C	1171 (ZIF-mix)	Membrane	9.1 × 10 ⁻²	200	-	0.20	101
35	PES-SO ₂ NH-Cr-MIL-101	-NH ₂ , -SO ₃ H, H ₃ PO ₄	390 °C	-	Membrane	4.1 × 10 ⁻²	160	-	0.21	102
36	SA-EIMS@MIL-101	SA, EIMS, ionic liquids	240 °C	-	Membrane	1.83 × 10 ⁻³	150	-	0.26	152
37	PSM2-10% OPBI	-SO ₃ H, OPOBI (aryl ether-type PBI)	~130 °C Fenton's reagent (3% H ₂ O ₂)	-	Membrane	3.08 × 10 ⁻³	160	-	0.15	153
38	(CS/(A+B), with A = UiO-66(SO ₃ H) and B = UiO-66(NH ₂))	-NH ₂ , -SO ₃ H	180 °C	-	Membrane	3.78 × 10 ⁻³	120	-	0.189	115
39	LiBr@((H ₃ O)[(UO ₂) ₄ (2pmb) ₃ (H ₂ O) ₃]-0.5H ₂ O)	H ₂ O (higher boiling), LiBr	290 °C	-	pellet	1.55 × 10 ⁻¹	110	Retained	0.36	120
Anhydrous Proton Conduction in COFs										
<i>Intrinsic Approach</i>										
1	Aza-COF-1	H ₂ SO ₄ (remained in pores as impurity)	250 °C/12 M HCl, 14 M KOH	99	Pellet	10 ⁻⁸ -10 ⁻⁹	50	-	0.49	154
2	Aza-COF-2	-SO ₃ H	<200 °C	102.2	Pellet	1.7 × 10 ⁻⁵	120	-	-	104
3	TpPa-SO ₃ H	-SO ₃ H	~248 °C	215	Pellet	1.52 × 10 ⁻⁴	120	-	0.37	108
4	CTF-MS	TFSA	>300 °C	-	Membrane	3.24 × 10 ⁻²	100	-	0.11	105
<i>Extrinsic Approach</i>										
5	PA@Tp-Azo	H ₃ PO ₄	~350 °C/9 (N) HCl, 1 (N) H ₃ PO ₄ , 1 (N) H ₂ SO ₄	1328 (parent)	Pellet	6.7 × 10 ⁻⁵	67	-	0.11	103
6	Im@Py-BT-COF-50	Im	~160 °C/1 M HCl, 1 M NaOH	1895 (Py-BT-COF), Negligible after Im loading	Pellet	2.92 × 10 ⁻³	130	Retained	0.36	155
7	Im@Py-BD-COF-50	H ₃ PO ₄	~550 °C/Fenton's reagent (100 h)	379 (post modification)	Membrane	3.09 × 10 ⁻¹	180	-	0.12	126
8	m-PBI-P@MCOF-10% (proton conducting)	H ₃ PO ₄	~525 °C/14.6 M H ₃ PO ₄ , 4 M Fenton's reagent	1909 (parent)	Pellet	1.27 × 10 ⁻²	160	-	0.17	107
9	H ₃ PO ₄ @NKCOF-54	H ₃ PO ₄	<250 °C/Acetone, H ₃ PO ₄	318 (parent)	Pellet	2.33 × 10 ⁻²	160	Retained	0.29	157
	H ₃ PO ₄ @NKCOF-52	H ₃ PO ₄		378 (parent)	Pellet	1.12 × 10 ⁻³		-	0.52	
	H ₃ PO ₄ @NKCOF-53	H ₃ PO ₄		564 (parent)	Pellet	1.24 × 10 ⁻²		-	0.27	
10	PA@TpBpy-ST	H ₃ PO ₄	<350 °C/9 N HCl, 3 N NaOH	80 (post modification)	Pellet	1.98 × 10 ⁻³	120	Retained	0.12	118
	PA@TpBpy-MC	H ₃ PO ₄			Pellet	2.5 × 10 ⁻³		-	0.11	
11	PA@EB-COF	H ₃ PO ₄	~350 °C	6.9 (post modification)	Pellet	2.77 × 10 ⁻²	180	-	0.35	158
	PA@DAAQ-COF			4.0 (post modification)		9.20 × 10 ⁻³	140		0.22	
	PA@PD-COF			0.75 (post modification)		5.51 × 10 ⁻³	140		0.24	
	PA@TAP-COF			13.0 (post modification)		2.65 × 10 ⁻³	140		0.46	
	tra@EB-COF	Tz		-		3.25 × 10 ⁻³	160		0.22	
	tra@DAAQ-COF			-		2.62 × 10 ⁻⁵	140		0.32	
	tra@PD-COF			-		4.98 × 10 ⁻⁵	140		0.34	
	tra@TAP-COF			-		3.82 × 10 ⁻³	150		0.26	

Table 2. continued

SL No.	Compound	Protonic Species (Carrier/Guest Molecule) ^a	Stability (Thermal/Chemical) <i>Extrinsic Approach</i>	BET Surface Area (m ² /g)	Form of Material	Conductivity (S/cm)	Temp (°C)	Stability Post PC Measurements	E _a (eV)	ref
12	PA@PyTTA-BMTP-COF	H ₃ PO ₄	~350 °C/1 M HCl, 1 M NaOH for 1 week	19 (post modification)	Tablet	2.6 × 10 ⁻²	140	-	0.22	159
	PA@PyTTA-DHTA-COF	H ₃ PO ₄	~450 °C/1 M HCl, 1 M NaOH for 1 week	21 (post modification)	Pellet	9.2 × 10 ⁻³	140	-	0.078	
13	COF-F6-H (H ₃ PO ₄ @COF-F6)	H ₃ PO ₄	~350 °C/H ₃ PO ₄ (85%), HCl (38%), and HNO ₃ (65%)	233 (parent)	Pellet	4.2 × 10 ⁻²	140	-	0.09–0.54	160
14	F6-[dema]HSO ₄ -1.5	[dema]HSO ₄	-	224 (parent)	Pellet	1.33 × 10 ⁻²	140	-	0.34	161
	C6-[dema]HSO ₄ -1.0	[dema]H ₂ PO ₄	-	531 (parent)	Pellet	2.84 × 10 ⁻³	140	-	0.38	
	C6-[dema]H ₂ PO ₄ -1.0	[dema]H ₂ PO ₄	-	3.27 × 10 ⁻⁵	Pellet	3.27 × 10 ⁻⁵	150	-	0.59	162
15	H ₃ PO ₄ @CTF-H	H ₃ PO ₄	Water, H ₃ PO ₄ , 12 M NaOH, 12 M HCl	551 (parent)	Pellet	1.6 × 10 ⁻¹	150	-	0.25	
	H ₃ PO ₄ @CTF-L	H ₃ PO ₄	-	551 (parent)	Membrane	5.1 × 10 ⁻²	130	-	0.26	163
16	trz@TAPB-DMTP-COF	Trz	-	20	Membrane	3.10 × 10 ⁻³	130	-	0.38	
	trz@TAPB-DMTP-COF _{0.1-BBA}	Trz	-	1890	Membrane	5.05 × 10 ⁻³	130	-	0.21	106
17	trz@TPB-DMTP-COF	Trz	210 °C	0.4	Pellet	1.10 × 10 ⁻³	130	-	0.21	
	im@TPB-DMTP-COF	Im	220 °C	2.3	Pellet	4.37 × 10 ⁻³	130	-	0.38	108
18	H ₃ PO ₄ @TPB-DMcTP-COF	H ₃ PO ₄	~440 °C/0.7 M H ₃ PO ₄ in THF, 12 M HCl, 14 M NaOH, Fenton's reagent	2894 (parent)	Pellet	1.91 × 10 ⁻¹	160	Retained	0.34	
	75% H ₃ PO ₄ @TPB-DMcTP-COF	H ₃ PO ₄	-	-	Pellet	3.05 × 10 ⁻²	140	-	0.40	
	50% H ₃ PO ₄ @TPB-DMcTP-COF	H ₃ PO ₄	-	-	Pellet	9.04 × 10 ⁻³	140	-	0.50	164
19	H ₃ PO ₄ @CPF-1/PVDF	H ₃ PO ₄	-	-	Pellet	9.77 × 10 ⁻³	140	-	0.15	
	H ₃ PO ₄ @CPF-BT-1/PVDF	H ₃ PO ₄	-	-	Pellet	1.30 × 10 ⁻²	120	-	0.16	165
20	H ₃ PO ₄ @CMP-F6-60%	H ₃ PO ₄	~120 °C strong acid and alkali solutions	287 (parent)	Membrane	4.39 × 10 ⁻³	120	-	0.35	
21	H ₃ PO ₄ @TPB-DMTP-COF	H ₃ PO ₄	-	2900 (parent)	Pellet	5.02 × 10 ⁻²	160	-	0.30	166
	H ₃ PO ₄ @Py-TMQPDA-COF	H ₃ PO ₄	THF, boiling water, Aq. H ₃ PO ₄ , 12 M HCl, 14 M NaOH, Fenton's reagent	1500 (parent)	Pellet	2.52 × 10 ⁻²	160	-	0.24	
	H ₃ PO ₄ @Py-2,2'-BPyPh-COF	H ₃ PO ₄	-	1710 (parent)	Pellet	1.09 × 10 ⁻²	120	-	0.45	
	H ₃ PO ₄ @HFPTP-BPDA-COF	H ₃ PO ₄	-	843 (parent)	Pellet	1.04 × 10 ⁻⁴	120	-	0.67	
	H ₃ PO ₄ @HFPTP-PDA-COF	H ₃ PO ₄	-	510 (parent)	Pellet	1.67 × 10 ⁻⁵	120	-	0.78	
	phytic@TpPa-Py	Phytic acid	-	-	-	3 × 10 ⁻⁴	120	-	0.10	105
2	phytic@TpPa-(SO ₃ H-Py)	[PSMIm][HSO ₄] (ionic liquid)	<200 °C	-	-	5 × 10 ⁻⁴	120	-	0.16	
3	PIL-TB-COF	Tz	~221 °C	-	Pellet	2.21 × 10 ⁻³	120	-	0.30	109
22	trz@XJCOF-1	Trz	~200 °C/3 M HCl	961 (parent)	Pellet	4.3 × 10 ⁻³	150	-	0.25	156
	trz@XJCOF-2	Trz	-	1.29 × 10 ⁻²	Pellet	1.29 × 10 ⁻²	160	-	0.27	
	trz@XJCOF-3	Trz	-	5.6 × 10 ⁻³	Pellet	5.6 × 10 ⁻³	160	-	0.28	
	im@XJCOF-1	Im	-	4.38 × 10 ⁻²	Pellet	4.38 × 10 ⁻²	140	-	0.21	
	im@XJCOF-2	Im	-	3.33 × 10 ⁻²	Pellet	3.33 × 10 ⁻²	140	-	0.24	
	im@XJCOF-3	Im	-	2.43 × 10 ⁻²	Pellet	2.43 × 10 ⁻²	140	-	0.20	

Table 2. continued

SL No.	Compound	Protonic Species (Carrier/Guest Molecule) ^a	Stability (Thermal/Chemical)	BET Surface Area (m ² /g)	Form of Material	Conductivity (S/cm)	Temp (°C)	Stability Post PC Measurements	E _a (eV)	ref
Anhydrous Proton Conduction in HOFs										
<i>Intrinsic Approach</i>										
1	Squaric acid derivative (<i>t</i> -Bu)	Squaric acid	150 °C	-	Pellet	2.3 × 10 ⁻³	110	-	0.41	109
2	Phosphoric acid imidazolium dihydrogen phosphate (1)	H ₃ PO ₄	~77 °C	-	Crystal	1.31 × 10 ⁻³	77	-	1.75	110
3	HOL-DMSO	4-Aminobenzenesulfonic acid	~100 °C	-	Pellet	2.21 × 10 ⁻²	100	-	0.40	111
	HOL-H ₂ O		~390 °C			7.07 × 10 ⁻⁶	60		1.16	
4	HOL		~383 °C			7.08 × 10 ⁻⁹	60		0.20	
4	Im-Suc	Im	~116 °C	-	Crystal	4.94 × 10 ⁻⁷	115	-	6.24	167
4	Im-Glu		~94 °C			2.40 × 10 ⁻⁶	94		4.87	
5	(2,5-H ₂ DABT ²⁺)(H ₃ PO ₄) ₂ ·(H ₃ PO ₄) ₂	H ₃ PO ₄	~164 °C	-	Pellet	2.6 × 10 ⁻⁵	164	-	0.65	168
6	(NH ₄ ⁺) ₂ (DPNDT ²⁻)	NH ₄ ⁺	~590 °C	-	Crystal	1.5 × 10 ⁻⁴	150	-	0.36	169
7	3,4-Bis(octyloxy)benzyl phosphonic acid (6e)	Free -OH group of phosphonic acid	150 °C	-	Pellet	8.0 × 10 ⁻²	140	-	0.09	170
Anhydrous Proton Conduction in POMs										
<i>Intrinsic Approach</i>										
1	H ₃ PW ₁₂ O ₄₀ ·6H ₂ O	Structural protons	~420 °C	-	Pellet	1 × 10 ⁻⁵	180	-	-	171
2	H ₆ KNa ₂ (H ₂ O) ₁₀ [Co(H ₂ O) ₂ (SINb ₈ O ₅₄)]·15H ₂ O (dehydrated blue)	Structural protons and coordinated water	MeOH, ACN, DMF, DMSO	-	Pellet	6.40 × 10 ⁻⁶	25	Retained	-	114
3	[(H ₂ O) _{0.03} @K ₆ (H ₂ O) ₁₂]H _{4.45} [PV _{7.45} Mo _{4.55} O ₄₀]·11H ₂ O	Structural protons and coordinated water	~330 °C	-	-	6.90 × 10 ⁻⁷	-24	-	0.44	115
4	Imid ₃ PW ₁₂ O ₄₀ ·4H ₂ O	Imidazolium cation	>500 °C	-	-	3.36 × 10 ⁻⁶	-1	-	0.50–0.26	56
5	Na ₆ (NH ₄) ₁₀ H ₈ [W ₁₄ Co ^{IV} O ₆₁](W ₃ Bi ₆ Co ^{III} ₃ (H ₂ O) ₃ O ₁₄)] [α-BiW ₉ O ₃₃] ₂ ·ca. 38 H ₂ O	Structural protons, ammonium cation, and coordinated water	~300 °C	-	Pellet	4.9 × 10 ⁻⁷	145	Retained	0.67	172

^aAbbreviations: TzH, triazolium; H₂dmbim, protonated dimethylbenzimidazole; ImH₂⁺, protonated imidazole; Tz, triazole; Im, imidazole; His, histamine; Hq, hydroquinone; Him, protonated imidazole; FA, formamidinium; Hmim, 2-methylimidazole; EIMS, 1-(1-ethyl-3-imidazolium)propane-3-sulfonate; HTFSA, N,N-bis(trifluoromethanesulfonyl)amide; NAPI, N-(3-aminopropyl)imidazole; SA, sulfate acid; dema, diethylmethylammonium.

be excellent candidates for achieving intrinsically high superproton conductivity in COFs, even under anhydrous conditions, and could eliminate the leaching concerns associated with the extrinsically doped COF materials.

Apart from the 2D COF materials, 3D COFs are also highly promising for their diversified pore structures that could facilitate efficient proton transportation via well-directed pore channels. Moreover, such structures could assist the accommodation of extrinsically incorporated proton carriers in the pore channels to facilitate the smooth transfer of protons even in the absence of humidity (under anhydrous conditions).¹²² 3D COFs could be advantageous in holding the extrinsically incorporated protonic species, compared to its 2D counterparts, through pore confinement and thus could eliminate the leaching issue of protonic guests to some extent. Despite possessing such fascinating structural features, 3D COFs are underexplored in the domain of proton conduction applications. However, recently a 3D COF material encapsulated with etidronic acid (**etidronic acid@COF-300**) was fabricated into a membrane that exhibited a superprotonic conductivity of 0.650 S/cm at 90 °C under 100% RH.¹²² Unfortunately, this material did not exhibit proton conduction under anhydrous conditions. In the context of anhydrous proton conductivity, recently Zheng and co-workers reported a thiazazole-based 5-fold-interpenetrated 3D COF material (**NUST-28**) that exhibited anhydrous proton conductivity of 8.4×10^{-2} S/cm at 120 °C post phosphoric acid doping.¹²³ It is quite striking to note that, to date, only one 3D COF material (**NUST-28**) has been noted to serve as an anhydrous PEM material, and thus huge research investments are deserved for further exploration on these materials as efficient future anhydrous proton conductors.

HOFs and POMs are highly less explored in the domain of anhydrous proton conductivities, with so far only 7 reports on HOFs and only 5 reports on native POMs. For both of them, the anhydrous proton conductivities mostly rely on a few intrinsic sources such as nonvolatile inorganic acid like H_3PO_4 ; organic acids like squaric acid and succinic acid; N-rich heterocycles like imidazole/imidazolium cations, etc. Thus, a large number of unexplored nonvolatile organic/inorganic species such as N-rich heterocycles like triazoles, tetrazoles, histamines, benzimidazoles, etc. or organic acids such as triflic acid, phytic acid, etc. could be incorporated in these frameworks either intrinsically (preferred) or through extrinsic methods to achieve anhydrous superprotonic conductivities. Moreover, *in situ* incorporation of ionic liquids such NAPI, EIMS, HTFSA, etc. into the channels of these unexplored crystalline platforms could also result in attaining high anhydrous conductivities.

Interestingly, in the majority of anhydrous extrinsic proton-conducting materials (specifically COFs), phosphoric acid (PA) is used as the main dopant (16 out of total 22 reports), which could be ascribed to the proton relay or switching mechanism in neat liquid PA being responsible for attaining such high proton conductivity.¹²⁴ Moreover, the strong, polarizable hydrogen bonds (three free $-\text{OH}$ groups) in PA produce coupled proton motion, with noticeable protic dielectric response, that aids in the establishment of frustrated networks of extended H-bonded matrices, resulting in ultrahigh superprotonic conductivities, even under anhydrous conditions. In fact, the proton mobility in PA is comparable to that of the aqueous systems with a higher degree of self-dissociation, giving rise to increased concentrations of intrinsic

proton carriers (7%) as compared to the water ($1.0 \times 10^{-5}\%$). Moreover, recently, in 2022, Jiang and co-workers reported exceptionally high anhydrous conductivity (1.91×10^{-1} S/cm at 160 °C) in porous COFs (**$\text{H}_3\text{PO}_4@\text{TPB-DMeTP-COF}$**) having hexagonal mesopores extrinsically impregnated with continuously H-bonded PA molecules.¹²⁵ It is important to mention that their work attained the highest anhydrous conductivity value thus far achieved by any crystalline materials and/or composites and exceeded the conductivity achieved by commercial Nafions under hydrous conditions.⁶ However, the intrinsic incorporation of these PA molecules (with continuous hydrogen-bonded arrays) into the crystal structures of these materials (MOFs, COF, HOFs, and POMs) is still unexplored and might be an interesting approach with high potentiality. The intrinsic pre-installation should not only enhance the inherent conductivities and assist the structure–function correlation (through structural visualization) but also reduce the chances of acid leaching at the electrodes and should contribute toward a decreased risk of fuel crossover that typically affects the output voltages (OCV) in real H_2/O_2 fuel cells.

5.2. Mechanical Stability. In the context of anhydrous conductivity, the thermal as well as mechanical stability of the solid-state electrolytes plays a pivotal role since it affects the performance of the materials under practical/real-time high-temperature ambiances (>100 °C). Despite significant improvements that have been achieved in enhancing the thermal stability of MOFs, the issues of enhancing the mechanical stability have not received sufficient considerations to date. In fact, during pellet preparation and fuel cell operation, the samples typically undergo cyclical stress/strain and mechanical pressures that makes the mechanical properties as essential concern when fabricating real-time PEM materials. To ameliorate the situation, organic linkers functionalized with linear alkyl polymeric chain can be utilized to fabricate new types of MOFs with upgraded mechanical properties. Moreover, the integration of these MOF materials with various polymers is an important tool to enhance their mechanical stability under high-temperature conditions. Hence, the *in situ* incorporation of linear polymers such poly(vinyl) alcohol (PVA), polyaniline (PA), poly(acrylic acid) (PAA), etc. within the channels of MOFs should not only assist the continuous proton hopping intrinsically but also boost the MEA performance by enhancing the mechanical stability. Here, it is important to mention that COF materials definitely score over MOF materials in this respect, since they possess higher thermal as well as mechanical stability while maintaining excellent conductivities at the same time, making them appropriate for real-time usage. That is the advantage being “all-organic”, suitable for easy processing in thin films or membranes. However, HOFs are made of simple molecular tectons and generally noted to exhibit poor mechanical stability due to the weak and flexible H-bonding interactions which eventually lower their stability even below than that of MOFs (built of coordinative framework interconnectivities). To address this issue, fabricating multicomponent-based HOFs through strategic selection of two types of molecular tectons, one with polymer functionalization and the other containing rigid organic backbones (restricting their free rotations) that are capable of forming strong and directional H-bonds along with several supramolecular interactions, could be a reliable option. In addition, the integration of HOF materials with organic polymers to form the mixed matrix membranes

(MMMs) could also be an effective option to enhance their mechanical endurance. Similarly for POMs, the integration of heteropolyacids (conjugate acids of POMs) with one or multiple proton-conducting polymers might improve their mechanical properties even under high-temperature anhydrous conditions. This has become evident from a recent report in 2022 by Li and co-workers, where the integration of a Keggin-type POM ($\text{H}_3\text{PW}_{12}\text{O}_{40}$ (PW)) with two types of organic polymers, (poly(terphenyl piperidine) (PTP), polyvinylpyrrolidone (PVP), not only offered excellent anhydrous conductivity but also demonstrated high mechanical stability, with a break strength of 7.0 ± 0.8 MPa and a storage modulus of 67 MPa, suggesting that both agents impart excellent mechanical durability on POM platforms.¹¹⁸

5.3. Durability. This is an important criterion that underlines the potentiality of these materials for successful real-time implementation as PEMs. In the majority of cases, there exists a trade-off between the high conductivity and the durability, a critical issue that needs to be considered for underlining the viability of such materials as real-time anhydrous conductors. Most of the MOFs that exhibit high/ultrahigh superprotonic anhydrous conductivities do suffer from the durability issues. As a matter of fact, the durability factor has not been investigated properly for the majority of MOFs in the domain of anhydrous conductivity both at high temperatures and at sub-ambient conditions, and whenever it was examined they exhibited poor durability. For example, in 2012 Kitagawa and co-workers reported $[\text{Zn}(\text{HPO}_4)(\text{H}_2\text{PO}_4)](\text{ImH}_2)_2$ that exhibited superprotonic conductivity of 2.5×10^{-4} S/cm at 130 °C for only 12 h but not beyond that. Similarly, in another report by the same group in 2014, a templated framework, $[\text{Zn}(\text{H}_2\text{PO}_4)_2(\text{HPO}_4)] \cdot (\text{H}_2\text{dmbim})_2$, was shown to exhibit a conductivity of 2×10^{-4} S/cm that could be retained only for 3 h. Again, Liu and co-workers in 2022 reported NNU-66a, which showed anhydrous conductivity of 1.94×10^{-3} S/cm at 180 °C that was perceived for roughly 24 h. The general lack of enough efforts to analyze/enhance the poor durability index of these frameworks under anhydrous conditions is a major obstacle that significantly hampers their real-time applications. The rational design of frameworks with strong coordination networks, adopting different strategies such as choosing organic ligands with hydrophobic backbones, insertion of pillars flanked with proton carrier functionalities via pore space partition (splitting a large channel into a number of smaller one) for framework stabilization, an interpenetration approach, or constructing the frameworks in accordance with Pearson's HSAB principle, might contribute toward enhancing the durability in performance of MOFs. Thus, long-term durability testing could be a regular practice to move MOFs a step forward for practical implementation in fuel cell technology, as was recently demonstrated by us with a 1D framework showing consistent conductivity for 5 days under extreme fuel cell operation conditions.¹⁴

In the context of COFs, although the durability factor is less explored, a phosphoric acid-doped COF material, $\text{H}_3\text{PO}_4@$ TPB-DMeTP-COF, exhibited ultrahigh conductivity as high as 1.91×10^{-1} S/cm under anhydrous conditions at 160 °C with durability maintained for 20 h, which in turn again questioned these materials' survival ability.¹²⁵ Another recent report in 2022 by Du and co-workers studying H@TPT-COF revealed high-temperature ultrahigh anhydrous conductivity (1.27×10^{-2} S/cm at 160 °C) that could be retained for 100 h.¹⁰⁷

Thus, it successfully balanced the trade-off between high conductivity and durability, which urges further development in COF materials for enhanced framework robustness through strengthening of the covalent linkages, pre-orientation of organic building blocks through efficient locking linkages by manipulating the inherent properties of organic precursors like steric tuning, hydrophobic engineering, etc. that could maintain a balance between high conductivity and durability.

It is of no surprise that, to date, the durability has never been investigated for the less explored HOFs and POMs as anhydrous proton conductors. Thus, strategic designing of stable HOFs with robust hydrophobic organic backbones like hexaphenylbenzene (HPB), metal-free porphyrin units, etc. and functionalizing them with strong and well-aligned H-bonding motifs such as diaminotriazinyl (DAT), $-\text{PO}_3\text{H}_2$, $-\text{SO}_3\text{H}$, $-\text{COOH}$, and $-\text{NH}_2$ via single-component/multi-component synthesis strategies could be an excellent approach to enhance the robustness, viability, and eventual durability of these materials. In the case of POMs, the only way to enhance the durability is by polymeric integration to obtain hybrid composites of heteropoly acids that could help in attainment of high conductivities with enhanced durability.

5.4. Membrane Fabrication. To satisfy the practical agenda of PEM materials in the domain of anhydrous fuel cells, balancing the critical trade-off among mechanical strength, chemical robustness, and thermal stability with high proton conductive performance is absolutely necessary. It is noted that although polymers such as PBI, SPEEK, PVPA, PES, SPES, etc. are highly flexible and processable and possess remarkable mechanical strength with thermal stability, they often suffer from poor proton conductive performances and are associated with leaching problems. Hence, the strategic integration of these polymeric matrices with crystalline materials (as fillers) for the formation of MMMs would serve as an excellent alternative, since it would combine the advantages of both the polymeric matrix and the inorganic crystalline materials for detailed structural guidelines. In the past decade, such sorts of composite membranes have been repeatedly synthesized through rational integration of tunable porous materials, specifically MOFs and COFs, with proton-conducting polymers such as SPEEK, PVPA, PEI, PBI, etc. to achieve significant improvements in the overall stability (chemical as well as mechanical) along with upgraded proton conductivities under hydrous conditions.⁹⁴ However, in the domain of anhydrous proton conductivity, the design and investigation of these MMMs as PEM materials is quite rare and limited to very few reports, specifically with MOFs only. For example, as mentioned earlier, Compan and co-workers synthesized a hybrid membrane based on PBI and a zinc/cobalt bimetallic ZIF (PBI/ H_3PO_4 -ZIF-mix), the oxidative, thermal, and mechanical stability of which (with enhanced elongation at break and material toughness) got significantly enhanced after the membrane fabrication and attained ultrahigh superprotonic anhydrous conductivity of 9.1×10^{-2} at 200 °C, comparable to that attained by with Nafion under hydrous conditions at lower temperatures (~ 85 °C).¹⁰¹

However, with the COF materials, despite containing organic backbones, the concept of membrane fabrication is still unexplored. Nevertheless, Jana and co-workers in 2023 reported a COF membrane composite with PBI as polymeric matrix that resulted in the formation of a stable membrane, *m*-PBI-P@MCOF-10%, with high thermal, mechanical, as well as oxidative stability and ultrahigh anhydrous superprotonic

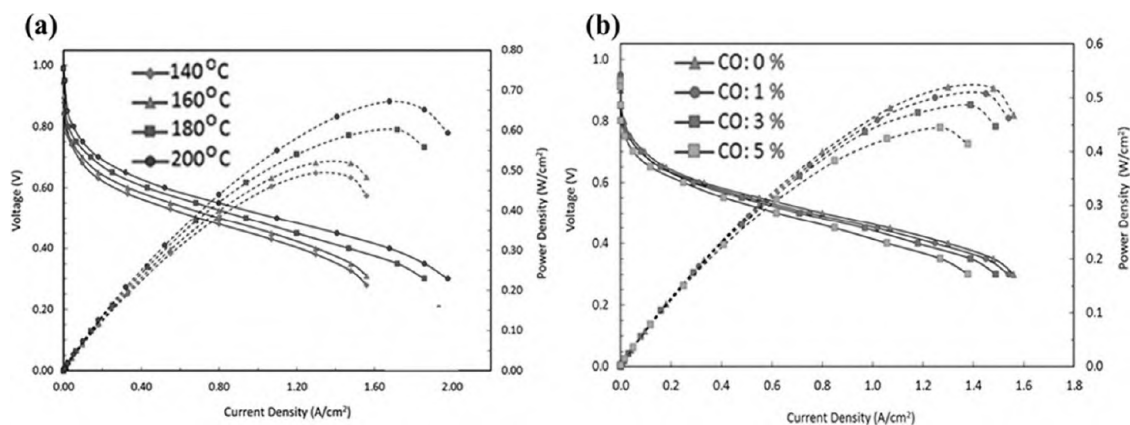


Figure 15. (a) Effect of working temperature on operation of HT-PEMFCs. (b) Effect of CO contents on HT-PEMFCs operating at 160 °C under anhydrous conditions. Reproduced with permission from ref 129. Copyright 2018, Elsevier.

conductivity (2.33×10^{-2} S/cm at 160 °C).¹²⁶ This should instigate further advanced research on COF materials as nanofillers in MMMs for achieving anhydrous conductivity. In the context of HOFs, it is highly surprising that, although these materials are highly processable and purely organic in nature, they have never been integrated with proton-conducting polymers for membrane fabrication to achieve high proton conductivities. Moreover, as stated before, membrane formation with HOFs could significantly enhance their thermal as well as mechanical endurance, making them potential solid-state conductors in anhydrous fuel cells. Coming to POM materials, they were also noted to be integrated with the polymers or polymeric mixtures to fabricate membranes that could be utilized directly in fuel cells. For example, Jiang, Xiang, and co-workers in 2010 assembled a VIM-30 wt% HPW/MCM-41 composite membrane by combining $\text{H}_3\text{PW}_{12}\text{O}_{40}$ (abbreviated as HPW) and mesoporous MCM-41 silica,¹²⁷ which exhibited ultrahigh superprotonic anhydrous proton conductivity of 4.5×10^{-2} S/cm at 150 °C, accredited to the continuous and smooth proton-transfer pathway via the Keggin-type HPW cluster inside the mesoporous silica structure.¹²⁵ However, one should be looking for the preparation of a defect-free membrane, which is challenging but required for better performance in PEMFCs.

In the context of fuel cell applications, it was noted in the previous section that only in three cases (NNU-66a@PVDF, CS/A-6+B-15, and SPES-SO₂NH-Cr-MIL-101) MOF-based membranes were used for MEA construction, and in all the other eight cases (five MOFs/CPs, two COFs, and one POM) the powdered samples were either sandwiched between the electrodes or installed in the electrode setup in the form of pellets. However, these pellets are not defect-free (in fact, it is too difficult to make them defect-free). Although such studies on pellet-based MEAs could provide us a clue toward future directions, they essentially could not assess the true potential of those MEAs. Ideally, the MEAs should be in the form of films or membranes (as thin as possible) without any defects. Hence, fabrication and deployment of thin films or membranes based on these crystalline materials (MOFs, COFs, HOFs, and POMs) are highly encouraged for evaluating the actual potential of these materials as PEMs in the fuel cells.

5.5. CO Tolerance Testing on PEMs and Scope of Improvements. Fuel processing is an aspect of utmost importance that determines the future of the fuel cell technology and its widespread global deployments. As

mentioned earlier, at lower temperatures, CO (present as an impurity in H₂ gas streams) binds strongly with the active sites of the catalysts (Pt-CO), which inhibits H₂ gas streams from reaching the catalyst surface at the anode side and causes remarkable deterioration in the fuel cell performance by virtue of CO toxicity or CO poisoning effects. However, such poisoning effects could be immensely reduced at higher temperatures since the thermodynamics of CO adsorption are highly disfavored at such conditions. In 2014, Li and co-workers investigated the effect of CO poisoning on traditional solid-state polymer electrolytes in the temperature range from 125 to 200 °C and assessed that the increment of temperature is associated with enhanced CO tolerance.¹²⁸ Although HT-PEMFCs exhibit superior performance in terms of CO tolerance, the increased working temperature might damage the cell components because of the high electrochemical potential and increased rate of carbon corrosion.^{129,130} Hence, it is necessary to determine the optimum temperature at which the highest performance could be secured. In this regard, Devrim and co-workers in 2018 investigated the effects of temperature (140–200 °C) and poisoning impurities (CO) on the operation of a fuel cell with a PA-doped PBI membrane as the electrolyte material.¹²⁹ In the temperature variation experiment, it was noted that, at 0.6 V constant potential, the current density increased from 0.29 A/cm² at 140 °C to 0.52 A/cm² at 200 °C (Figure 15a). Thus, it again became evident that, at higher operational temperatures, the PEMFCs performed better on account of enhanced electrode kinetics; however, at such working conditions the lifetime of the cell was decreased. Hence, considering the inevitable deformation of the cell connections and gaskets at higher temperatures, the operational temperature of the fuel cell was optimized to 160 °C, which would meet both ends in achieving higher CO tolerance as well as attaining increased cell performance with minimal deformations. Next, to interrogate the effects of CO on its performance at the optimized temperature (160 °C), the HT-PEMFCs were fed with varying concentrations of CO (1–5 vol%) in the anode gas stream. According to the performance curve obtained at 0.6 V, it was noted that the current density decreased from 0.33 to 0.31, 0.29, and 0.25 A/cm² for H₂ streams containing 0, 1, 3, and 5 vol% of CO, respectively (Figure 15b). Thus, with increase in the volume percentage of CO, the current densities progressively showed decreasing trends. As can be seen from Figure 15b, although at lower current densities the effect of CO poisoning is not much

pronounced, at higher current densities the active sites of the catalysts become insufficient for the electro-oxidation of H₂ at the anode, which eventually experiences a pronounced performance drop. After careful analysis, it was noted that increasing the CO concentration beyond 3 vol% caused a marked decrease in the cell performance, associated with such types of traditional amorphous organic solid-state polymer electrolytes.

In the context of crystalline proton-conducting MOFs, COFs, HOFs, and POMs as anhydrous electrolyte materials in HT-PEMFCs (as discussed in this Perspective), strategic screening of operational temperature (in the high-temperature window) and detailed assessment of the effect of CO impurities on the membranes' effective performance (current density) could be an innovative approach to discover the actual durability of fuel cells to minimize the deformation on the cell components, PEMs, cell connections and gaskets under operational conditions. Such rational testing with these crystalline anhydrous electrolytes (MOFs, COFs, HOFs, and POMs) in PEMFCs by varying the concentrations of CO impurities in the H₂ gas at the optimized operation temperature would give us an idea about the extent of CO toxicity and the CO tolerance of the membrane materials made out of those particular crystalline platforms.

5.6. Performance Evaluation of Anhydrous Proton Conductors with Fuel Cell Test Stands. Fuel cell test stations are important for research and development purposes, since they can replicate the real-world operational conditions through careful regulation of the environmental factors (temperature, humidity), alter gas (fuel) compositions, and examine the long-term durability/longevity of PEMs through accelerated stress testing and cyclic experiments etc. before they are actually utilized for regular operation in large units. Ideally, in PEMFC test stations the following factors are primarily evaluated: (i) gross performance of fuel cells (including *I*-*V* characteristics and power outputs), (ii) durability and lifetime testing, (iii) environmental testing (including temperature and humidity controlling), (iv) fuel and oxidant supply testing (with flow and pressure controllers), (v) data acquisition and monitoring, and (vi) safety and protection assessment (leak detection and emergency shutdown). Although quite a few companies could provide such large setups, integrating all the testing units into portable bench management of PEM fuel cells would aid research and university educational programs.^{173,174} The anhydrous proton-conducting crystalline materials with impressive conductivities in the ultrahigh superprotonic regions discussed in this Perspective could thus find a way to be implemented practically after assessment of their performances with such testing systems, with the anticipation of a smooth transition from academia to industry.

5.7. It Is Important to Address the Question, "How dry is anhydrous?". From the applied viewpoint, anhydrous fuel cells should operate at temperatures well above 100 °C without any need for humidification. This is mostly in order to overcome the CO adsorption issue at elevated temperatures to combat the dilemma of CO toxicity and to simplify the water management system during cyclic operations, in addition to several other advantages as pointed out in the [Introduction](#) section. For example, as stated therein, polymeric blends like PBI/H₃PO₄, PEO/H₃PO₄, PEI/H₃PO₄, Nylon/H₃PO₄, PEO/PMMA/H₃PO₄, etc. were used as anhydrous proton conductors earlier, though the reported conductivities were

mostly below 100 °C within the range of 10⁻³–10⁻⁶ S/cm, ascribed to their chemical as well as mechanical instability beyond 100 °C.¹⁶ In another report, PBI/H₃PO₄ blends were considered as HT-PEMs within a temperature range of 60–200 °C; however, minimal humidity (in the range of 5–30% RH) was applied to attain such superprotonic conductivities.¹⁷⁵ Thus, these blends may *not* be considered as absolute anhydrous proton conductors. It is essential to report the drying processes of the SSPCs before deploying them in anhydrous proton conduction measurements (for example, dry glovebox, molecular sieves, Ar/N₂ atmosphere, vacuum drying, drying at elevated temperature, etc.). Also, when anhydrous conductivity measurements are carried out below 100 °C, care must be taken in introducing inert gases into the measurement chambers in order to eliminate traces of humidity.

In the context of crystalline regimes, a certain number of MOF-based reports prevail in the literature where good proton conductive performance was attained at high temperatures in the presence of high relative humidity. For example, in 2017, Stock *et al.* reported a 3D porous Al-MOF (Al-MIL-68-Mes) that exhibited a proton conductivity of 1.1 × 10⁻⁵ S/cm in the simultaneous coexistence of high temperature (130 °C) as well as high humidity (100% RH).¹⁷⁶ Likewise, they reported a Ga-based MOF revealing a conductivity of 1.0 × 10⁻³ S/cm at 130 °C, accompanied by high relative humidity (100% RH).¹⁷⁷ Along the same line, Vivani and co-workers reported a Zr-based phosphonate MOF that exhibited high-temperature proton conductive performance (1.0 × 10⁻³ S/cm at 140 °C) in the presence of 95% RH.¹⁷⁸ Nevertheless, it is important to mention that all the examples discussed, tabulated, and analyzed in this Perspective typically exhibit proton conductivities under absolute anhydrous conditions in all the temperature domains (including high temperature as well as low to intermediate temperature). For example, as mentioned earlier, in 2016, Zhang, Xiang and co-workers reported an imidazole-templated framework, FJU-25-Fe, that exhibited conductivities of 5.15 × 10⁻⁵ and 1.30 × 10⁻⁴ S/cm at sub-zero (-10 °C) and at high temperature (90 °C) under purely anhydrous conditions through N₂ flushing into the measurement chamber to remove the existence of even trace moisture.⁹⁸ Along the same line, in 2022, Dekura, Mori, and co-workers reported a 3D phosphate-based HOF (1) that exhibited an intermediate temperature (77 °C) superprotonic conductivity of 1.31 × 10⁻³ S/cm across the crystallographic *c*-axis solely under anhydrous conditions.¹¹⁰ Needless to say, a majority of the materials discussed here show anhydrous conductivity at temperatures above 100 °C, but only a few materials report anhydrous conductivity at intermediate and sub-zero temperatures.

6. COMPARATIVE ANALYSIS OF FOUR TYPES OF CRYSTALLINE ANHYDROUS PROTON CONDUCTORS

In this section, we intend to analyze and compare the four types of crystalline platforms—MOFs, COFs, HOFs, and POMs—discussed in this Perspective to evaluate their overall performances in the domain of anhydrous proton conduction. Considering the total number of literature reports so far published on anhydrous proton conduction, the maximum number of reports have mostly focused on MOFs (39), followed by COFs (22), whereas the reports on HOFs (7) and POMs (5) are significantly less in number, leaving a huge scope for further exploration ([Figure 16a,b](#)). For anhydrous

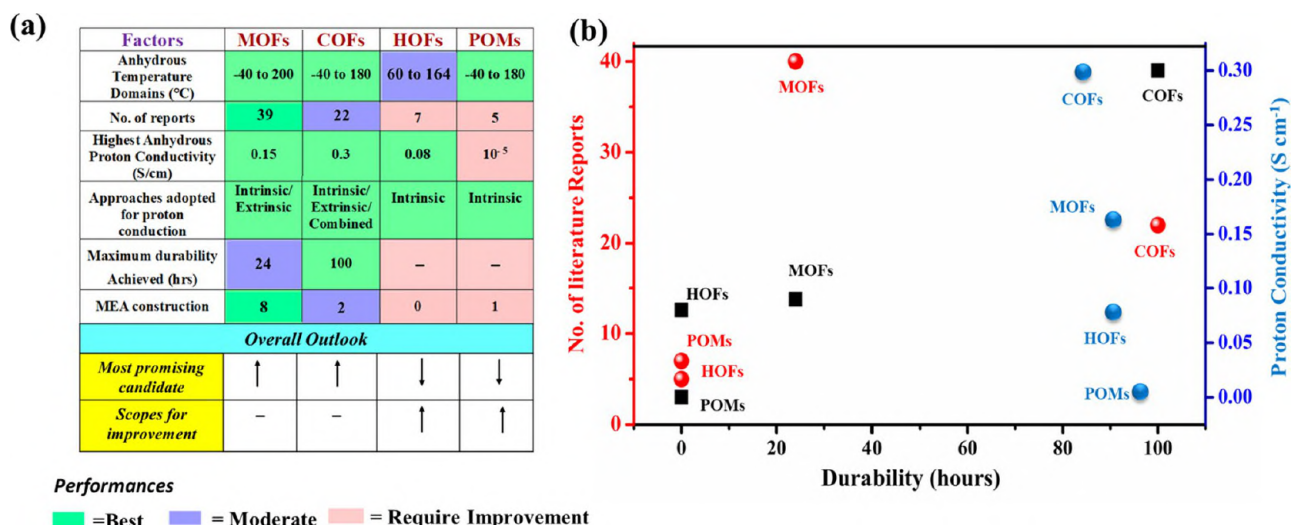


Figure 16. (a) Checklist depicting the overall performance of the MOFs, COFs, HOFs, POMs with all essential features in the domain of anhydrous proton conduction. (b) Comparison of crystalline platforms based on the number of published reports, maximum anhydrous proton conductivity achieved and durability.

proton conductivity measurements, the temperature domain is highly crucial since it plays an essential role in evaluating the practicality of SSPCs under different ambiances. It is pointed out that, although MOFs, COFs, and POMs witnessed anhydrous proton conductive performances from sub-zero to high-temperature conditions, HOFs typically exhibits anhydrous proton conductivity from the intermediate to high-temperature domain, which in turn limits their practicality in the context of sub-zero anhydrous proton conduction. Further, considering the highest anhydrous conductivity achieved so far, COFs ($\sigma = 3 \times 10^{-1}$ S/cm) and MOFs ($\sigma = 1.55 \times 10^{-1}$ S/cm) run ahead of HOFs ($\sigma = 8 \times 10^{-2}$ S/cm), whereas POMs ($\sigma = 1 \times 10^{-5}$ S/cm) significantly lag behind from the other three crystalline platforms, which thus creates another huge scope for further improvements. Graphical comparisons of the performances of these materials with key structural features are depicted in Figure 16.

Overall, these frameworks possess some inherent pros and cons those need to be taken into consideration while designing anhydrous proton conductors, as listed below:

6.1. MOFs. Pros. They possess high structural tunability and fascinating framework architectures, leading to superior design ability as *intrinsic* anhydrous proton conductors with the aid of detailed structural elucidation for plausible proton conduction pathways through single-crystal X-ray analysis. Moreover, MOFs exhibit permanent porosity with high surface area that allow for extrinsic loading of nonvolatile/high-boiling proton carriers into the pore spaces through well-established postsynthetic modification procedures, that in turn facilitate the smooth hopping of protons in the absence of humidity. Further, in order to validate the real-time practicality of these materials in anhydrous fuel cells, a handful of MOFs have been successfully deployed as PEM materials in MEA construction and yielded excellent output voltages (OCV values), as evident from the literature reports (8 reports).

Cons. Typically, due to the presence of coordination bonds in MOFs, they exhibit poor mechanical strength when compared to that of COFs (built of stronger covalent bonds). On a similar note, MOFs are generally noted to exhibit moderate durability for anhydrous proton conduction measurements (with the maximum durability achieved to date

being 24 h), which is indeed a drawback and needs some improvements. In addition, the high porosity of MOFs makes them susceptible to the problem of fuel crossover, that in turn can reduce the efficiency of proton conduction.

6.2. COFs. Pros. They are amenable to controllable synthesis strategies with structural predesignability and tailorable functionalities that are beneficial for effective fabrication of proton-conducting COFs.

Akin to MOFs, they are also porous, with high surface area that allows for extrinsic loading of nonvolatile proton carrier guests to improve proton transfer under completely anhydrous conditions. Further, COF skeletons are built of strong covalent bonds that improve their thermochemical stability as well as mechanical strength, a criterion essential for MEA construction. Moreover, COF-based PEMs exhibit comparatively better durability (with maximum 100 h durable performances being achieved to date) with respect to the other three crystalline architectures (MOFs/HOFs/POMs). Besides, COFs, being purely organic in nature, are highly compatible with organic polymers for membrane fabrication as well. In the context of MEA construction under anhydrous conditions, COFs are moderately explored, with literature reports limited to 2 examples to date.

Cons. It is difficult to get the single crystals in COFs (compared to MOFs and HOFs); hence, the detailed structural elucidation for visualization of plausible proton conduction pathways is often difficult. In the context of anhydrous proton conduction in COFs, although extrinsic loading strategies (nonvolatile carriers) are heavily explored, the strategy of attaining superprotonic anhydrous proton conductivities with intrinsic proton sources is left underexplored. In addition, because of extrinsic impregnation of proton carriers (nonvolatile and high-boiling), sometimes they suffer from weak host–guest interactions, leading to external leaching of loaded guest proton carriers. Further, COFs are highly porous in nature and thus are prone to the problem of fuel crossover which can reduce the overall performance of HT-PEMFCs.

6.3. HOFs. Pros. Due to the rich library of organic synthons available in the literature (with functionalized proton donors, acceptors, and hopping sites), HOFs offer fascinating structural

diversities. H-bonding constitutes an essential component in building HOF skeletons, and the fundamental feature for attaining high proton conductivity in SSPCs is the presence of continuous H-bonded networks; hence, it is obvious that they offer great promise for providing ultrahigh conductivity by virtue of their intrinsic H-bonded matrices. Moreover, they can be scaled up easily under mild synthesis conditions, offer feasibility for growth of bigger single crystals for structural elucidation, and possess healing properties as well. Akin to the COFs, being made of pure organic backbones, HOFs also have high compatibility toward organic polymers and thus offer an easy way to construct PEMs, though they are not well-explored to date.

Cons. They suffer from stability issues due to the weak and flexible nature of H-bonding interactions. One of the major drawbacks of HOF material is their very poor mechanical stability (as compared to MOFs and COFs), which could be improved by integrating them with polymers, although the aspect of membrane fabrication with HOFs remains surprisingly unexplored to date. Durability could be another critical issue (none of the anhydrous proton-conducting HOFs exhibited durability to date) that requires improvement. In addition, HOFs tend to crystallize in different polymorphs at the same time, which can induce problems with phase purity in HOF synthesis. Unfortunately, none of the HOF materials have been tested in real-time potentiality checks through MEA construction under anhydrous conditions, which thus leaves a huge scope for further exploration and investigation.

6.4. POMs. Pros. Similar to the other three crystalline platforms, POMs also possess a highly structurally tunable nature with oxygen-rich exterior interfaces that facilitate the spontaneous long-range transfer of the intrinsic structural protons, which is indeed important to achieve superprotonic conductivity. The most exciting factor about POMs is their aqueous medium synthesis, which not only follows green chemistry principles but also leads to occupation by a high number of proton sources inside the cavities (e.g., organic azoles, inorganic acids, etc.). Moreover, the huge number of strong metal–oxygen bonds provides enormous thermal stability, thus fulfilling one of the major prerequisites of anhydrous proton conductors.

Cons. The major challenge for POMs as anhydrous proton conductors lies in the retention of the intrinsic proton source, lattice water, within the framework, which is prone to be liberated at higher temperatures. To improve the water retention capacity at higher temperatures, integration of POMs with polymers/plasticizers is being explored; however, from the anhydrous perspective, there is still huge room for further exploration. Similar to HOFs, durability of anhydrous POMs is another critical factor that is mostly underappreciated. It is also very surprising that, despite their well-resolved single-crystal structures, exploration of the proton conduction pathways *via* SC-XRD is very limited (as in most cases structural protons such as the protons in HPA units that are responsible for conduction are difficult to locate in a difference Fourier map), and there has been none in the anhydrous scenario. Thus, further research could be progressed toward these directions. Among the very few reports on anhydrous proton-conducting POMs, one has been tested via MEA construction; however, it is still in the infancy stage and thus requires extensive propulsion for real-time implementation in anhydrous fuel cells.

Thus, it is noted that although all the crystalline materials have their respective advantages as well as disadvantages (challenges), from an overall outlook (Figure 16a,b) it is evaluated that so far MOFs and COFs have proven themselves as the most promising ones (based on the comparison chart and performance graph), whereas the HOFs and POMs (possessing immense potential as SSPCs) leave a huge scope for further exploration and improvement in the domain of anhydrous proton conduction.

7. CONCLUSION

On a concluding note, in this Perspective we have summarized the exponential progress made with the crystalline platforms in the domain of anhydrous proton conduction, that are divided into four categories—MOFs, COFs, HOFs, and POMs—based on their structural backbones and framework engineering. In order to acquire high anhydrous proton conductivities, all the crystalline platforms (MOFs/COFs/HOFs/POMs) must fulfill two prior criteria: (a) They must maintain highly extended H-bonded networks offered by proton carriers (other than water molecules). In order to maintain the proton conduction route completely intact for facile proton migration under anhydrous condition, the intrinsic pre-installation or extrinsic incorporation of various nonvolatile, high-boiling proton carriers such as heterocyclic organic molecules like imidazoles, triazoles, tetrazoles, and benzimidazoles; high-boiling organic hydroxyls like hydroquinone; nonvolatile amino acids such as histamines; or nonvolatile inorganic acids or their conjugate bases such as H_3PO_4 , H_2PO_4^- , HPO_4^{2-} , and H_2SO_4 inside the pores of the framework backbone is highly crucial that plays a pivotal role for improving proton transfer even in the absence of water molecules. (b) The given material must be stable under the experimental measurement conditions.

The handful of crystalline materials that have been fabricated based on the above-mentioned prior criteria have been noted to attain conductivities ranging from the superprotonic region ($\geq 10^{-4}$ S/cm) up to the ultrahigh superprotonic zone ($\geq 10^{-1}$ S/cm) under anhydrous conditions in the past decade and thus proved themselves as excellent alternatives to the traditionally used state-of-the-art Nafion or PBI/ H_3PO_4 polymers that mostly work under hydrous conditions. As can be seen from Table 2, many of these crystalline materials exhibit anhydrous conductivities in the range of 10^{-2} – 10^{-1} S/cm, which can also be achieved with Nafion but only in its hydrous state. When it comes to comparisons with other anhydrous proton-conducting materials, not many materials appear in the picture to be compared. However, as stated in the Introduction section, only a few H_3PO_4 -blended amorphous polymers and crystalline phosphates/phosphonates of tetravalent metals like Zr(IV) have been tested as anhydrous proton conductors, with typical conductivities in the range of 10^{-3} – 10^{-6} S/cm below 100 °C and 10^{-5} – 10^{-8} S/cm above 100 °C. This clearly shows the great potential of crystalline MOFs, COFs, HOFs, and POMs as anhydrous proton conductors for plausible usage as PEMs in the near future, largely solving the bottleneck issue of water management systems in Nafion-based hydrous PEMFCs. We have provided a clear timeline representing the evolution of MOFs as crystalline anhydrous proton conductors since the first report in 2009 by Shimizu and Kitagawa et al., followed by the subsequent rise of anhydrous proton conductive HOFs, COFs, and POMs in 2012, 2014, and 2019, respectively. However, considering the arrival of a relatively larger number

of reports on anhydrous proton conductivities, specifically with MOFs and COFs, two separate timelines regarding their individual advancements to date are also provided for quick visualization by readers. The crystalline MOFs and COFs are further sub-divided into “intrinsic” and “extrinsic” anhydrous conductivities based on the origin and installation of proton sources and/or proton carriers that are responsible for continuous proton hopping to yield high conductivities. Moreover, for MOFs, the intrinsic anhydrous conductivities are further categorized based on their working temperature (sub-zero temperature, i.e. -10 to -40 °C, and high temperature, ~ 100 to 200 °C), whereas the extrinsic conductivity in MOFs is also sub-classified based on the incorporation/integration of nonvolatile proton sources/carriers or proton-conducting polymers. In the context of HOFs and POMs, they are primarily noted to exhibit intrinsic anhydrous conductivity and attract much more attention for being utilized on practical scales. All the developed crystalline anhydrous conductors are summarized and tabulated in Table 2, based on the strategies adopted for proton conduction as well as other prominent features such as working conditions, activation energies, stability (thermal and chemical), etc. that are cooperatively responsible for attaining ultrahigh anhydrous conductivity in these materials. So far, the $\text{H}_3\text{PO}_4@ \text{TPB-DMeTP-COF}$ reported recently, in 2024, by Jiang and co-workers has exhibited the highest conductivity of 3.1×10^{-1} S/cm at 160 °C, achieved by extrinsic encapsulation of H_3PO_4 into the nicely tuned pore spaces of a COF, which in turn draws special attention to the role of phosphoric acid as a proton source/carrier under anhydrous conditions, ascribed to its quick proton relay and switching mechanism. Among the MOFs and their composites, the extrinsic LiBr-encapsulated MOF $\text{LiBr}@(\text{H}_3\text{O})[(\text{UO}_2)_4(2\text{pmb})_3(\text{H}_2\text{O})_3] \cdot 0.5\text{H}_2\text{O}$ achieved the highest ultrahigh superprotonic anhydrous conductivity of 1.55×10^{-1} at 110 °C. Thus, such MOF-integrated polymeric materials offer huge potential to replace the state-of-the-art Nafion for utilization on the commercial scale as well by satisfying the practical agenda for PEM materials (Nafion shows such a magnitude of conductivity under $80\text{--}85$ °C and at $95\text{--}100\%$ RH). Toward further progress in this research field, some of the crystalline materials, such as a few MOFs, COFs, and POMs, have been explored in the fabrication of MEAs for practical potentiality checks. Although significant achievements have been made in this research field, still many challenges and underdeveloped issues remain unexcavated that demand higher attention for future advancements in this field. Specifically, as discussed in the previous section, CO tolerance is an important factor that critically affects fuel cell performance; however, measures to investigate the CO tolerance as well as to assess the fuel upgradation require prior attention to justify the sustainability of these crystalline anhydrous conductors. Similarly, performance assessments must be carried out with these anhydrous conductors as PEMs in benchtop fuel cell test stands in laboratories, as highlighted. Thus, encouraged by the terrific progress in the domain of anhydrous proton conductivities, it is reasonable to trust that these crystalline platforms shall definitely attract more and more attention in the near future and will surely motivate researchers to put extensive efforts into fixing the issues critically discussed herein to make allow them to be implemented as anhydrous PEMs in PEMFC technology.

Corresponding Authors

Dirk Volkmer – Chair of Solid State and Materials Chemistry, Institute of Physics, Augsburg University, 86159 Augsburg, Germany; orcid.org/0000-0002-8105-2157; Email: dirk.volkmer@physik.uni-augsburg.de
Madhab C. Das – Department of Chemistry, Indian Institute of Technology Kharagpur, Kharagpur 721302, India; orcid.org/0000-0002-6571-8705; Email: mcdas@chem.iitkgp.ac.in

Authors

Debolina Mukherjee – Department of Chemistry, Indian Institute of Technology Kharagpur, Kharagpur 721302, India
Apu Saha – Department of Chemistry, Indian Institute of Technology Kharagpur, Kharagpur 721302, India
Subhdeep Moni – Department of Chemistry, Indian Institute of Technology Kharagpur, Kharagpur 721302, India

Complete contact information is available at:
<https://pubs.acs.org/10.1021/jacs.4c14029>

Notes

The authors declare no competing financial interest.

ACKNOWLEDGMENTS

D.M. and A.S. thank IIT Kharagpur for their research fellowships. M.C.D. acknowledges the CSIR, New Delhi, for the EMR Research Grant (01/3113/23/EMR-II) for financial support and the AvH Foundation Germany for a Humboldt Research Fellowship for “Experienced Researchers”.

REFERENCES

- (1) International Energy Outlook, DOE/EIA-0484(2016); U.S. Energy Information Administration (EIA), Washington, DC, May 2016. [https://www.eia.gov/outlooks/ieo/pdf/0484\(2016\).pdf](https://www.eia.gov/outlooks/ieo/pdf/0484(2016).pdf)
- (2) Staffell, I.; Scamman, D.; Abad, A. V.; Balcombe, P.; Dodds, P. E.; Ekins, P.; Shah, N.; Ward, K. R. The role of hydrogen and fuel cells in the global energy system. *Energy Environ. Sci.* **2019**, *12*, 463.
- (3) Ramaswamy, P.; Wong, N. E.; Shimizu, G. K. H. MOFs as proton conductors – challenges and opportunities. *Chem. Soc. Rev.* **2014**, *43*, 5913.
- (4) Colomban, P. *Proton Conductors: Solids, Membranes and Gels—Materials and Devices*, Vol. 2; Cambridge University Press: Cambridge, 1992.
- (5) Sahoo, R.; Mondal, S.; Pal, S. C.; Mukherjee, D.; Das, M. C. Covalent-Organic Frameworks (COFs) as Proton Conductors. *Adv. Energy Mater.* **2021**, *11*, No. 2102300.
- (6) Pal, S. C.; Das, M. C. Superprotonic Conductivity of MOFs and Other Crystalline Platforms Beyond 10^{-1} S/cm. *Adv. Funct. Mater.* **2021**, *31*, No. 2101584.
- (7) Alaswad, A.; Omran, A.; Sodre, J. R.; Wilberforce, T.; Pignatelli, G.; Dassisi, M.; Baroutaji, A.; Olabi, A. G. Technical and Commercial Challenges of Proton-Exchange Membrane (PEM) Fuel Cells. *Energies* **2021**, *14*, 144.
- (8) Office of Fossil Energy, Hydrogen Strategy: Enabling a Low-Carbon Economy; U.S. Department of Energy, Washington, DC, July 2020. https://www.energy.gov/sites/prod/files/2020/07/f76/USDOE_FE_Hydrogen_Strategy_July2020.pdf
- (9) Zhao, Y.; Mao, Y.; Zhang, W.; Tang, Y.; Wang, P. Reviews on the effects of contaminations and research methodologies for PEMFC. *Int. J. Hydrogen Energy* **2020**, *45*, 23174.
- (10) Yan, W. M.; Chu, H.-S.; Lu, M.-X.; Weng, F.-B.; Jung, G.-B.; Lee, C.-Y. Degradation of proton exchange membrane fuel cells due to CO and CO₂ poisoning. *J. Power Sources* **2009**, *188*, 141.

- (11) Baschuk, J. J.; Li, X. Carbon monoxide poisoning of proton exchange membrane fuel cells. *Int. J. Energy Res.* **2001**, *25*, 695.
- (12) Divisek, J.; Oetjen, H. F.; Peinecke, V.; Schmidt, V. M.; Stimming, U. Components for PEM fuel cell systems using hydrogen and CO containing fuels. *Electrochim. Acta* **1998**, *43*, 3811.
- (13) Bose, S.; Kuila, T.; Nguyen, T. X. H.; Kim, N. H.; Lau, K.-t.; Lee, J. H. Polymer membranes for high temperature proton exchange membrane fuel cell: Recent advances and challenges. *Prog. Polym. Sci.* **2011**, *36*, 813.
- (14) Pal, S. C.; Mukherjee, D.; Oruganti, Y.; Lee, B. G.; Lim, D. W.; Pramanik, B.; Manna, A. K.; Das, M. C. Room-Temperature Superprotonic Conductivity beyond 10^{-1} S/cm in a Co(II) Coordination Polymer. *J. Am. Chem. Soc.* **2024**, *146*, 14546.
- (15) Xiang, F.; Chen, S.; Zheng, S.; Yang, Y.; Huang, J.; Lin, Q.; Wang, L.; Xiang, S.; Zhang, Z. Anhydrous Proton Conduction in Crystalline Porous Materials with a Wide Working Temperature Range. *ACS Appl. Mater. Interfaces* **2021**, *13*, 41363.
- (16) Schuster, M. F. H.; Meyer, W. H. Anhydrous Proton-Conducting Polymers. *Annu. Rev. Mater. Res.* **2003**, *33*, 233.
- (17) Ye, Y.; Gong, L.; Xiang, S.; Zhang, Z.; Chen, B. Metal–Organic Frameworks as a Versatile Platform for Proton Conductors. *Adv. Mater.* **2020**, *32*, No. 1907090.
- (18) Lim, D.-W.; Kitagawa, H. Proton Transport in Metal–Organic Frameworks. *Chem. Rev.* **2020**, *120*, 8416.
- (19) Yamada, T.; Otsubo, K.; Makiura, R.; Kitagawa, H. Designer coordination polymers: dimensional crossover architectures and proton conduction. *Chem. Soc. Rev.* **2013**, *42*, 6655.
- (20) Elahi, S. M.; Chand, S.; Deng, W. H.; Pal, A.; Das, M. C. Polycarboxylate-Templated Coordination Polymers: Role of Templates for Superprotonic Conductivities of up to 10^{-1} S/cm. *Angew. Chem., Int. Ed.* **2018**, *57*, 6662.
- (21) Tominaka, S.; Coudert, F.-X.; Dao, T. D.; Nagao, T.; Cheetham, A. K. Insulator-to-Proton-Conductor Transition in a Dense Metal–Organic Framework. *J. Am. Chem. Soc.* **2015**, *137*, 6428.
- (22) Bao, S.; Shimizu, G. K. H.; Zheng, L.-M. Proton conductive metal phosphonate frameworks. *Coord. Chem. Rev.* **2019**, *378*, 577.
- (23) Sahoo, R.; Pal, S. C.; Das, M. C. Solid-State Proton Conduction Driven by Coordinated Water Molecules in Metal–Organic Frameworks and Coordination Polymers. *ACS Energy Lett.* **2022**, *7*, 4490.
- (24) Lim, D.-W.; Sadakiyo, M.; Kitagawa, H. Proton transfer in hydrogen-bonded degenerate systems of water and ammonia in metal–organic frameworks. *Chem. Sci.* **2019**, *10*, 16.
- (25) Bunzen, H.; Javed, A.; Klawinski, D.; Lamp, A.; Grzywa, M.; Kalytta-Mewes, A.; Tiemann, M.; von Nidda, H.-A. K.; Wagner, T.; Volkmer, D. Anisotropic Water-Mediated Proton Conductivity in Large Iron(II) Metal–Organic Framework Single Crystals for Proton-Exchange Membrane Fuel Cells. *ACS Appl. Nano Mater.* **2019**, *2*, 291.
- (26) Kitagawa, H. Transported into fuel cells. *Nat. Chem.* **2009**, *1*, 689.
- (27) Sadakiyo, M.; Yamada, T.; Kitagawa, H. Rational Designs for Highly Proton-Conductive Metal–Organic Frameworks. *J. Am. Chem. Soc.* **2009**, *131*, 9906.
- (28) Bureekaew, S.; Horike, S.; Higuchi, M.; Mizuno, M.; Kawamura, T.; Tanaka, D.; Yanai, N.; Kitagawa, S. One-dimensional imidazole aggregate in aluminium porous coordination polymers with high proton conductivity. *Nat. Mater.* **2009**, *8*, 831.
- (29) Umeyama, D.; Horike, S.; Inukai, M.; Hijikata, Y.; Kitagawa, S. Confinement of Mobile Histamine in Coordination Nanochannels for Fast Proton Transfer. *Angew. Chem., Int. Ed.* **2011**, *50*, 11706.
- (30) Taylor, J. M.; Dawson, K. W.; Shimizu, G. K. H. A Water-Stable Metal–Organic Framework with Highly Acidic Pores for Proton-Conducting Applications. *J. Am. Chem. Soc.* **2013**, *135*, 1193.
- (31) Kim, S.; Dawson, K. W.; Gelfand, B. S.; Taylor, J. M.; Shimizu, G. K. H. Enhancing Proton Conduction in a Metal–Organic Framework by Isomorphous Ligand Replacement. *J. Am. Chem. Soc.* **2013**, *135*, 963.
- (32) Yoon, M.; Suh, K.; Natarajan, S.; Kim, K. Proton Conduction in Metal–Organic Frameworks and Related Modularly Built Porous Solids. *Angew. Chem., Int. Ed.* **2013**, *52*, 2688.
- (33) Shimizu, G. K. H.; Taylor, J. M.; Kim, S. R. Proton Conduction with Metal–Organic Frameworks. *Science* **2013**, *341*, 354.
- (34) Colodrero, R. M. P.; Papathanasiou, K. E.; Stavlianoudaki, N.; Olivera-Pastor, P.; Losilla, E. R.; Aranda, M. A. G.; León-Reina, L.; Sanz, J.; Sobrados, I.; Choquesillo-Lazarte, D.; García-Ruiz, J. M.; Atienzar, P.; Rey, F.; Demadis, K. D.; Cabeza, A. Multifunctional Luminescent and Proton-Conducting Lanthanide Carboxyphosphate Open-Framework Hybrids Exhibiting Crystalline-to-Amorphous-to-Crystalline Transformations. *Chem. Mater.* **2012**, *24*, 3780.
- (35) Liu, Y.-R.; Chen, Y.-Y.; Zhao, H.-Y.; Li, G. Exploration of single-crystal proton conduction in ordered networks. *Coord. Chem. Rev.* **2024**, *499*, No. 215516.
- (36) Ponomareva, V. G.; Kovalenko, K. A.; Chupakhin, A. P.; Dybtsev, D. N.; Shutova, E. S.; Fedin, V. P. Imparting High Proton Conductivity to a Metal–Organic Framework Material by Controlled Acid Impregnation. *J. Am. Chem. Soc.* **2012**, *134*, 15640.
- (37) Xue, W.-L.; Deng, W.-H.; Chen, H.; Liu, R.-H.; Taylor, J. M.; Li, Y.-k.; Wang, L.; Deng, Y.-H.; Li, W.-H.; Wen, Y.-Y.; Wang, G.-E.; Wan, C.-Q.; Xu, G. MOF-Directed Synthesis of Crystalline Ionic Liquids with Enhanced Proton Conduction. *Angew. Chem., Int. Ed.* **2021**, *60*, 1290.
- (38) Sahoo, R.; Luo, S.; Pendyala, N. K.; Chand, S.; Fu, Z.-H.; Das, M. C. Coordinated water molecule-induced solid-state superprotonic conduction by a highly scalable and pH-stable coordination polymer (CP). *Mater. Chem. Front.* **2023**, *7*, 3373.
- (39) Chand, S.; Elahi, S. M.; Pal, A.; Das, M. C. Metal–Organic Frameworks and Other Crystalline Materials for Ultrahigh Superprotonic Conductivities of 10^{-2} S/cm or Higher. *Chem.—Eur. J.* **2019**, *25*, 6259.
- (40) Pal, S. C.; Chand, S.; Kumar, A. G.; Mileo, P. G. M.; Silverwood, I.; Maurin, G.; Banerjee, S.; Elahi, S. M.; Das, M. C. A Co(ii)-coordination polymer for ultrahigh superprotonic conduction: an atomistic insight through molecular simulations and QENS experiments. *J. Mater. Chem. A* **2020**, *8*, 7847.
- (41) Chand, S.; Pal, S. C.; Lim, D.-W.; Otsubo, K.; Pal, A.; Kitagawa, H.; Das, M. C. A 2D Mg(II)-MOF with High Density of Coordinated Waters as Sole Intrinsic Proton Sources for Ultrahigh Superprotonic Conduction. *ACS Materials Lett.* **2020**, *2*, 1343.
- (42) Geng, K.; He, T.; Liu, R.; Dalapati, S.; Tan, K. T.; Li, Z.; Tao, S.; Gong, Y.; Jiang, Q.; Jiang, D. Covalent Organic Frameworks: Design, Synthesis, and Functions. *Chem. Rev.* **2020**, *120*, 8814.
- (43) Hao, L.; Jia, S.; Qiao, X.; Lin, E.; Yang, Y.; Chen, Y.; Cheng, P.; Zhang, Z. Pore Geometry and Surface Engineering of Covalent Organic Frameworks for Anhydrous Proton Conduction. *Angew. Chem., Int. Ed.* **2023**, *62*, e202217240.
- (44) Huang, N.; Zhai, L.; Couprie, D. E.; Addicoat, M. A.; Okushita, K.; Nishimura, K.; Heine, T.; Jiang, D. Multiple-component covalent organic frameworks. *Nat. Commun.* **2016**, *7*, 12325.
- (45) Feng, X.; Ding, X.; Jiang, D. Covalent organic frameworks. *Chem. Soc. Rev.* **2012**, *41*, 6010.
- (46) Pal, S. C.; Mukherjee, D.; Sahoo, R.; Mondal, S.; Das, M. C. Proton-Conducting Hydrogen-Bonded Organic Frameworks. *ACS Energy Lett.* **2021**, *6*, 4431.
- (47) Lin, R.-B.; He, Y.; Li, P.; Wang, H.; Zhou, W.; Chen, B. Multifunctional porous hydrogen-bonded organic framework materials. *Chem. Soc. Rev.* **2019**, *48*, 1362.
- (48) Wang, B.; Lin, R.-B.; Zhang, Z.; Xiang, S.; Chen, B. Hydrogen-Bonded Organic Frameworks as a Tunable Platform for Functional Materials. *J. Am. Chem. Soc.* **2020**, *142*, 14399.
- (49) Hisaki, I.; Xin, C.; Takahashi, K.; Nakamura, T. Designing Hydrogen-Bonded Organic Frameworks (HOFs) with Permanent Porosity. *Angew. Chem., Int. Ed.* **2019**, *58*, 11160.
- (50) Xing, G.; Yan, T.; Das, S.; Ben, T.; Qiu, S. Synthesis of Crystalline Porous Organic Salts with High Proton Conductivity. *Angew. Chem., Int. Ed.* **2018**, *57*, 5345.
- (51) Kang, D. W.; Kang, M.; Kim, H.; Choe, J. H.; Kim, D. W.; Park, J. R.; Lee, W. R.; Moon, D.; Hong, C. S. A Hydrogen-Bonded Organic Framework (HOF) with Type IV NH₃ Adsorption Behavior. *Angew. Chem., Int. Ed.* **2019**, *58*, 16152.

- (52) Karmakar, A.; Illathvalappil, R.; Anothumakkool, B.; Sen, A.; Samanta, P.; Desai, A. V.; Kurungot, S.; Ghosh, S. K. Hydrogen-Bonded Organic Frameworks (HOFs): A New Class of Porous Crystalline Proton-Conducting Materials. *Angew. Chem., Int. Ed.* **2016**, *55*, 10667.
- (53) Ogiwara, N.; Iwano, T.; Ito, T.; Uchida, S. Proton conduction in ionic crystals based on polyoxometalates. *Coord. Chem. Rev.* **2022**, *462*, No. 214524.
- (54) Sun, X.; Liu, S.; Zhang, S.; Dang, T.; Tian, H.; Lu, Y.; Liu, S. High Proton Conductivity Achieved by the Self-Assembly of POM-Based Acid–Base Adduct in SBA-15 over a Wide Range from -40 to 85 °C. *ACS Appl. Energy Mater.* **2020**, *3*, 1242.
- (55) Lin, J.; Li, N.; Yang, S.; Jia, M.; Liu, J.; Li, X.-M.; An, L.; Tian, Q.; Dong, L.-Z.; Lan, Y.-Q. Self-Assembly of Giant Mo240 Hollow Opening Dodecahedra. *J. Am. Chem. Soc.* **2020**, *142*, 13982.
- (56) Martinelli, A.; Otero-Mato, J. M.; Garaga, M. N.; Elamin, K.; Rahman, S. M. H.; Zwanziger, J. W.; Werner-Zwanziger, U.; Varela, L. M. A New Solid-State Proton Conductor: The Salt Hydrate Based on Imidazolium and 12-Tungstophosphate. *J. Am. Chem. Soc.* **2021**, *143*, 13895.
- (57) Zhou, H.-C.; Kitagawa, S. Metal–Organic Frameworks (MOFs). *Chem. Soc. Rev.* **2014**, *43*, 5415.
- (58) Zhou, H.-C.; Long, J. R.; Yaghi, O. M. Introduction to Metal–Organic Frameworks. *Chem. Rev.* **2012**, *112*, 673.
- (59) Sahoo, R.; Mondal, S.; Mukherjee, D.; Das, M. C. Metal–Organic Frameworks for CO₂ Separation from Flue and Biogas Mixtures. *Adv. Funct. Mater.* **2022**, *32*, No. 2207197.
- (60) Lin, R.-B.; Xiang, S.; Xing, H.; Zhou, W.; Chen, B. Exploration of porous metal–organic frameworks for gas separation and purification. *Coord. Chem. Rev.* **2019**, *378*, 87.
- (61) Lin, R.-B.; Zhang, Z.; Chen, B. Achieving High Performance Metal–Organic Framework Materials through Pore Engineering. *Acc. Chem. Res.* **2021**, *54*, 3362.
- (62) Mukherjee, D.; Behera, J.; Mondal, S.; Pal, S. C.; Volkmer, D.; Das, M. C. Critical Perspectives on Metal–Organic Frameworks and Their Composites for the Adsorptive Removal of Antibiotics from Wastewater Matrices. *Cryst. Growth Des.* **2023**, *23*, 7612.
- (63) Mukherjee, D.; Pal, S. C.; Das, G.; Gore, K. R.; Das, M. C. Devising robust hydrophobic MOFs and its membrane for ultra-sensitive aqueous phase detection of antibiotics and toxic nitro-explosives and adsorption of TNP. *J. Environ. Chem. Eng.* **2023**, *11*, No. 110528.
- (64) Lustig, W. P.; Mukherjee, S.; Rudd, N. D.; Desai, A. V.; Li, J.; Ghosh, S. K. Metal–organic frameworks: functional luminescent and photonic materials for sensing applications. *Chem. Soc. Rev.* **2017**, *46*, 3242.
- (65) Newar, R.; Akhtar, N.; Antil, N.; Kumar, A.; Shukla, S.; Begum, W.; Manna, K. Amino Acid-Functionalized Metal-Organic Frameworks for Asymmetric Base–Metal Catalysis. *Angew. Chem., Int. Ed.* **2021**, *60*, 10964.
- (66) Sahoo, R.; Pramanik, B.; Mondal, S.; Das, M. C. A Highly Chemically Robust 3D Interpenetrated MOF Heterogeneous Catalyst for the Synthesis of Hantzsch1,4-Dihydropyridines and Drug Molecules. *Small* **2024**, *20*, No. 2309281.
- (67) Mukherjee, D.; Saha, A.; Basak, D.; Sahoo, R.; Das, M. C. Highly scalable and robust ribbon-like coordination polymer as green catalyst for Hantzsch condensation in synthesis of DHPs and bioactive drug molecule. *Mater. Today Catal.* **2024**, *5*, No. 100051.
- (68) Behera, J.; Pal, A.; Sahoo, R.; Das, M. C. Variation in Catalytic Efficacies of a 2D pH-Stable MOF by Altering Activation Methods. *Chem. – Eur. J.* **2024**, *30*, No. e202400375.
- (69) Saha, A.; Pal, A.; Mukherjee, D.; Pal, S. C.; Das, M. C. Two-Dimensional Cu(II)-MOF with Lewis Acid–Base Bifunctional Sites for Chemical Fixation of CO₂ and Bioactive 1,4-DHP Synthesis via Hantzsch Condensation. *Inorg. Chem.* **2024**, *63*, 10832.
- (70) Mondal, S.; Samanta, P.; Sahoo, R.; Kuila, T.; Das, M. C. Porous and chemically robust MIL-100(V) MOF as an efficient cathode material for zinc-ion batteries. *Chem. Eng. J.* **2023**, *470*, No. 144340.
- (71) Kanda, S.; Yamashita, K.; Ohkawa, K. A proton conductive coordination polymer. I. [N, N'-bis (2-hydroxyethyl)-dithiooxamido] copper (II). *Bull. Chem. Soc. Jpn.* **1979**, *52*, 3296.
- (72) Hurd, J. A.; Vaidhyanathan, R.; Thangadurai, V.; Ratcliffe, C. I.; Moudrakovski, I. L.; Shimizu, G. K. H. Anhydrous proton conduction at 150 °C in a crystalline metal-organic framework. *Nat. Chem.* **2009**, *1*, 705.
- (73) Umeyama, D.; Horike, S.; Inukai, M.; Itakura, T.; Kitagawa, S. Inherent Proton Conduction in a 2D Coordination Framework. *J. Am. Chem. Soc.* **2012**, *134*, 12780.
- (74) Inukai, M.; Horike, S.; Chen, W.; Umeyama, D.; Itakura, T.; Kitagawa, S. Template-directed proton conduction pathways in a coordination framework. *J. Mater. Chem. A* **2014**, *2*, 10404.
- (75) Horike, S.; Umeyama, D.; Inukai, M.; Itakura, T.; Kitagawa, S. Coordination-Network-Based Ionic Plastic Crystal for Anhydrous Proton Conductivity. *J. Am. Chem. Soc.* **2012**, *134*, 7612.
- (76) Wei, Y.-S.; Hu, X.-P.; Han, Z.; Dong, X.-Y.; Zang, S.-Q.; Mak, T. C. W. Unique Proton Dynamics in an Efficient MOF-Based Proton Conductor. *J. Am. Chem. Soc.* **2017**, *139*, 3505.
- (77) Haase, F.; Lotsch, B. V. Solving the COF trilemma: towards crystalline, stable and functional covalent organic frameworks. *Chem. Soc. Rev.* **2020**, *49*, 8469.
- (78) Wang, H.; Zeng, Z.; Xu, P.; Li, L.; Zeng, G.; Xiao, R.; Tang, Z.; Huang, D.; Tang, L.; Lai, C.; Jiang, D.; Liu, Y.; Yi, H.; Qin, L.; Ye, S.; Ren, X.; Tang, W. Recent progress in covalent organic framework thin films: fabrications, applications and perspectives. *Chem. Soc. Rev.* **2019**, *48*, 488.
- (79) Huang, N.; Wang, P.; Jiang, D. Covalent organic frameworks: a materials platform for structural and functional designs. *Nat. Rev. Mater.* **2016**, *1*, 16068.
- (80) Li, Z.; He, T.; Gong, Y.; Jiang, D. Covalent Organic Frameworks: Pore Design and Interface Engineering. *Acc. Chem. Res.* **2020**, *53*, 1672.
- (81) Diercks, C. S.; Yaghi, O. M. The Atom, The Molecule, and The Covalent Organic Framework. *Science* **2017**, *355*, No. eaal1585.
- (82) Guan, X.; Chen, F.; Fang, Q.; Qiu, S. Design and Applications of Three Dimensional Covalent Organic Frameworks. *Chem. Soc. Rev.* **2020**, *49*, 1357.
- (83) Alahakoon, S. B.; Diwakara, S. D.; Thompson, C. M.; Smaldone, R. A. Supramolecular Design in 2D Covalent Organic Frameworks. *Chem. Soc. Rev.* **2020**, *49*, 1344.
- (84) Zhao, X.; Pachfule, P.; Thomas, A. Covalent Organic Frameworks (COFs) for Electrochemical Applications. *Chem. Soc. Rev.* **2021**, *50*, 6871.
- (85) Jiménez-García, L.; Kaltbeitzel, A.; Pisula, W.; Gutmann, J. S.; Klapper, M.; Müllen, K. Phosphonated Hexaphenylbenzene: A Crystalline Proton Conductor. *Angew. Chem., Int. Ed.* **2009**, *48*, 9951.
- (86) Tholen, P.; Peeples, C. A.; Schaper, R.; Bayraktar, C.; Erkal, T. S.; Ayhan, M. M.; Çoşut, B.; Beckmann, J.; Yazaydin, A. O.; Wark, M.; Hanna, G.; Zorlu, Y.; Yücesan, G. Semiconductive Microporous Hydrogen-Bonded Organophosphonic Acid Frameworks. *Nat. Commun.* **2020**, *11*, 3180.
- (87) Chand, S.; Pal, S. C.; Pal, A.; Ye, Y.; Lin, Q.; Zhang, Z.; Xiang, S.; Das, M. C. Metallo Hydrogen-Bonded Organic Frameworks (MHOFs) as New Class of Crystalline Materials for Protonic Conduction. *Chem. – Eur. J.* **2019**, *25*, 1691.
- (88) Wang, Y.; Yin, J.; Liu, D.; Gao, C.; Kang, Z.; Wang, R.; Sun, D.; Jiang, J. Guest-tuned Proton Conductivity of a Porphyrinylphosphonate-Based Hydrogen-Bonded Organic Framework. *J. Mater. Chem. A* **2021**, *9*, 2683.
- (89) Sun, Y.; Wei, J.; Fu, Z.; Zhang, M.; Zhao, S.; Xu, G.; Li, C.; Zhang, J.; Zhou, T. Bio-Inspired Synthetic Hydrogen-Bonded Organic Frameworks for Efficient Proton Conduction. *Adv. Mater.* **2023**, *35*, No. 2208625.
- (90) Nakamura, O.; Kodama, T.; Oginio, I.; Miyake, Y. High-Conductivity Solid Proton Conductors: Dodecamolybdophosphoric Acid And Dodecatungstophosphoric Acid Crystals. *Chem. Lett.* **1979**, *8*, 17.

- (91) Yoon, M.; Suh, K.; Natarajan, S.; Kim, K. Proton Conduction in Metal–Organic Frameworks and Related Modularly Built Porous Solids. *Angew. Chem., Int. Ed.* **2013**, *52*, 2688.
- (92) Li, A.-L.; Gao, Q.; Xu, J.; Bu, X.-H. Proton-Conductive Metal–Organic Frameworks: Recent Advances and Perspectives. *Coord. Chem. Rev.* **2017**, *344*, 54.
- (93) Sadakiyo, M.; Yamada, T.; Kitagawa, H. Hydrated Proton-Conductive Metal–Organic Frameworks. *ChemPlusChem.* **2016**, *81*, 691.
- (94) Escorihuela, J.; Narducci, R.; Compañ, V.; Costantino, F. Proton Conductivity of Composite Polyelectrolyte Membranes with Metal–Organic Frameworks for Fuel Cell Applications. *Adv. Mater. Interfaces* **2019**, *6*, No. 1801146.
- (95) Watanabe, M.; Thomas, M. L.; Zhang, S.; Ueno, K.; Yasuda, T.; Dokko, K. Application of Ionic Liquids to Energy Storage and Conversion Materials and Devices. *Chem. Rev.* **2017**, *117*, 7190.
- (96) Bao, S.-S.; Shimizu, G. K.H.; Zheng, L.-M. Proton conductive metal phosphonate frameworks. *Coord. Chem. Rev.* **2019**, *378*, 577.
- (97) Li, S.; Zhou, Z.; Zhang, Y.; Liu, M.; Li, W. 1H-1,2,4-Triazole: An Effective Solvent for Proton-Conducting Electrolytes. *Chem. Mater.* **2005**, *17*, 5884–5886.
- (98) Su, X.; Yao, Z.; Ye, Y.; Zeng, H.; Xu, G.; Wu, L.; Ma, X.; Chen, Q.-H.; Wang, L.; Zhang, Z.; Xiang, S. 40-Fold Enhanced Intrinsic Proton Conductivity in Coordination Polymers with the Same Proton-Conducting Pathway by Tuning Metal Cation Nodes. *Inorg. Chem.* **2016**, *55*, 983.
- (99) Liu, L.; Yao, Z.; Ye, Y.; Lin, Q.; Chen, S.; Zhang, Z.; Xiang, S. Enhanced Intrinsic Proton Conductivity of Metal–Organic Frameworks by Tuning the Degree of Interpenetration. *Cryst. Growth Des.* **2018**, *18*, 3724.
- (100) Ye, Y.; Wu, X.; Yao, Z.; Wu, L.; Cai, Z.; Wang, L.; Ma, X.; Chen, Q.-H.; Zhang, Z.; Xiang, S. Metal–Organic Frameworks with a Large Breathing Effect to Host Hydroxyl Compounds for High Anhydrous Proton Conductivity over a Wide Temperature Range from Subzero to 125 °C. *J. Mater. Chem. A* **2016**, *4*, 4062.
- (101) Escorihuela, J.; Sahuquillo, Ó.; García-Bernabé, A.; Giménez, E.; Compañ, V. Phosphoric Acid Doped Polybenzimidazole (PBI)/Zeolitic Imidazolate Framework Composite Membranes with Significantly Enhanced Proton Conductivity under Low Humidity Conditions. *Nanomaterials* **2018**, *8*, 775.
- (102) Anahidzade, N.; Abdolmaleki, A.; Dinari, M.; Firouz Tadavani, K.; Zhiani, M. Metal–Organic Framework Anchored Sulfonated Poly (Ether Sulfone) as a High Temperature Proton Exchange Membrane for Fuel Cells. *J. Membr. Sci.* **2018**, *565*, 281.
- (103) Chandra, S.; Kundu, T.; Kandambeth, S.; BabaRao, R.; Marathe, Y.; Kunjir, S. M.; Banerjee, R. Phosphoric Acid Loaded Azo (–N=N–) Based Covalent Organic Framework for Proton Conduction. *J. Am. Chem. Soc.* **2014**, *136*, 6570.
- (104) Chandra, S.; Kundu, T.; Dey, K.; Addicoat, M.; Heine, T.; Banerjee, R. Interplaying Intrinsic and Extrinsic Proton Conductivities in Covalent Organic Frameworks. *Chem. Mater.* **2016**, *28*, 1489.
- (105) Huang, W.; Li, B.; Wu, Y.; Zhang, Y.; Zhang, W.; Chen, S.; Fu, Y.; Yan, T.; Ma, H. In Situ-Doped Superacid in the Covalent Triazine Framework Membrane for Anhydrous Proton Conduction in a Wide Temperature Range from Subzero to Elevated Temperature. *ACS Appl. Mater. Interfaces* **2021**, *13*, 13604.
- (106) Xu, H.; Tao, S.; Jiang, D. Proton Conduction in Crystalline and Porous Covalent Organic Frameworks. *Nat. Mater.* **2016**, *15*, 722.
- (107) Jiang, G.; Zou, W.; Ou, Z.; Zhang, L.; Zhang, W.; Wang, X.; Song, H.; Cui, Z.; Liang, Z.; Du, L. Tuning the Interlayer Interactions of 2D Covalent Organic Frameworks Enables an Ultrastable Platform for Anhydrous Proton Transport. *Angew. Chem., Int. Ed.* **2022**, *61*, e202208086.
- (108) Guo, Y.; Zou, X.; Li, W.; Hu, Y.; Jin, Z.; Sun, Z.; Gong, S.; Guo, S.; Yan, F. High-Density Sulfonic Acid-Grafted Covalent Organic Frameworks with Efficient Anhydrous Proton Conduction. *J. Mater. Chem. A* **2022**, *10*, 6499.
- (109) Basak, D.; Verseck, C.; Toscano, D. T.; Christensen, S.; Tuominen, M. T.; Venkataraman, D. Anhydrous Proton Conductivities of Squaric Acid Derivatives. *Chem. Commun.* **2012**, *48*, 5922.
- (110) Dekura, S.; Mizuno, M.; Mori, H. Isotropic Anhydrous Superprotonic Conductivity Cooperated with Installed Imidazolium Molecular Motions in a 3D Hydrogen-Bonded Phosphate Network. *Angew. Chem., Int. Ed.* **2022**, *61*, No. e202212872.
- (111) Wang, X.-L.; Niu, K.-Y.; Yang, F.-F.; Wang, J.-H.; Liang, L.; Zhang, X.-M. Boosting Proton Conductivity in Hydrogen-Bonded Organic Layers by Modulating Embedded Guest Molecules. *Cryst. Growth Des.* **2023**, *23*, 6221.
- (112) Shi, N.; Wang, Y.-J.; Li, X.-X.; Sun, Y.-Q.; Zheng, S.-T. An Inorganic Co-containing Heteropolyoxoniobate: Reversible Chromism and H₂O-dependent Proton Conductivity Properties. *Inorg. Chem. Front.* **2021**, *8*, 5225.
- (113) Yao, Z.-Y.; Zhang, G.-Q.; Liu, J.-L.; Zhang, J.; Liu, W.-L.; Ren, X.-M. A CsCl-type Inorganic Cluster-Based High Symmetry Crystal Built from {Mo_{4.55}V_{7.45}PO₄₀}^{10.45-} with a High Ratio of Vanadium to Molybdenum and {(H₂O)_{0.3}@K₆(H₂O)₁₂}⁶⁺ Clusters Exhibiting Proton Conduction below the Freezing Point of Water. *Dalton Trans.* **2019**, *48*, 17210.
- (114) Gui, D.; Dai, X.; Tao, Z.; Zheng, T.; Wang, X.; Silver, M. A.; Shu, J.; Chen, L.; Wang, Y.; Zhang, T.; Xie, J.; Zou, L.; Xia, Y.; Zhang, J.; Zhang, J.; Zhao, L.; Diwu, J.; Zhou, R.; Chai, Z.; Wang, S. Unique Proton Transportation Pathway in a Robust Inorganic Coordination Polymer Leading to Intrinsically High and Sustainable Anhydrous Proton Conductivity. *J. Am. Chem. Soc.* **2018**, *140*, 6146.
- (115) Dong, X.-Y.; Wang, J.-H.; Liu, S.-S.; Han, Z.; Tang, Q.-J.; Li, F.-F.; Zang, S.-Q. Synergy between Isomorphous Acid and Basic Metal–Organic Frameworks for Anhydrous Proton Conduction of Low-Cost Hybrid Membranes at High Temperatures. *ACS Appl. Mater. Interfaces* **2018**, *10*, 38209.
- (116) Li, X.-M.; Dong, L.-Z.; Liu, J.; Ji, W.-X.; Li, S.-L.; Lan, Y.-Q. Intermediate-Temperature Anhydrous High Proton Conductivity Triggered by Dynamic Molecular Migration in Trinuclear Cluster Lattice. *Chem.* **2020**, *6*, 2272.
- (117) Shinde, D. B.; Aiyappa, H. B.; Bhadra, M.; Biswal, B. P.; Wadge, P.; Kandambeth, S.; Garai, B.; Kundu, T.; Kurungot, S.; Banerjee, R. A Mechanochemically Synthesized Covalent Organic Framework as a Proton-Conducting Solid Electrolyte. *J. Mater. Chem. A* **2016**, *4*, 2682.
- (118) Zeng, M.; Liu, W.; Guo, H.; Li, T.; Li, Q.; Zhao, C.; Li, X.; Li, H. Polyoxometalate-Cross-Linked Proton Exchange Membranes with Post-Assembled Nanostructures for High-Temperature Proton Conduction. *ACS Appl. Energy Mater.* **2022**, *5*, 9058.
- (119) Bao, S.-S.; Shimizu, G. K. H.; Zheng, L.-M. Proton conductive metal phosphonate frameworks. *Coord. Chem. Rev.* **2019**, *378*, 577–594.
- (120) Zhang, K.; Wen, G.-H.; Yang, X.-J.; Lim, D.-W.; Bao, S. S.; Donoshita, M.; Wu, L.-Q.; Kitagawa, H.; Zheng, L.-M. Anhydrous Superprotonic Conductivity of a Uranyl-Based MOF from Ambient Temperature to 110 °C. *ACS Materials Lett.* **2021**, *3*, 744–751.
- (121) Li, J.; Wang, J.; Shui, F.; Yi, M.; Zhang, Z.; Liu, X.; Zhang, L.; You, Z.; Yang, R.; Yang, S.; Li, B.; Bu, X.-H. Superhigh intrinsic proton conductivity in densely carboxylic covalent organic framework. *Chin. Chem. Lett.* **2023**, *34*, No. 107917.
- (122) Fan, C.; Geng, H.; Wu, H.; Peng, Q.; Wang, X.; Shi, B.; Kong, Y.; Yin, Z.; Liu, Y.; Jiang, Z. Three-dimensional covalent organic framework membrane for efficient proton conduction. *J. Mater. Chem. A* **2021**, *9*, 17720–17723.
- (123) Pan, Y.; Shan, Z.; Liu, Z.; Su, J.; Zhang, G. Thiadiazole-based 3D Covalent Organic Framework for Efficient Anhydrous Proton Conduction. *CrystEngComm.* **2024**, *27*, 111.
- (124) Vilčiauskas, L.; Tuckerman, M. E.; Bester, G.; Paddison, S. J.; Kreuer, K.-D. The Mechanism of Proton Conduction in Phosphoric Acid. *Nat. Chem.* **2012**, *4*, 461.
- (125) Tao, S.; Zhai, L.; Dinga Wonanke, A. D.; Addicoat, M. A.; Jiang, Q.; Jiang, D. Confining H₃PO₄ Network in Covalent Organic

- Frameworks Enables Proton Super Flow. *Nat. Commun.* **2020**, *11*, 1981.
- (126) Das, A.; Hazarika, M.; Sana, B.; Jana, T. Nanoporous Covalent Organic Framework and Polybenzimidazole Composites for Proton Exchange Membranes. *ACS Appl. Nano Mater.* **2023**, *6*, 12016.
- (127) Lu, S.; Wang, D.; Jiang, S. P.; Xiang, Y.; Lu, J.; Zeng, J. HPW/MCM-41 Phosphotungstic Acid/Mesoporous Silica Composites as Novel Proton-Exchange Membranes for Elevated-Temperature Fuel Cells. *Adv. Mater.* **2010**, *22*, 971.
- (128) Li, J.; Li, X.; Yu, S.; Hao, J.; Lu, W.; Shao, Z.; Yi, B. Porous Polybenzimidazole Membranes Doped with Phosphoric Acid: Preparation and Application in High-Temperature Proton-Exchange-Membrane Fuel Cells. *Energy Convers. Manag.* **2014**, *85*, 323.
- (129) Devrim, Y.; Albostan, A.; Devrim, H. Experimental Investigation of CO Tolerance in High Temperature PEM Fuel Cells. *Int. J. Hydrogen Energy* **2018**, *43*, 18672.
- (130) Zhao, J.; Huang, X.; Chang, H.; Chan, S. H.; Tu, Z. Effects of Operating Temperature on the Carbon Corrosion in a Proton Exchange Membrane Fuel Cell under High Current Density. *Energy Convers. Manag. X* **2021**, *10*, No. 100087.
- (131) Cao, J.; Ma, W.; Lyu, K.; Zhuang, L.; Cong, H.; Deng, H. Twist and Sliding Dynamics between Interpenetrated Frames in Ti-MOF Revealing High Proton Conductivity. *Chem. Sci.* **2020**, *11*, 3978.
- (132) Nagarkar, S. S.; Unni, S. M.; Sharma, A.; Kurungot, S.; Ghosh, S. K. Two-in-One: Inherent Anhydrous and Water-Assisted High Proton Conduction in a 3D Metal–Organic Framework. *Angew. Chem., Int. Ed.* **2014**, *53*, 2638.
- (133) Panda, T.; Kundu, T.; Banerjee, R. Structural Isomerism Leading to Variable Proton Conductivity in Indium(III) Isophthalic Acid Based Frameworks. *Chem. Commun.* **2013**, *49*, 6197.
- (134) Horike, S.; Chen, W.; Itakura, T.; Inukai, M.; Umeyama, D.; Asakura, H.; Kitagawa, S. Order-to-disorder Structural Transformation of a Coordination Polymer and Its Influence on Proton Conduction. *Chem. Commun.* **2014**, *50*, 10241.
- (135) Qu, J.-X.; Fu, Y.-M.; Meng, X.; He, Y.-O.; Sun, H.-X.; Yang, R.-g.; Wang, H.-N.; Su, Z.-M. A Porous Ti-based Metal–Organic Framework for CO₂ Photoreduction and Imidazole-Dependent Anhydrous Proton Conduction. *Chem. Commun.* **2023**, *59*, 1070.
- (136) Liu, S.; Yue, Z.; Liu, Y. Incorporation of Imidazole within the Metal–Organic Framework UiO-67 for Enhanced Anhydrous Proton Conductivity. *Dalton Trans.* **2015**, *44*, 12976.
- (137) Yu, S.-S.; Liu, S.-X.; Duan, H.-B. Dielectric Response and Anhydrous Proton Conductivity in a Chiral Framework Containing a Non-Polar Molecular Rotor. *Dalton Trans.* **2015**, *44*, 20822.
- (138) Homburg, T.; Hartwig, C.; Reinsch, H.; Wark, M.; Stock, N. Structure Property Relationships Affecting the Proton Conductivity in Imidazole Loaded Al-MOFs. *Dalton Trans.* **2016**, *45*, 15041.
- (139) Wang, K.; Si, L.; Tian, Y.; Yang, F. Ionization of a Neutral MOF to Disperse and Anchor Acid for Boosting Anhydrous Proton Conductivity. *Microporous & Mesoporous Mater.* **2024**, *363*, No. 112825.
- (140) Inukai, M.; Horike, S.; Itakura, T.; Shinozaki, R.; Ogiwara, N.; Umeyama, D.; Nagarkar, S.; Nishiyama, Y.; Malon, M.; Hayashi, A.; Ohhara, T.; Kiyonagi, R.; Kitagawa, S. Encapsulating Mobile Proton Carriers into Structural Defects in Coordination Polymer Crystals: High Anhydrous Proton Conduction and Fuel Cell Application. *J. Am. Chem. Soc.* **2016**, *138*, 8505.
- (141) Tang, Q.; Liu, Y.; Liu, S.; He, D.; Miao, J.; Wang, X.; Yang, G.; Shi, Z.; Zheng, Z. High Proton Conduction at above 100 °C Mediated by Hydrogen Bonding in a Lanthanide Metal–Organic Framework. *J. Am. Chem. Soc.* **2014**, *136*, 12444.
- (142) Liu, L.; Yao, Z.; Ye, Y.; Liu, C.; Lin, Q.; Chen, S.; Xiang, S.; Zhang, Z. Enhancement of Intrinsic Proton Conductivity and Aniline Sensitivity by Introducing Dye Molecules into the MOF Channel. *ACS Appl. Mater. Interfaces* **2019**, *11*, 16490.
- (143) Lupa, M.; Kozyra, P.; Matoga, D. Solvent-Free Mechanochemical Dense Pore Filling Yields CPO-27/MOF-74 Metal–Organic Frameworks with High Anhydrous and Water-Assisted Proton Conductivity. *ACS Appl. Energy Mater.* **2023**, *6*, 9118.
- (144) Lin, Q.; Ye, Y.; Liu, L.; Yao, Z.; Li, Z.; Wang, L.; Liu, C.; Zhang, Z.; Xiang, S. High Proton Conductivity in Metalloring-Cluster Based Metal–Organic Nanotubes. *Nano Res.* **2021**, *14*, 387.
- (145) Wang, L.; Deng, N.; Wang, G.; Ju, J.; Wang, M.; Cheng, B.; Kang, W. Construction of Interpenetrating Transport Channels and Compatible Interfaces via a Zeolitic Imidazolate Framework “Bridge” for Nanofibrous Hybrid PEMs with Enhanced Proton Conduction and Methanol Resistance. *ACS Sustainable Chem. Eng.* **2020**, *8*, 12976.
- (146) Chen, W.; Horike, S.; Umeyama, D.; Ogiwara, N.; Itakura, T.; Tassel, C.; Goto, Y.; Kageyama, H.; Kitagawa, S. Glass Formation of a Coordination Polymer Crystal for Enhanced Proton Conductivity and Material Flexibility. *Angew. Chem., Int. Ed.* **2016**, *55*, 5195.
- (147) Sun, X.-L.; Deng, W.-H.; Chen, H.; Han, H.-L.; Taylor, J. M.; Wan, C.-Q.; Xu, G. A Metal–Organic Framework Impregnated with a Binary Ionic Liquid for Safe Proton Conduction above 100 °C. *Chem.—Eur. J.* **2017**, *23*, 1248.
- (148) Qu, J.-X.; Fu, Y.-M.; Meng, X.; He, Y.-O.; Li, C.-J.; Sun, H.-X.; Yang, R.-G.; Wang, H.-N.; Su, Z.-M. Construction of Zr-Metal–Organic Frameworks-Based Composite Materials toward Anhydrous Proton Conduction and Photocatalytic CO₂ Reduction. *Inorg. Chem.* **2023**, *62*, 15992.
- (149) Umeyama, D.; Horike, S.; Inukai, M.; Kitagawa, S. Integration of Intrinsic Proton Conduction and Guest-Accessible Nanospace into a Coordination Polymer. *J. Am. Chem. Soc.* **2013**, *135*, 11345.
- (150) Wu, B.; Liang, G.; Lin, X.; Wu, L.; Luo, J.; Xu, T. Immobilization of N-(3-aminopropyl)-Imidazole through MOFs in Proton Conductive Membrane for Elevated Temperature Anhydrous Applications. *J. Membr. Sci.* **2014**, *458*, 86.
- (151) Rao, Z.; Feng, K.; Tang, B.; Wu, P. Construction of Well Interconnected Metal–Organic Framework Structure for Effectively Promoting Proton Conductivity of Proton Exchange Membrane. *J. Membr. Sci.* **2017**, *533*, 160.
- (152) Chen, H.; Han, S.-Y.; Liu, R.-H.; Chen, T.-F.; Bi, K.-L.; Liang, J.-B.; Deng, Y.-H.; Wan, C.-Q. High Conductive, Long-Term Durable, Anhydrous Proton Conductive Solid-State Electrolyte Based on a Metal–Organic Framework Impregnated with Binary Ionic Liquids: Synthesis, Characteristic and Effect of Anion. *J. Power Sources* **2018**, *376*, 168.
- (153) Mukhopadhyay, S.; Das, A.; Jana, T.; Das, S. K. Fabricating a MOF Material with Polybenzimidazole into an Efficient Proton Exchange Membrane. *ACS Appl. Energy Mater.* **2020**, *3*, 7964.
- (154) Meng, Z.; Aykanat, A.; Mirica, K. A. Proton Conduction in 2D Aza-Fused Covalent Organic Frameworks. *Chem. Mater.* **2019**, *31*, 819.
- (155) Li, S.; Liu, Y.; Li, L.; Liu, C.; Li, J.; Ashraf, S.; Li, P.; Wang, B. Enhanced Proton Conductivity of Imidazole-Doped Thiophene-Based Covalent Organic Frameworks via Subtle Hydrogen Bonding Modulation. *ACS Appl. Mater. Interfaces* **2020**, *12*, 22910.
- (156) Fu, Y.; Wu, Y.; Chen, S.; Zhang, W.; Zhang, Y.; Yan, T.; Yang, B.; Ma, H. Zwitterionic Covalent Organic Frameworks: Attractive Porous Host for Gas Separation and Anhydrous Proton Conduction. *ACS Nano* **2021**, *15*, 19743.
- (157) Hao, L.; Jia, S.; Qiao, X.; Lin, E.; Yang, Y.; Chen, Y.; Cheng, P.; Zhang, Z. Pore Geometry and Surface Engineering of Covalent Organic Frameworks for Anhydrous Proton Conduction. *Angew. Chem., Int. Ed.* **2023**, *62*, No. e202217240.
- (158) Chen, S.; Wu, Y.; Zhang, Y.; Zhang, W.; Fu, Y.; Huang, W.; Yan, T.; Ma, H. Tuning Proton Dissociation Energy in Proton Carrier Doped 2D Covalent Organic Frameworks for Anhydrous Proton Conduction at Elevated Temperature. *J. Mater. Chem. A* **2020**, *8*, 13702.
- (159) Liu, S.; Liu, M.; Li, X.; Xu, Q.; Sun, Y.; Zeng, G. Construction of Dense H-bond Acceptors in the Channels of Covalent Organic Frameworks for Proton Conduction. *J. Mater. Chem. A* **2023**, *11*, 13965.
- (160) Wu, X.; Hong, Y.-l.; Xu, B.; Nishiyama, Y.; Jiang, W.; Zhu, J.; Zhang, G.; Kitagawa, S.; Horike, S. Perfluoroalkyl-Functionalized Covalent Organic Frameworks with Superhydrophobicity for Anhydrous Proton Conduction. *J. Am. Chem. Soc.* **2020**, *142*, 14357.

(161) Wu, X.; Liu, Z.; Guo, H.; Hong, Y.-l.; Xu, B.; Zhang, K.; Nishiyama, Y.; Jiang, W.; Horike, S.; Kitagawa, S.; Zhang, G. Host-Guest Assembly of H-Bonding Networks in Covalent Organic Frameworks for Ultrafast and Anhydrous Proton Transfer. *ACS Appl. Mater. Interfaces* **2021**, *13*, 37172.

(162) Liu, M.; Deng, W.-H.; Wang, X.; Liu, J.; Jin, S.; Xu, G.; Tan, B. Hydrogen Bond Activation by Pyridinic Nitrogen for the High Proton Conductivity of Covalent Triazine Framework Loaded with H₃PO₄. *ChemSusChem* **2022**, *15*, No. e202201298.

(163) Liu, S.; Lin, Z.; Wang, C.; Guo, J. Dual-Sided Symmetric Crystalline Orientation of Covalent Organic Framework Membranes for Unidirectional Anhydrous Proton Conduction. *Sci. China Chem.* **2022**, *65*, 2548.

(164) Zhong, Y.; Li, C.; Yang, F.; Guan, L.; Jin, S. Covalent Pyrimidine Frameworks via a Tandem Polycondensation Method for Photocatalytic Hydrogen Production and Proton Conduction. *Small* **2023**, *19*, No. 2204515.

(165) Jiang, X.; Zhang, K.; Huang, Y.; Xu, B.; Xu, X.; Zhang, J.; Liu, Z.; Wang, Y.; Pan, Y.; Bian, S.; Chen, Q.; Wu, X.; Zhang, G. Conjugated Microporous Polymer with C≡C and C–F Bonds: Achieving Remarkable Stability and Super Anhydrous Proton Conductivity. *ACS Appl. Mater. Interfaces* **2021**, *13*, 15536.

(166) Tao, S.; Jiang, D. Accelerating Anhydrous Proton Transport in Covalent Organic Frameworks: Pore Chemistry and its Impacts. *Angew. Chem., Int. Ed.* **2024**, *63*, e202408296.

(167) Sunairi, Y.; Ueda, A.; Yoshida, J.; Suzuki, K.; Mori, H. Anisotropic Proton Conductivity Arising from Hydrogen-Bond Patterns in Anhydrous Organic Single Crystals, Imidazolium Carboxylates. *J. Phys. Chem. C* **2018**, *122*, 11623.

(168) Yuan, G.; Takeda, T.; Hoshino, N.; Akutagawa, T. Highly Proton-Conducting Mixed Proton-Transferred [(H₂PO₄⁻)(H₃PO₄)_n][∞] Networks Supported by 2,2'-Diaminobithiazolium in Crystals. *J. Phys. Chem. C* **2020**, *124*, 1861.

(169) Ide, R.; Kawasaki, A.; Takeda, T.; Dekura, S.; Hoshino, N.; Matsuda, W.; Seki, S.; Akutagawa, T. Proton Conduction Crossover and Pyrophosphate Bond Formation of –PO₃H⁻ Substituted Naphtalenediimide Salts. *J. Phys. Chem. C* **2023**, *127*, 16709.

(170) Kumar, A.; Pisula, W.; Sieber, C.; Klapper, M.; Mullen, K. Anhydrous Proton Conduction in Self-assembled and Disassembled Ionic Molecules. *J. Mater. Chem. A* **2018**, *6*, 6074.

(171) Slade, R. C. T.; Omana, M. J. Protonic Conductivity of 12-Tungstophosphoric Acid (TPA, H₃PW₁₂O₄₀) at Elevated Temperatures. *Solid State Ionics* **1992**, *58*, 195.

(172) Liu, J.-C.; Han, Q.; Chen, L.-J.; Zhao, J.-W.; Streb, C.; Song, Y.-F. Aggregation of Giant Cerium–Bismuth Tungstate Clusters into a 3D Porous Framework with High Proton Conductivity. *Angew. Chem.* **2018**, *57*, 8416.

(173) PEM Fuel Cell Test Station. <https://hyfindr.com/en/page/pem-fuel-cell-test-station> (accessed 2024-09-03).

(174) 840 Fuel Cell Test System. <https://www.scribner.com/products/fuel-cell-test-systems/840-fuel-cell-test-system/> (accessed 2024-09-03).

(175) Ma, Y.-L.; Wainright, J. S.; Litt, M. H.; Savinell, R. F. Conductivity of PBI Membranes for High-Temperature Polymer Electrolyte Fuel Cells. *J. Electrochem. Soc.* **2004**, *151*, A8.

(176) Reinsch, H.; Homburg, T.; Heidenreich, N.; Frohlich, D.; Henninger, S.; Wark, M.; Stock, N. Green Synthesis of a New Al-MOF Based on the Aliphatic Linker Mesaconic Acid: Structure, Properties and In Situ Crystallisation Studies of Al-MIL-68-Mes. *Chem.—Eur. J.* **2018**, *24*, 2173.

(177) Homburg, T.; Tschense, C. B. L.; Wolkersdoerfer, K.; Reinsch, H.; Wark, M.; Többens, D.; Zander, S.; Senker, J.; Stock, N. Magnesium doped Gallium Phosphonates Ga_{1-x}Mg_x[H_{3+x}(O₃PCH₂)₃N] (x = 0, 0.20) and the Influence on Proton Conductivity. *Z. Anorg. Allg. Chem.* **2018**, *644*, 86.

(178) Donnadio, A.; Nocchetti, M.; Costantino, F.; Taddei, M.; Casciola, M.; Lisboa, F. S.; Vivani, R. A Layered Mixed Zirconium Phosphate/Phosphonate with Exposed Carboxylic and Phosphonic

Groups: X-ray Powder Structure and Proton Conductivity Properties. *Inorg. Chem.* **2014**, *53*, 13220.